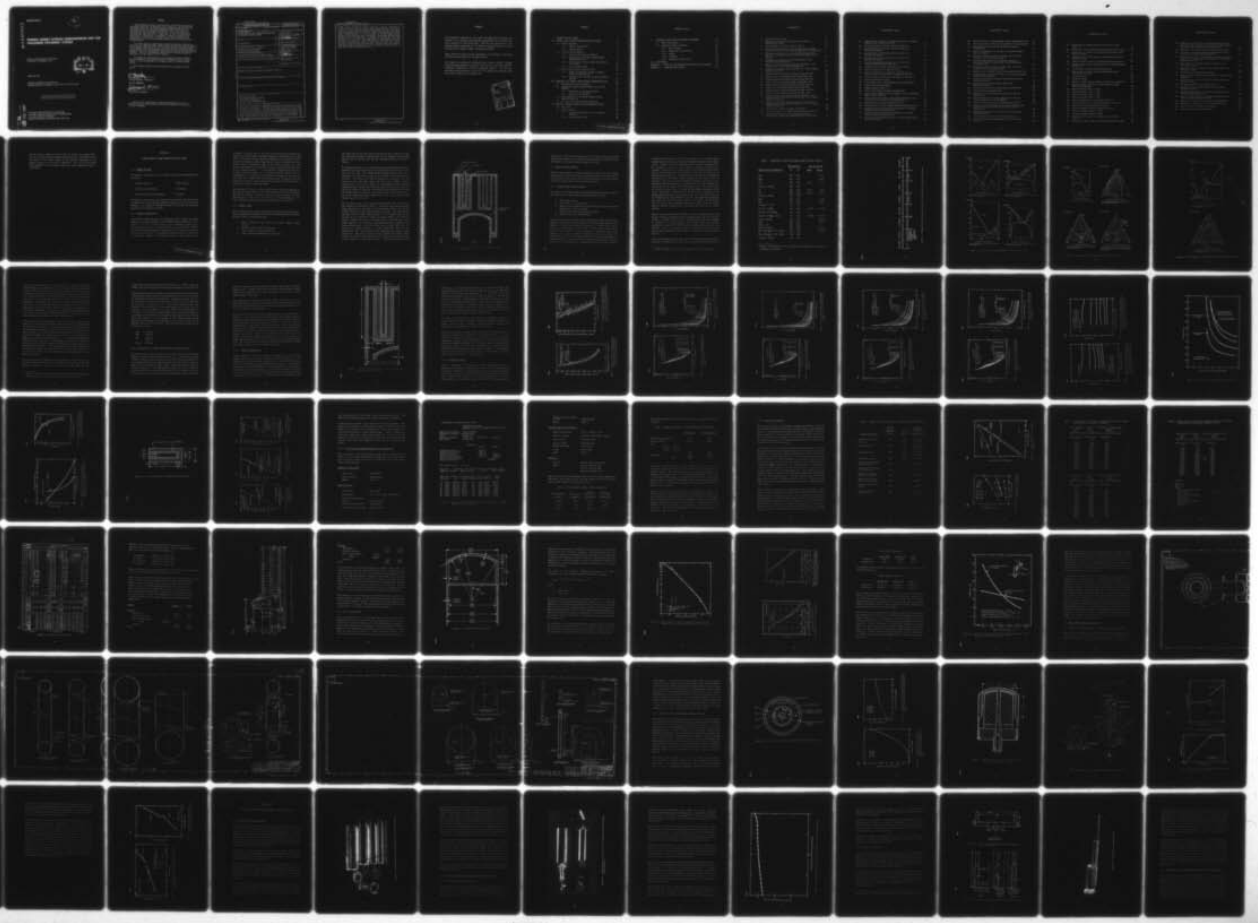
AD-A040 895 XEROX CORP/ELECTRO-OPTICAL SYSTEMS PASADENA CALIF F/G 10/2
THERMAL ENERGY STORAGE DEMONSTRATION UNIT FOR VUILLEUMIER CRYOG--ETC(U)
FEB 77 R RICHTER F33615-75-C-2045
UNCLASSIFIED 2340-I-1 AFAPL-TR-76-110 NL

1 OF 2
AD A040895



AD A040895

AFAPL-TR-76-110

12 NW

# THERMAL ENERGY STORAGE DEMONSTRATION UNIT FOR VUILLEUMIER CRYOGENIC COOLER

*XEROX ELECTRO-OPTICAL SYSTEMS*
*PASADENA, CALIFORNIA 91107*

DDC
RECEIVED
JUN 23 1977
B

FEBRUARY 1977

TECHNICAL REPORT AFAPL-TR-76-110
INTERIM REPORT FOR PERIOD 2 JUNE 1975 to 31 AUGUST 1976

Approved for public release; distribution unlimited

DDC FILE COPY

AIR FORCE AERO PROPULSION LABORATORY
AIR FORCE WRIGHT AERONAUTICAL LABORATORIES
AIR FORCE SYSTEMS COMMAND
WRIGHT-PATTERSON AIR FORCE BASE, OHIO 45433

## NOTICE

When Government drawings, specifications, or other data are used for any purpose other than in connection with a definitely related government procurement operation, the United States Government thereby incurs no responsibility nor any obligation whatsoever; and the fact that the government may have formulated, furnished, or in any way supplied the said drawings, specifications, or other data, is not to be regarded by implication or otherwise as in any manner licensing the holder or any other person or corporation, or conveying any rights or permission to manufacture, use, or sell any patented invention that may in any way be related thereto.

This final report was submitted by Xerox/Electro Optical Systems Inc. under Contract F3361575-C-2045. Robert Richter was the principal investigator. The effort was sponsored by the Air Force Space and Missile Systems Organization (SAMSO), under the technical direction of the Air Force Aero Propulsion Laboratory, with E.T. Mahefkey/AFAPL/POE-2/513-255-6237 the cognizant project engineer. The Air Force greatfully acknowledges Dr. Richter's technical contribution in the conduct of this research.

This report has been reviewed by the Information Office, (ASD/OIP) and is releasable to the National Technical Information Service (NTIS). At NTIS, it will be available to the general public, including foreign nations.

This technical report has been reviewed and is approved for publication.

E.T. Mahefkey
Project Engineer, AFAPL/POE-2

FOR THE COMMANDER

J.F. Wise
Technical Area Manager

Copies of this report should not be returned unless return is required by security considerations, contractual obligations, or notice on a specific document.

AIR FORCE - 18 APRIL 77 - 100

UNCLASSIFIED

SECURITY CLASSIFICATION OF THIS PAGE (When Data Entered)

## REPORT DOCUMENTATION PAGE

READ INSTRUCTIONS BEFORE COMPLETING FORM

1. REPORT NUMBER: AFAPL-TR-76-110
2. GOVT ACCESSION NO.
3. RECIPIENT'S CATALOG NUMBER

4. TITLE (and Subtitle): THERMAL ENERGY STORAGE DEMONSTRATION UNIT FOR VUILLEUMIER CRYOGENIC COOLER

5. TYPE OF REPORT & PERIOD COVERED: Interim Report, 2 June 1975 to 31 August 1976

6. PERFORMING ORG. REPORT NUMBER: 2340-Interim-1

7. AUTHOR(s): Robert Richter

8. CONTRACT OR GRANT NUMBER(s): F33615-75-C-2045

9. PERFORMING ORGANIZATION NAME AND ADDRESS:
Xerox Electro-Optical Systems
300 North Halstead Street
Pasadena, California 91107

10. PROGRAM ELEMENT, PROJECT, TASK AREA & WORK UNIT NUMBERS:
Project No. 2126
Task No. 03
Work Unit No. 10

11. CONTROLLING OFFICE NAME AND ADDRESS:
Air Force Aero Propulsion Laboratory/POE
Wright Patterson Air Force Base, Ohio 45433

12. REPORT DATE: February 1977

13. NUMBER OF PAGES: 154

14. MONITORING AGENCY NAME & ADDRESS (if different from Controlling Office)

15. SECURITY CLASS. (of this report): Unclassified

15a. DECLASSIFICATION DOWNGRADING SCHEDULE

16. DISTRIBUTION STATEMENT (of this Report)

Approved for public release; distribution unlimited.

Interim rept. 2 Jun 75–31 Aug 76

17. DISTRIBUTION STATEMENT (of the abstract entered in Block 20, if different from Report)

18. SUPPLEMENTARY NOTES

19. KEY WORDS (Continue on reverse side if necessary and identify by block number)

Thermal Space Power
Heat Pipe and Energy Transport
Space Power System Study
Thermal Energy Storage Material

20. ABSTRACT (Continue on reverse side if necessary and identify by block number)

This report covers the work performed under the Thermal Energy Storage Demonstration Unit Program. The report presents the analysis, design, fabrication, and testing of a thermal energy storage demonstration unit which was to be mated to an existing Vuilleumier cooler (AFLIR) to demonstrate the concept of powering such a device directly with stored thermal energy. The Thermal Energy Storage Demonstration Unit was to be sized for delivering 1000 watts thermal power for one hour at a temperature of 1250° ±25°F. The

DD FORM 1 JAN 73 1473 EDITION OF 1 NOV 65 IS OBSOLETE

UNCLASSIFIED

SECURITY CLASSIFICATION OF THIS PAGE (When Data Entered)

ternary eutectic 64 $MgF_2$-30 LiF-6 KF, which has a eutectic temperature of 1310°F, was selected as the thermal energy storage material. The report presents the approach and the assumptions underlying the design of the unit, which incorporates a heat pipe for the transfer of energy from the thermal energy storage material to the hot cylinder of the Vuilleumier cooler. Details of the fabrication and the testing of the Thermal Energy Storage Demonstration Unit are presented. The analysis of the test data led to the conclusion that the basic design satisfied all requirements that were established for a TES unit. The thermal energy storage material, however, was found to apparently release its latent heat of fusion over a wider temperature range than had been anticipated. This fact can be attributed to nonisothermal phase transformation or a bulk thermal conductivity that is lower than had been assumed for the salt.

# FOREWORD

The information presented in this report was generated during the performance of the Thermal Energy Storage Demonstration Unit contract, Air Force Contract No. F33615-75-C-2045. The work was carried out in the Advanced Systems Department of the Radiation Systems Division of Xerox Electro-Optical Systems, (XEOS), Pasadena, California.

Robert Richter was the principal investigator of the program. Individual contributors were members of the XEOS Division.

The program was sponsored by SAMSO/SZ under Project 21260310, "Thermal Energy Storage Demonstration Program," with the Air Force Aero Propulsion Laboratory (AFAPL/POE-2) acting as technical monitor. The work was performed during the period 1 June 1975 to 31 August 1976 with the draft final report submitted in November 1976.



CONTENTS


| | | | |
|---|---|---|---|
| I. | INTRODUCTION AND SUMMARY | | 1 |
| II. | THERMAL ENERGY STORAGE DEMONSTRATION UNIT DESIGN | | 5 |
| | 2.1 | General Approach | 5 |
| | | 2.1.1 Heating Configuration | 5 |
| | | 2.1.2 General Layout | 6 |
| | 2.2 | Detailed Design Approach | 9 |
| | | 2.2.1 Thermal Energy Storage Material | 9 |
| | | 2.2.2 Optimization of Thermal Energy Storage Demonstration Unit | 19 |
| | | 2.2.3 Final Thermal Energy Storage Demonstration Unit Design | 45 |
| | | 2.2.4 Hot Cylinder Design | 49 |
| | 2.3 | Special Heat Transfer Considerations | 56 |
| | | 2.3.1 Effect of Volumetric Change of Thermal Energy Storage Material | 56 |
| | | 2.3.2 Cooling of Hot Cylinder During Performance Testing | 63 |
| III. | FABRICATION OF THERMAL ENERGY STORAGE DEMONSTRATION UNIT | | 73 |
| | 3.1 | Machining and Initial Assembly | 73 |
| | 3.2 | Loading of Thermal Energy Storage Unit with TES Material | 75 |
| | | 3.2.1 Evaluation of Loading Procedures | 75 |
| | | 3.2.2 Casting of TES Material | 79 |
| | 3.3 | Final Assembly of the Thermal Energy Storage Demonstration Unit | 82 |
| | 3.4 | Filling of Heat Pipe With Working Fluid | 84 |
| IV. | TESTING OF THERMAL ENERGY STORAGE DEMONSTRATION UNIT | | 91 |
| | 4.1 | Test Setup | 91 |
| | 4.2 | Initial Testing | 93 |
| | | 4.2.1 Steady State Thermal Losses and Thermal Capacity | 93 |
| | | 4.2.2 Test Data Evaluation | 98 |




PRECEDING PAGE BLANK-NOT FILMED

CONTENTS (Contd)


V. CONCEPTUAL FLIGHT DEVICE PARAMETER DEVELOPMENT 119

5.1 Basic Requirements 119

5.2 Conceptual Design Parameters 120

5.2.1 Basic Design 120

5.2.2 Temperature Distributions 123

5.2.3 Weight 123

5.2.4 Structure 128

5.2.5 Conceptual Flight Device 132

VI. CONCLUSIONS 135

APPENDIX A - EFFECT OF NONCONDENSABLE GAS ON HEAT PIPE OPERATION 137

APPENDIX B - TRANSIENT WICK EFFECTS 141

ILLUSTRATIONS


| | | |
|---|---|---|
| 1 | General TES Unit Lay-out | 8 |
| 2 | Temperature Distribution Along the Solar Collector Thermal Power System | 12 |
| 3 | Phase Diagrams of Fluoride Eutectic Salts | 13 |
| 4 | Temperature Distribution in the Thermal Energy Storage Unit for a VM Cooler with 64 LiF-30 $MgF_2$-6 KF as TES Material | 17 |
| 5 | Temperature Distribution in the Thermal Energy Storage Unit for a Vuilleumier Cooler with 67 LiF-33 $MgF_2$ as TES Material | 17 |
| 6 | Parameters Investigated in the Optimization of the Thermal Energy Storage Unit | 21 |
| 7 | Effect of Thermal Energy Storage Salt Thickness on the Length of the Thermal Energy Storage Unit | 23 |
| 8 | Correlation Between Primary Dimensions of 1 kW-Hr Thermal Energy Storage Unit | 23 |
| 9 | Thermal Losses from Thermal Energy Storage Heat Pipe | 24 |
| 10 | Power Losses from Thermal Energy Storage Heat Pipe | 24 |
| 11 | Thermal Losses from Thermal Energy Storage Heat Pipe | 25 |
| 12 | Power Losses from Thermal Energy Storage Heat Pipe | 25 |
| 13 | Thermal Losses from Thermal Energy Storage Heat Pipe | 26 |
| 14 | Power Loss from Thermal Energy Storage Heat Pipe | 26 |
| 15 | Thermal Losses from Thermal Energy Storage Heat Pipe | 27 |
| 16 | Power Loss from Thermal Energy Storage Heat Pipe | 27 |
| 17 | Effect of Vapor Flow Annular Width and Thermal Energy Storage Material Thickness on Thermal Loss of the Thermal Energy Storage Unit | 28 |
| 18 | Effect of Vapor Flow Annular Width and Thermal Energy Storage Material Thickness on Thermal Loss of the Thermal Energy Storage Unit | 28 |
| 19 | Power Losses from Hot Cylinder of VM Cooler | 29 |
| 20 | Optimum Design for a 1 kW-Hr Thermal Energy Storage Unit | 30 |
| 21 | Power Loss as Function of Insulation Thickness of Final Thermal Energy Storage Demonstration Unit Design | 32 |

ILLUSTRATIONS (Contd)


| | | |
|---|---|---|
| 22 | Temperature Distribution in Thermal Insulation of Thermal Energy Storage Demonstration Unit | 32 |
| 23 | Insulation Design of Thermal Energy Storage Unit | 33 |
| 24 | Pressure Drops and Available Suction Pressure for Various Wire Screens | 34 |
| 25 | Pressure Drops and Available Suction Pressure for Various Wire Screens | 34 |
| 26 | Pressure Drops and Available Suction Pressure for Various Wire Screens | 34 |
| 27 | Heat Pipe Design Calculations for Final Design of a 1 kW-Hr Thermal Energy Storage Unit | 36 |
| 28 | Conductivity of Various Combinations of Fiberfrax | 41 |
| 29 | Thermal Conductivity of Super Insulation | 41 |
| 30 | Effect of Insulation Thickness on the Total Loss of Thermal Energy from the Thermal Energy Storage Unit | 44 |
| 31 | Thermal Losses as Affected by the Amount of Insulation | 44 |
| 32 | Available Inconel 600 Pipes | 46 |
| 33 | Final Design for a 1 kW-Hr Thermal Energy Storage Unit | 48 |
| 34 | Original Hot Cylinder Design | 50 |
| 35 | Rupture Stress of René 41 | 52 |
| 36 | Life of Cold-Rolled, Annealed and Aged Sheet | 53 |
| 37 | Larson-Miller Parameter Plot of Rupture Life of Cold-Rolled Sheet, 0.025-0.250-Inch | 53 |
| 38 | Effect of Plate Thickness on the Maximum Stresses in the Hot Cylinder of the AFLIR Vuilleumier Cooler | 55 |
| 39 | Thermal Energy Storage Demonstration Unit | 57 |
| 40 | Configuration of Thermal Energy Storage Demonstration Unit | 64 |
| 41 | Volumetric Void as a Function of Half Angle for Thermal Energy Storage Demonstration Unit | 65 |
| 42 | Volumetric Void and Surface Void Relation for Thermal Energy Storage Demonstration Unit | 65 |
| 43 | Gas Flow for Performance Testing of Thermal Energy Storage Demonstration Unit | 66 |

ILLUSTRATIONS (Contd)


| | | |
|---|---|---|
| 44 | Flow Test Insert - Thermal Energy Storage Demonstration Unit | 67 |
| 45 | Total Heat Transfer from the Hot Cylinder to the Cooling Air | 68 |
| 46 | Power Extraction from the Hot Cylinder as Function of Flow Rate | 68 |
| 47 | Final Air Temperature as Function of Flow Rate Through the Hot Cylinder | 70 |
| 48 | Pressure Drop Along the Heat Transfer Path of the Hot Cylinder of the Vuilleumier Cooler | 70 |
| 49 | Flow Rate Requirement for Cooling Hot Cylinder of Vuilleumier Cooler During Thermal Energy Storage Unit Performance Test | 72 |
| 50 | Pressure Drop Along the Heat Transfer Path of the Hot Cylinder of the Vuilleumier Cooler | 72 |
| 51 | Exploded View of Thermal Energy Storage Demonstration Unit | 74 |
| 52 | Thermal Energy Storage Unit Prior to Loading with Thermal Energy Storage Material | 76 |
| 53 | Temperature of Thermal Energy Storage Material Capsule During Melt-Down | 78 |
| 54 | Bottom Plate of Casting Fixture SK2340-004-1 Material: Graphite | 80 |
| 55 | Tubes and Center Rod of Casting Fixture SK2340-004-2 | 80 |
| 56 | Casting Fixture (Exploded View) | 81 |
| 57 | Distribution of Wick Material Consisting of Mesh 70 Bolting Cloth | 83 |
| 58 | TES Demonstration Unit After Application of Wicking Structure and Prior to Final Welding | 85 |
| 59 | Completed Thermal Energy Storage Demonstration Unit | 85 |
| 60 | Insulation and Thermocouple Locations of Thermal Energy Storage Demonstration Unit for Vuilleumier Cooler Application | 86 |
| 61 | Predicted Thermal Losses from Thermal Energy Storage Demonstration Unit | 87 |
| 62 | Fully Thermally Insulated TES Demonstration Unit | 88 |
| 63 | Thermal Energy Storage Demonstration Unit Test Setup (View I) | 92 |

ILLUSTRATIONS (Contd)


| | | |
|---|---|---|
| 64 | Thermal Energy Storage Demonstration Unit Test Setup (View II) | 92 |
| 65 | Energy Loss from Thermal Energy Storage Demonstration Unit | 95 |
| 66 | Temperature of Thermal Energy Storage Demonstration Unit During Cool-Down | 100 |
| 67 | Temperature of Thermal Energy Storage Demonstration Unit During Cool-Down | 100 |
| 68 | Apparent Thermal Capacity of Thermal Energy Storage Unit | 101 |
| 69 | Measured Temperature of Thermocouple No. 3 During Charging of TES Unit | 101 |
| 70 | Cooling Data of Thermal Energy Storage Unit | 105 |
| 71 | Temperature of Thermal Energy Storage Demonstration Unit During Cool-Down | 106 |
| 72 | Extracted Energy | 107 |
| 73 | Extracted Energy | 107 |
| 74 | Amount of Stored Thermal Energy as Function of Temperature | 109 |
| 75 | Apparent Thermal Capacity of Thermal Energy Storage Unit During Charging | 109 |
| 76 | Extracted Energy (June 7, 1976) | 111 |
| 77 | Extracted Energy (June 7, 1976) | 111 |
| 78 | Extracted Energy (June 4, 1976) | 112 |
| 79 | Extracted Energy (June 4, 1976) | 112 |
| 80 | Measured Temperatures During Energy Extraction | 114 |
| 81 | Measured Temperatures by Thermocouples Nos. 10 and 12 | 114 |
| 82 | Temperatures During Charging of TES Unit | 115 |
| 83 | Measured Temperature During Energy Extraction | 117 |
| 84 | Extracted Energy (August 5, 1976) | 118 |
| 85 | Extracted Energy (August 5, 1976) | 118 |
| 86 | Thermal Energy Storage Unit Mounted on a Hi-Cap Hot Cylinder | 121 |
| 87 | Correlation Between Power Requirement and TES Unit Length | 122 |

ILLUSTRATIONS (Contd)


| | | |
|---|---|---|
| 88 | Temperature Distribution in the Thermal Energy Storage Unit and the Hot Cylinder of the Long Life, High Capacity Vuilleumier Refrigerator for Space Application | 124 |
| 89 | Temperature Drop Across Thermal Energy Storage Material | 125 |
| 90 | Vuilleumier Refrigerator Operating Temperature During Discharge of Thermal Energy Storage Unit | 125 |
| 91 | Operating Temperature of Vuilleumier Refrigerator During a Full Cycle of Charging and Discharging of the Thermal Energy Storage Unit | 126 |
| 92 | Total Weight of a Thermal Energy Storage Unit for a Vuilleumier Cooler | 127 |
| 93 | Specific Energy of a Thermal Energy Storage Unit for a Vuilleumier Cooler | 129 |
| 94 | Thermal Energy Storage Material Weight | 130 |
| 95 | Total Container Weight Including Insulation and Heat Pipe Components | 130 |
| 96 | Dynamic Modulus of Elasticity E and Yield Strength of Inconel 600 Alloy | 131 |
| 97 | Collapsing Pressure of Thin-Walled Vessel | 131 |
| 98 | Conceptual Thermal Energy Storage Unit for Hi-Cap Vuilleumier Cooler | 133 |
| 99 | Long Life, High Capacity Vuilleumier Refrigerator with Thermal Energy Storage Units | 134 |
| 100 | Long Life, High Capacity Vuilleumier Refrigerator with Battery Energized Electric Heaters | 134 |
| A-1 | Temperature Differentials and Pressure Differentials | 138 |
| A-2 | Temperature Differential Due to Noncondensable Gas | 139 |
| A-3 | Vapor Pressure of Sodium and Potassium | 139 |
| B-1 | Test Fixture for Wick Investigation | 143 |

# SECTION I

## INTRODUCTION AND SUMMARY

The objective of the Thermal Energy Storage Demonstration Unit program was the demonstration of a thermal energy storage (TES) unit capable of providing thermal energy to a Vuilleumier (VM) cooler by releasing thermal energy which had been stored in the form a latent heat of fusion of a salt. The requirements were to deliver 1 kW of thermal power for 1 hour at a temperature between 1200° and 1400°F to the hot cylinder of a Vuilleumier cooler. In addition, the TES capability had to be sufficient to account for all thermal losses occurring due to limitations on the size and weight of thermal insulation of the TES unit.

The program was to generate background data for the design of flight test devices which can operate in a power range of 1 to 3 kW, while having a lifetime of better than 5 years. The data were to include costing for the design, fabrication, testing, and delivery of such devices, projected efficiency in satellite application, their weight, volume, and the operating temperature as a function of load.

The program was organized into seven major tasks:

I. Analytical Studies
II. Design
III. Fabrication
IV. Test Setup
V. Testing
VI. Conceptual Flight Device Parameter Development
VII. Reporting

The total technical effort of the program extended over a period of 12-months, and was concluded with the delivery of the tested TES unit mounted on a hot cylinder of a Vuilleumier cooler.

For successful mating of the thermal energy storage unit with the Vuilleumier cooler, the heat pipe concept was considered for transferring the stored energy from the storage material to the point of energy requirement. This appeared most valid in this application in which the amount of thermal energy is large and the heat transfer surface of the hot cylinder over which the thermal energy had to be applied was relatively small.

As the optimization studies indicated, weight considerations and thermal loss considerations dictated a unit with a relatively large diameter, which was about one-third the length of the unit. The largest acceptable diameter of the unit was determined by the restriction that the temperature at the hot cylinder of the Vuilleumier cooler should not vary by more than $50^{\circ}F$ from the beginning of the energy extraction process until the completion of the freezing of the thermal energy storage salt. This stipulation determined the largest thermal energy storage material thickness in the unit and, thus, the greatest diameter for an annular design of the storage compartment.

During the heat pipe design, the elevation pressure drop, which is determined by the height to which the working fluid of the heat pipe has to be raised, proved to be the major pressure drop component. The final wick design of the heat pipe had to utilize almost 75 percent of its theoretical suction capacity to overcome the elevation pressure drop. The wick design proved to be adequate, although great uncertainty existed for a time when the heat pipe did not function properly for reasons which later were traced to a gas leak. The dynamic behavior of wick structures has not been fully investigated and therefore introduced uncertainties into the design of large diameter heat pipe structures which have to be operated in a 1-g environment.

The test results seemed to indicate that the eutectic salt, $MgF_2$-LiF-KF, used in the thermal energy storage demonstration unit, released only about 50 percent of the fusion energy of the individual components of the eutectic mixture at the eutectic temperature. The total stored energy could therefore not be extracted within the design temperature range of $1250^{o} \pm 25^{o}F$.

SECTION II

# THERMAL ENERGY STORAGE DEMONSTRATION UNIT DESIGN

## 2.1. GENERAL APPROACH

The specific requirements for the thermal energy storage demonstration unit were:

| | |
|---|---|
| Thermal capacity to | 1 kW-hr thermal |
| Power to the hot cylinder | 1 kW thermal |
| Hot cylinder operating tempeature | 1250 $\pm 25^{o}$F |

The energy to the unit was to be supplied from an electric source which was to energize the thermal energy storage unit without the use of electrical heaters, i.e., using the container material of the unit as resistance elements for the electrical current.

### 2.1.1 HEATING CONFIGURATION

Considerable thought was given to eliminating electric heaters and using solely the structural material of the thermal energy storage unit as the electrical pass for resistance heating. For a reasonable current level, the electric pass has to be long and, therefore, many structural elements of the thermal energy storage unit would have had to be placed electrically in series with each other. This would have required electrical insulation of structural components by insulating material, which appeared very



PRECEDING PAGE BLANK-NOT FILMED

difficult to achieve when at the same time requiring high thermal conductivity for maintaining a reasonable temperature distribution in the TES unit. An even more serious problem was thought to be the galvanic effect to which the thermal energy storage material would be exposed and about which little or nothing was known for the ternary eutectic salt. Any galvanic separation of the individual elements could cause a serious attack on the container material. It was therefore suggested that the electrically resistive heating of the container material should first be investigated in a smaller device specifically developed for such a test. This test could furnish long time operating data in parallel with the operation of the full scale thermal energy storage unit which could be heated with standard resistance heaters.

The elimination of electric heaters appeared to be of great advantage, as many electric heater failures have been experienced with the VM cooler. When the hot cylinder is heated directly by electric heaters, the heat transfer area is only 7.241 $in.^2$ (46.7 $cm^2$). For a power input of 1 kW, this indicates the relatively high power density of 21.4 $watt/cm^2$.

### 2.1.2 GENERAL LAYOUT

After electing separate electric heating for the power input into the unit, the most appropriate configuration for that heating scheme was considered. The most critical considerations were:

a. Lowest temperature drop across the thermal energy storage material
b. Smallest thermal losses from the unit
c. Lowest weight of structural material
d. Lowest operating temperature of the heaters

The design that evolved from these considerations was a tubular unit with two interconnected annular compartments for the thermal energy storage material and an annular well for the resistance heaters as shown in Figure 1.

The highest temperature drop across the thermal energy storage material is determined by the greatest thickness of the TES material and the heat flow rate per unit area. The annular design provides large surfaces for a relatively low heat flux as well as a relatively small TES material thickness. By placing the electric heaters into an annular well, the heaters can give off their power from their entire surface, thereby operating at a lower power density and corresponding lower operating temperature than a heater that transfers energy only from one side while having its other side insulated. Furthermore, by placing the heater inside the thermal energy storage unit, the outer surface of the TES unit is at the lowest temperature during heating of the unit. This minimizes the thermal losses from the unit.

For the initial layout of the thermal energy storage unit, the effective heat transfer area was about 1700 $cm^2$. During the time when the heaters supply energy for the operation of the Vuilleumier cooler as well as for storage, the highest power density is only 1 watt/$cm^2$. This compares very favorably with the heater power density of 21.4 watt/$cm^2$ when the hot cylinder of the Vuilleumier cooler is heated directly with electric heaters. Despite the fact that the heaters have to transfer power to the higher temperature of the thermal energy storage material, compared to the operating temperature of the hot cylinder which is about 90°F lower, the heaters will actually operate at a lower temperature because of the considerably lower power density when energizing the thermal energy storage unit. Thus, the reliability of the heaters in the thermal energy storage unit would be higher than that of the heaters that directly power the hot cylinder of a Vuilleumier cooler. This might suggest that the

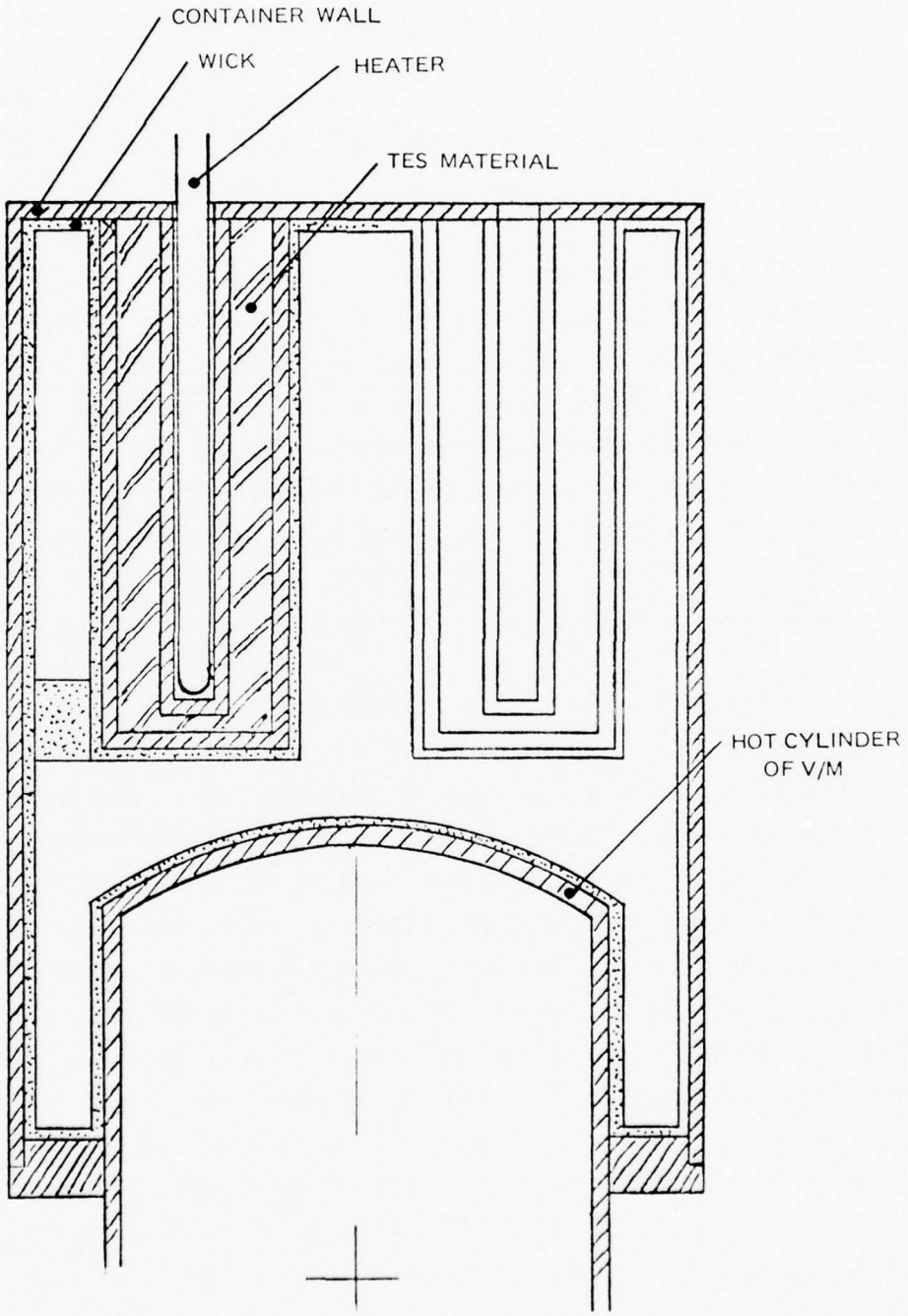



Figure 1. General TES Unit Layout (Center Cut Through Cylindrical Configuration)

urgency for eliminating the heaters and for turning to resistance heating the container material of the thermal energy storage unit might have been eliminated by the thermal energy storage unit design.

## 2.2 DETAILED DESIGN APPROACH

With the establishment of the general approach to the design of the thermal energy storage demonstration unit, the detailed design of the unit required the selection of the thermal energy storage material and the optimization of the unit with respect to size and thermal losses.

### 2.2.1 THERMAL ENERGY STORAGE MATERIAL

The design of the thermal energy storage demonstration unit had to consider the selection of a thermal energy storage material that had:

a. High fusion energy
b. Low volume, i.e., high density
c. Melting point appropriate for maintaining the desired operating temperature of the hot cylinder
d. Compatibility with the structural material
e. Stability over many melting cycles

In the Solar Collector Thermal Power System program which preceded this program, lithium fluoride was selected as the the thermal energy storage material. Lithium fluoride has a melting point of 1558$^{o}$F and a heat of fusion of 0.259 kWh/kg. For the solar collector thermal power train, lithium fluoride proved to be the appropriate thermal energy storage material as it had the melting temperature that could provide the Vuilleumier cooler with the thermal energy at the desired temperature as shown in Figure 2. Since in the present application the thermal energy did not have to be transferred across a thermal radiation joint, which required

a temperature differential of 220°F in the thermal train, a thermal energy storage material with a lower melting temperature appeared to be appropriate. A number of the most promising thermal energy storage materials are presented in Table 1, while Figure 3 presents pertinent phase diagrams.[1] From Table 1 the binary eutectic 67 LiF-33 $MgF_2$ and the ternary eutectic 64 LiF-30 $MgF_2$-6 KF were selected for possible application in the thermal energy storage unit. In Figures 4 and 5 the calculated temperature distributions in the thermal energy storage unit are shown for the two materials. The ternary eutectic LiF-$MgF_2$-KF appeared to provide the more appropriate melting temperature for achieving the desired operating conditions at the hot cylinder of the Vuilleumier cooler. The inner surface of the hot cylinder, which is cooled by the flowing helium gas in the cooler, would have a temperature of 1267.5°F at the beginning of the thermal energy extraction cycle, while at the end of the extraction cycle the temperature will have dropped to 1227.5°F. This temperature range was well within the desired operating range of 1250 $\pm$25°F. The temperature level as well as the temperature range for a system using the binary eutectic LiF-$MgF_2$ appeared not to be better than that of the ternary eutectic.

Another ternary system which appeared to have a melting point near the desired operating temperature for the storage material was 62 LiF-19 NaF-19 $MgF_2$. It fuses at 708°C (1306°F). However, this system was recognized as unstable as it can transition into a system which has a melting temperature of only 630°C (1166°F) when NaF and $MgF_2$ form the double salt $MgF_2$ NaF. This is in conformance with the double melting point of the binary system consisting of NaF and $MgF_2$, as shown in the phase diagram of Figure 3.

The assumed thermal energy storage capacity of the ternary eutectic mixture composed of LiF-$MgF_2$-KF was based on the published data of the heat of

---

1. "Phase Diagrams for Ceramists," American Ceramic Society (1964).

TABLE 1. PROPERTIES OF APPLICABLE THERMAL ENERGY STORAGE MATERIALS

| Eutectic Molar Composition | Melting Point °C | Melting Point °F | Heat of Fusion* kWh/ℓ | Heat of Fusion* kWh/kg |
|---|---|---|---|---|
| $CaF_2$ | 1382 | 2520 | | 0.105 |
| $MgF_2$ | 1263 | 2305 | | 0.265 |
| NaF | 996 | 1825 | 0.603 | 0.216 |
| 56 $CaF_2$ + 44 $MgF_2$ | 985 | 1805 | | |
| KF | 860 | 1580 | 0.310 | 0.125 |
| LiF | 848 | 1558 | 0.464 | 0.259 |
| 67 $CaF_2$ + 33 NaF | 813 | 1495 | | |
| NaCl | 800 | 1472 | | 0.132 |
| KCl | 776 | 1429 | | 0.098 |
| 79 $CaF_2$ + 21 LiF | 765 | 1409 | | |
| 67 LiF + 33 $MgF_2$ | 742 | 1368 | (0.537) | (0.238) |
| 42.5 LiF + 57.5 $MgF_2$ | 735 | 1355 | | |
| 64 LiF + 30 $MgF_2$ + 6 KF | 713 | 1315 | (0.465) | (0.219) |
| 40 KF + 60 NaF | 710 | 1310 | | (0.172) |
| LiH | 686 | 1267 | | 0.716 |
| 50 KF + LiF | 650 | 1202 | | |
| 48 LiF + 52 NaF | 652 | 1206 | | (0.261) |
| NaF + NaF-$MgF_2$ + LiF + $MgF_2$ | 630 | 1166 | | (0.261) |
| NaF + NaF-$MgF_2$ + LiF + $MgF_2$ | 708 | 1306 | | |
| 62 $ZnF_2$ + 38 LiF | 622 | 1152 | | |

* Values in parentheses are of questionable accuracy and subject to modifying definitions.

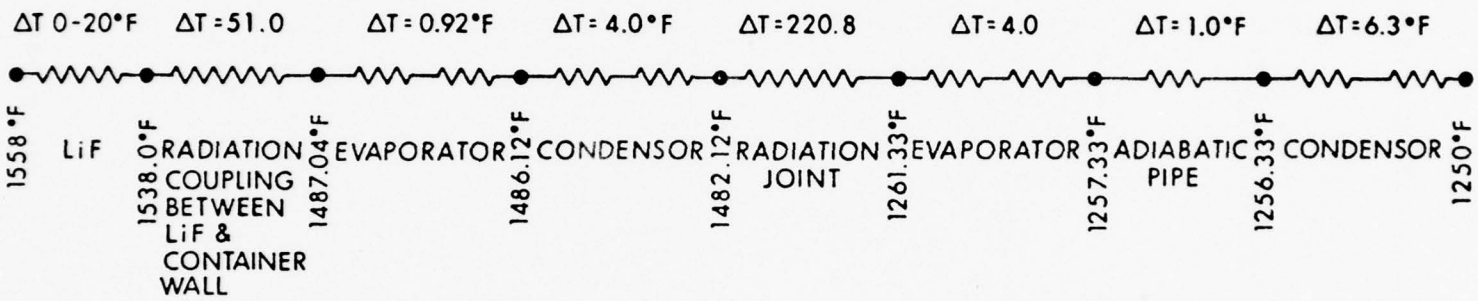



Figure 2. Temperature Distribution Along the Solar Collector Thermal Power System

LiF-NaF

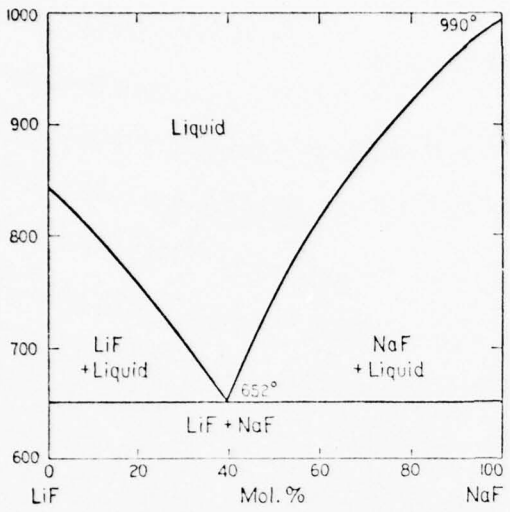



FIG. 1467.—System LiF–NaF.

A. G. Bergman and E. P. Dergunov, *Compt. rend. acad. sci., U.R.S.S.*, **31**, 755 (1941).

$LiF-MgF_2$

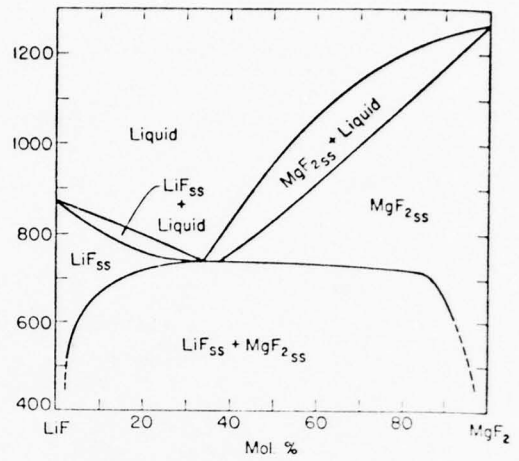



FIG. 1471.—System $LiF–MgF_2$.

W. E. Counts, Rustum Roy, and E. F. Osborn, *J. Am. Ceram. Soc.*, **36** [1] 15 (1953).

$NaF-CaF_2$

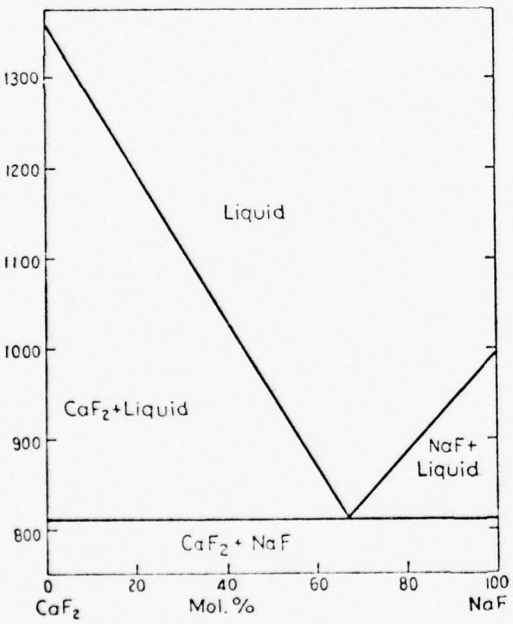



FIG. 1483.—System $NaF–CaF_2$.

P. P. Fedotieff and W. P. Iljinskiĭ, *Z. anorg. u. allgem. Chem.*, **129**, 101 (1923).

$LiF-ZnF_2$

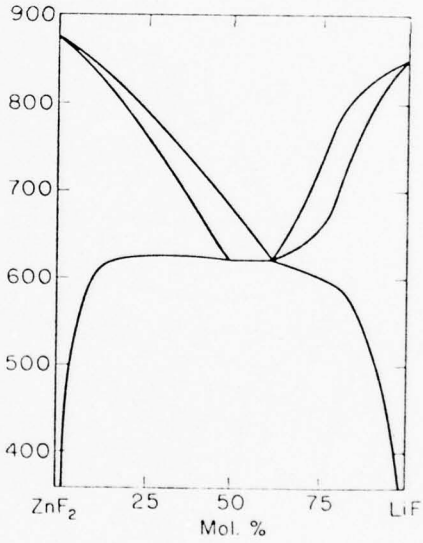



FIG. 1472.—System $LiF–ZnF_2$.

O. Schmitz-Dumont and Horst Bornefeld, *Z. anorg. u. allgem. Chem.*, **287**, 121 (1956).

Figure 3. Phase Diagrams of Fluoride Eutectic Salts (sheet 1 of 4)

LiF–$CaF_2$

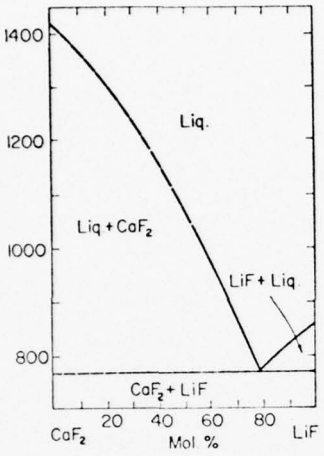



FIG. 1470.—System LiF–$CaF_2$.

W. E. Roake, *J. Electrochem. Soc.*, 104, 661 (1957).

KF–LiF–$MgF_2$

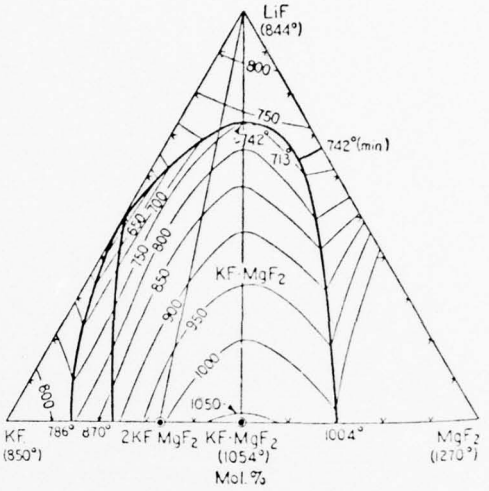



FIG. 1531.—System KF–LiF–$MgF_2$.

A. G. Bergman and S. P. Parlenko, *Compt. rend. acad. sci., U.R.S.S.*, **31**, 818–19 (1941).

KF–LiF–NaF

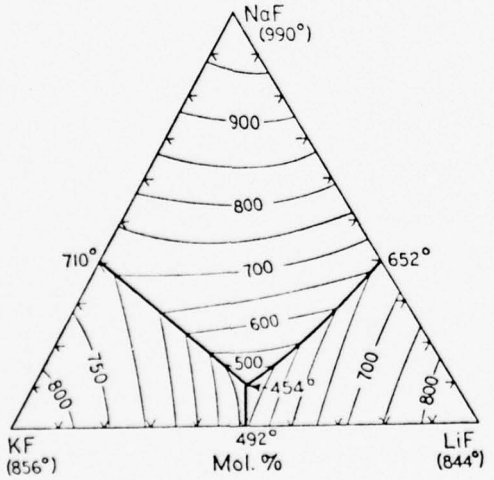



FIG. 1529.—System KF–LiF–NaF.

A. G. Bergman and E. P. Dergunov, *Compt. rend. acad sci., U.R.S.S.*, **31**, 754 (1941).

NaF–$CaF_2$–$MgF_2$

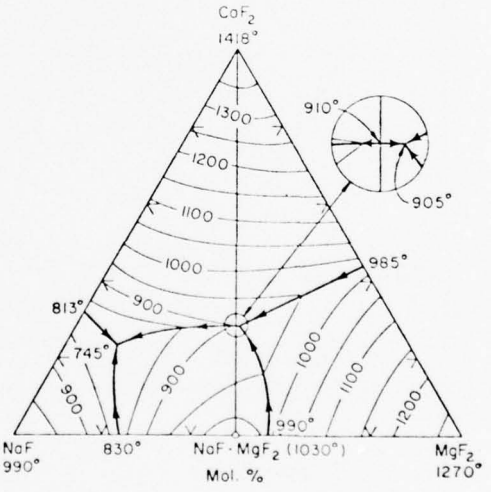



FIG. 1565.—System NaF–$CaF_2$–$MgF_2$; preliminary.

C. J. Barton, L. M. Bratcher, J. P. Blakely, and W. R. Grimes, Oak Ridge National Laboratory, Phase Diagrams of Nuclear Reactor Materials, R. E. Thoma, ed., ORNL-2548, p. 30 (1959).

Figure 3. Phase Diagrams of Fluoride Eutectic Salts (sheet 2 of 4)

$NaF-MgF_2$

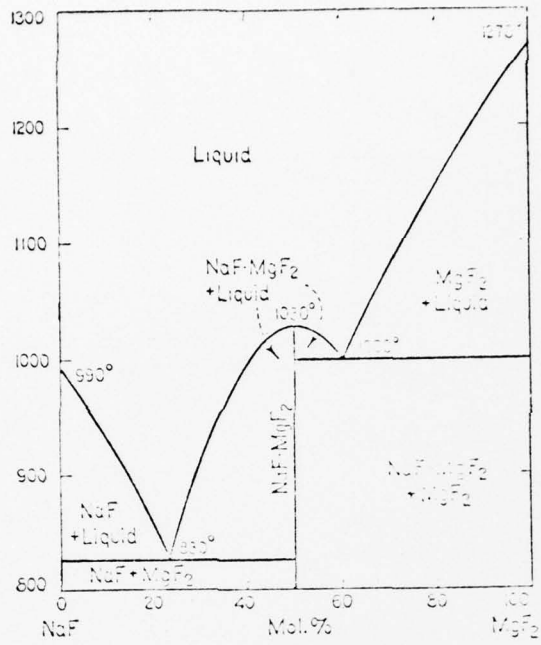



FIG. 1430.—System $NaF-MgF_2$.

A. G. Bergman and E. P. Dergunov, *Compt. rend. acad. sci., U.R.S.S.*, **31**, 755 (1941).

$LiF-NaF-MgF_2$

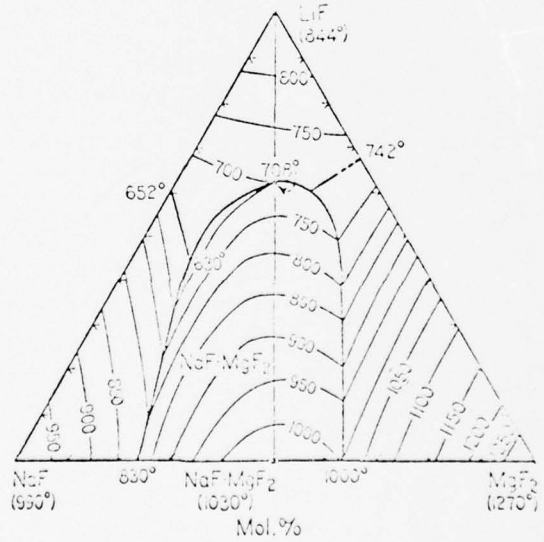



FIG. 1545.—System $LiF-NaF-MgF_2$.

A. G. Bergman and E. P. Dergunov, *Compt. rend. acad. sci., U.R.S.S.*, **31**, 755 (1941).

Figure 3. Phase Diagrams of Fluoride Eutectic Salts (sheet 3 of 4)

BEST AVAILABLE COPY

**KF–$MgF_2$**

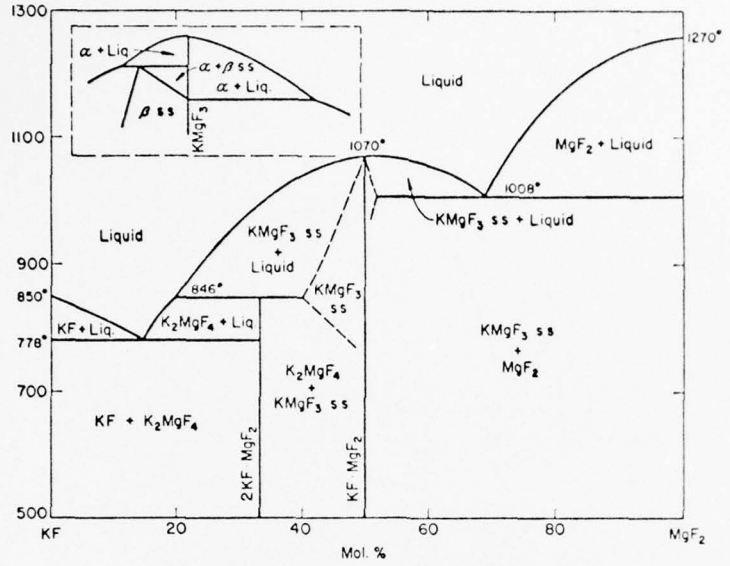



FIG. 1458.—System $KF–MgF_2$. Insert shows possible alternative for high-temperature region near $KF \cdot MgF_2$.

R. C. DeVries and Rustum Roy, *J. Am. Chem. Soc.*, 75, 2481 (1953).

**KF–$NiF_2$**

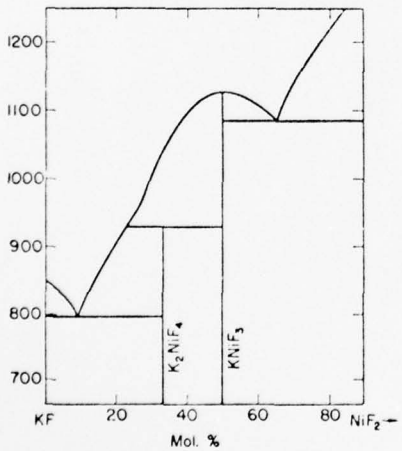



FIG. 1459.—System $KF–NiF_2$.

G. Wagner and D. Balz, *Z. Elektrochem.*, 56, 576 (1952).

**KF–$ZnF_2$**

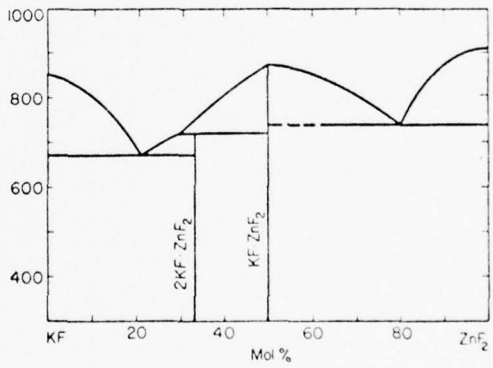



FIG. 1460.—System $KF–ZnF_2$, tentative.

C. J. Barton, L. M. Bratcher, and W. R. Grimes, Oak Ridge National Laboratory, Phase Diagrams of Nuclear Reactor Materials, R. E. Thoma, ed., ORNL-2548, p. 49 (1959).

See also O. Schmitz-Dumont and Horst Bornefeld, *Z. anorg. u. allgem. Chem.*, 287, 122 (1956).

Figure 3. Phase Diagrams of Fluoride Eutectic Salts (sheet 4 of 4)

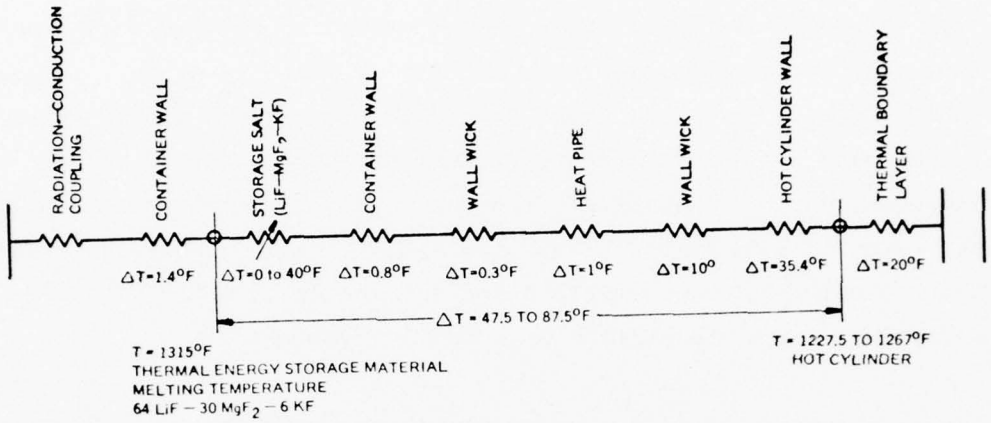



Figure 4. Temperature Distribution in the Thermal Energy Storage Unit for a VM Cooler with 64 LiF-30 $MgF_2$-6 KF as TES Material

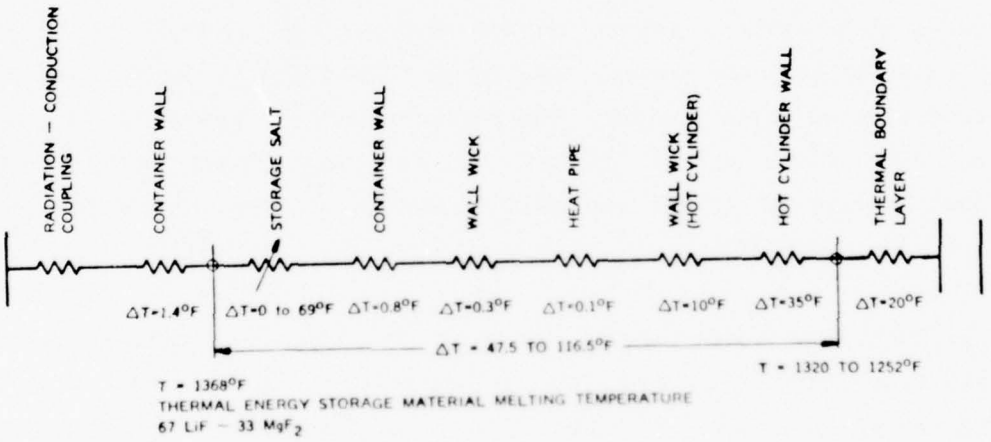



Figure 5. Temperature Distribution in the Thermal Energy Storage Unit for a Vuilleumier Cooler with 67 LiF-33 $MgF_2$ as TES Material

fusion which were given as 944 joules/gram in Ref. 2 and as 788 joules/gram (0.219 kWh/kg) in a communication by North American Philips Corporation. It appears now that the heat of fusion of the ternary salt of Ref. 2 was not a measured value but had been calculated with the assumption of "ideality," i.e., the heat of fusion of the ternary eutectic is the sum of the heat of fusion of its constituents when melting as a single salt at the eutectic temperature. The latent heat quoted by the second source was an ideal value based on the difference in thermal energy content of the salt at temperatures above and below the eutectic temperature and extrapolated to the eutectic temperature. The underlying assumption must have been that the eutectic salt increases its thermal energy in a step function at the eutectic temperature similar to a single component salt.

The test results of this program have shown that the heat of fusion of the ternary salt is only about 50 percent the heat of fusion calculated under the assumption of ideality. It should have been obvious that ideality was an inappropriate assumption when looking at the phase diagram of the salt shown in Figure 3. The phase diagram indicates clearly the formation of a double salt, KF-$MgF_2$, and transition lines. While the instrumentation and general test setup of this program was not sophisticated enough for performing basic research on thermodynamic properties of binary and ternary salts, some general behavior and thermodynamic properties could be demonstrated quite clearly. The results which are presented in Section IV of this report proved the selection of the ternary salt without the availability of proven and well documented thermodynamic data to be a technical liability.

The ternary eutectic LiF-$MgF_2$-KF is not available as a commercial salt. It had to be prepared by combining its constituents in a retort. Based on the molecular fraction of 0.64, 0.30, and 0.06 for LiF, $MgF_2$, and KF,

---

2. "Summary and Selection of Inorganic Salts for Application to Thermal Energy Storage," by Alina Borucka, Report ERDA 59, June 1975.

respectively, the weight fractions of the eutectic are 0.4281, 0.4820, and 0.0899. The specific weight of the eutectic was given as 2.1233 gram/$cm^3$.

Preliminary heat transfer calculations indicated that the losses from the thermal energy storage unit would be approximately 200 watts, if the unit is insulated with Flexible Min-K material. This predicted value proved to be correct for the steady state condition at 1300$^{o}$F, as will be seen from the test data in Subsection 4.2.1. The thermal energy storage unit therefore had to be sized for a total power release of 1.2 kW for 1 hour of operation. This corresponds to a total energy storage requirement of 1.2 kWh or $4.32 \times 10^6$ joules. When the lower value of the heat of fusion of 0.219 kWh/kg or 0.465 kWh/liter (based on the liquid density at the melting point) was accepted, the total weight of the thermal energy storage material was calculated to be 5.480 kg and the required volume of the material 2.581 liter (157.481 $in.^3$). Thus, the total material required for the eutectic salt was

| | |
|---|---|
| LiF | 2.346 kg |
| $MgF_2$ | 2.641 kg |
| KF | 0.493 kg |
| Total | 5.480 kg |

### 2.2.2 OPTIMIZATION OF THERMAL ENERGY STORAGE DEMONSTRATION UNIT

The thermal energy storage unit has as its purpose the storing of thermal energy in the form of fusion energy of a salt. It is expected that by using a thermal energy storage system, the overall weight of the power supply for a Vuilleumier cooler will be lighter and that the power system will have an equal or better reliability than a power supply which stores energy in electrical batteries. For achieving this goal, the overall structure containing the thermal energy storage material had to be made as small as possible so that, by itself, it will be light and will require the least

amount of insulation for containing the thermal energy with the lowest thermal losses. Thermal losses from the thermal energy storage unit are reflected in additional solar panel requirements as well as a larger thermal energy storage unit.

The requirement of testing the thermal energy storage unit in a 1-g environment imposed limitations on the design which would not exist if the unit could have been designed for exclusive space application and would not have to be tested in the laboratory.

The general lay-out of the thermal energy storage unit was presented in Figure 1. It was indicated that electric heaters would supply energy to the thermal energy storage salt and that thermal energy for the operation of the hot cylinder of the Vuilleumier cooler would be transferred from the thermal energy storage material by heat pipe action. Direct transfer from the salt to the hot cylinder could not be considered as the heat transfer area of the hot cylinder is very small relative to the required amount of thermal energy salt. Direct energy transfer would therefore not only result in a very high temperature differential, but would alo encompass a large temperature variation during the extraction of the energy from the salt. The aim was to find an optimum configuration with respect to weight and thermal losses for the basic design of the unit.

2.2.2.1 Overall Configuration

Several parameters affect the weight and configuration of the thermal energy storage unit. The most important parameters appeared to be the thickness of the thermal energy storage salt, $t_s$, the heater diameter, $D_H$, and the wick thickness, $t_w$, which are indicated in Figure 6. For maintaining the most uniform temperature of the hot cylinder and the heat pipe, it is desirable to make the thickness, $t_s$, of the thermal energy storage salt as small as possible and to achieve a large surface area and a small depth across which heat flux occurs. The effect of the salt thickness on the

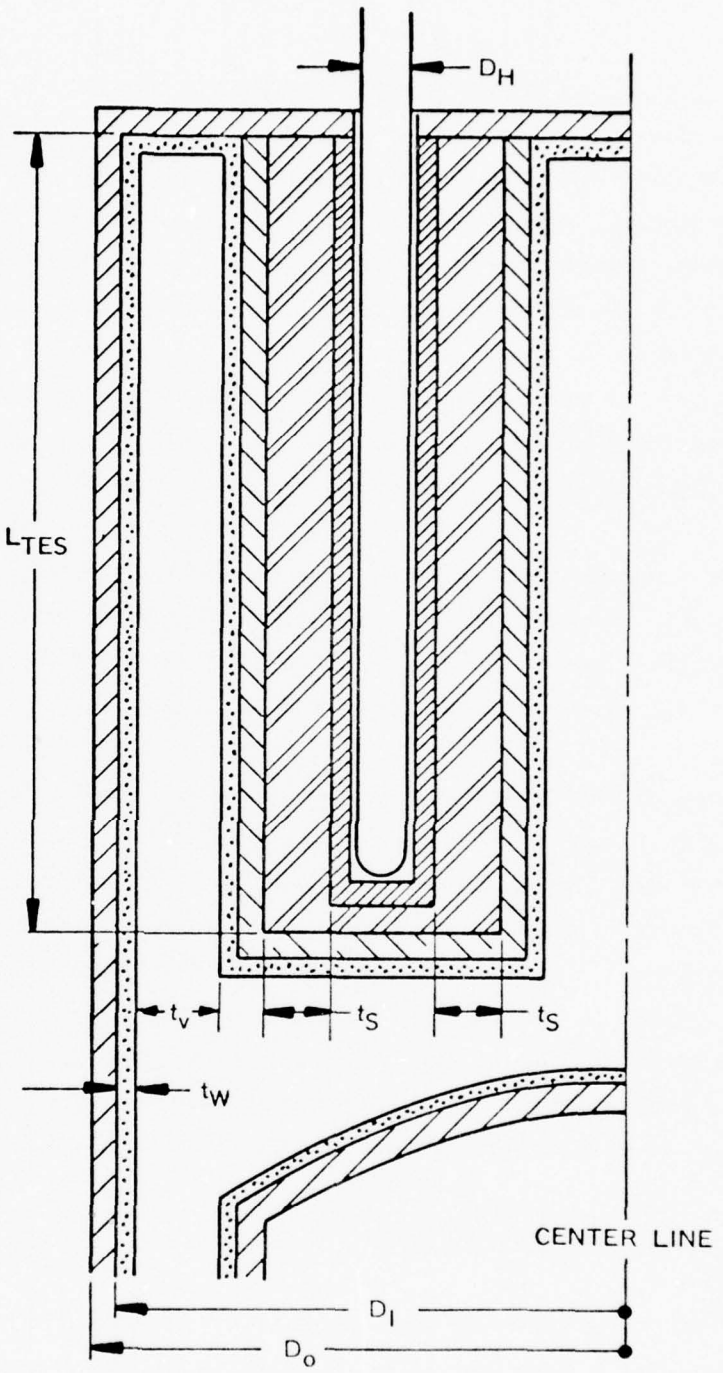



Figure 6. Parameters Investigated in the Optimization of the Thermal Energy Storage Unit

56684

length, $L_{TES}$, of the thermal energy storage unit is shown in Figure 7 for two designs which differ solely with respect to the size of the heater diameter, $D_H$, and the vapor flow area, $A_v$. A correlation of all the dimensional parameters of the unit are shown in Figure 8. The thermal losses for the various configurations are presented in Figures 9 through 16. It is quite obvious that, for the lowest losses, the thermal energy storage salt should have a thickness of about 0.8 inch. Figures 10, 12, 14, and 16 also indicate that, after a certain insulation thickness has been reached, additional insulation will only add weight to the unit without substantially further reducing thermal losses.

The results of the thermal loss calculations are summarized in Figures 17 and 18. They confirm that the vapor flow width has a minimal effect on the thermal losses and that, therefore, a minimal effort is required for optimizing on this parameter in the sizing of the unit.

Based on the parametric design study of the thermal energy storage unit, the heat loss from the unit appeared to be between 185 watts for an outer insulation diameter of 10 inches and 124 watts for an outer insulation diameter of 15 inches. These losses compare with the losses of a directly electrically heated hot cylinder of a Vuilleumier cooler of about 50 watts as shown in Figure 19 for the same type insulation. The design that evolved from the optimization study is shown in Figure 20. The length of the unit is about three times the diameter. In this design, the thermal load at the heater surface is only 1 watt/cm$^2$.

2.2.2.2 Insulation Design

Prior to optimizing the insulation of the TES demonstration unit by employing a superinsulation consisting of radiation shields between layers of conduction insulation, it was decided to use less expensive insulation made of two conduction insulation materials, Flexible Min-K and Cerafelt. The insulation layers exposed to the highest temperature were to be Flexible Min-K. For insulating the unit below 600$^{o}$F, Cerafelt was chosen.

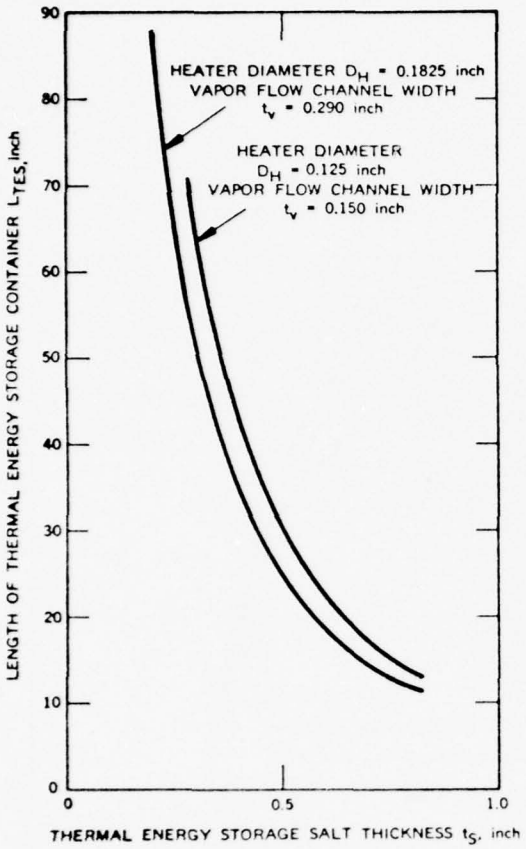



Figure 7. Effect of Thermal Energy Storage Salt Thickness on the Length of the Thermal Energy Storage Unit

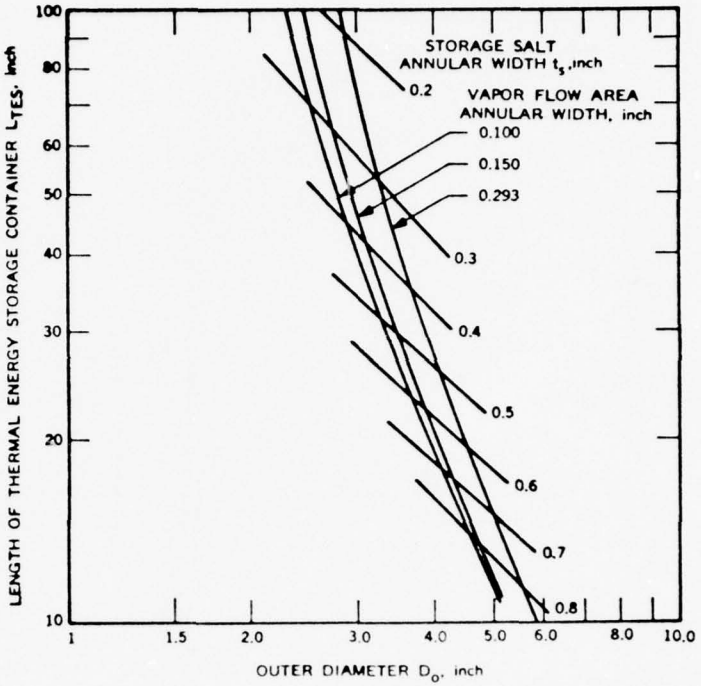



Figure 8. Correlation Between Primary Dimensions of 1-kW-Hr Thermal Energy Storage Unit (Required Thermal Energy Storage Material Volume $V_{TES}$ = 157.481 Inch$^3$)

56700

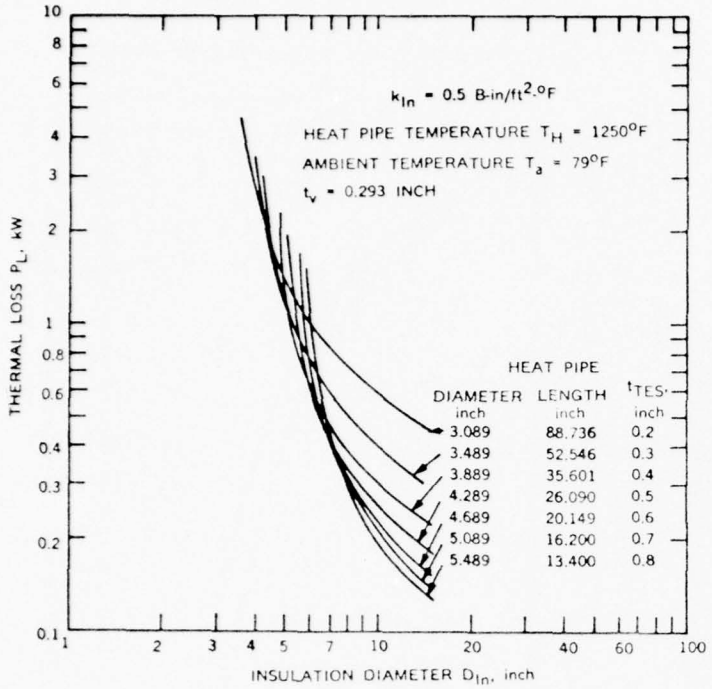



Figure 9. Thermal Losses from Thermal Energy Storage Heat Pipe (0.1825-inch Dia. Heater)

54802

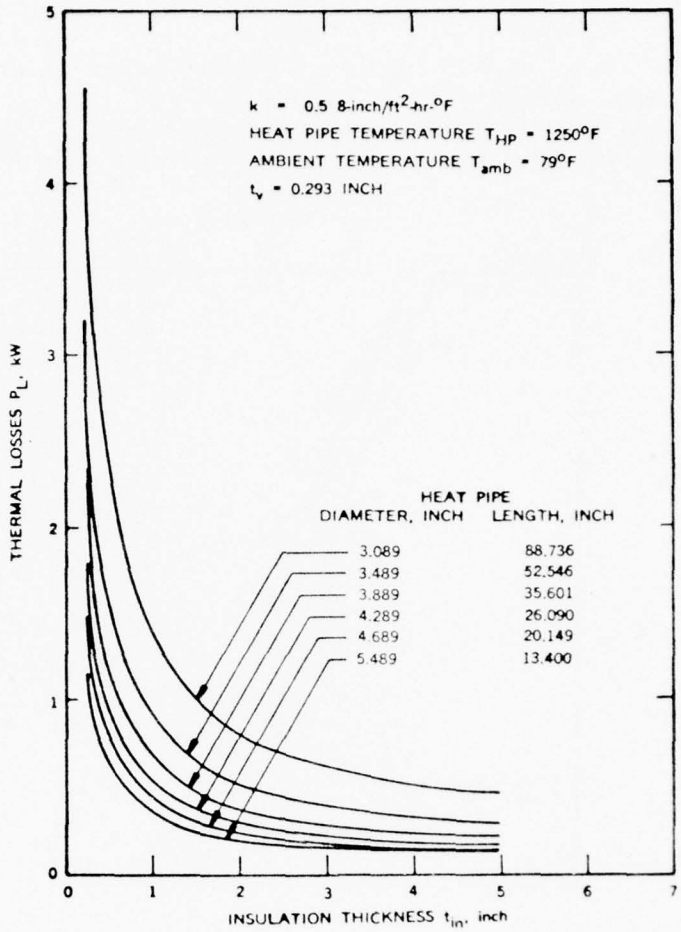



Figure 10. Power Losses from Thermal Energy Storage Heat Pipe (0.1825-inch Dia. Heater)

56702

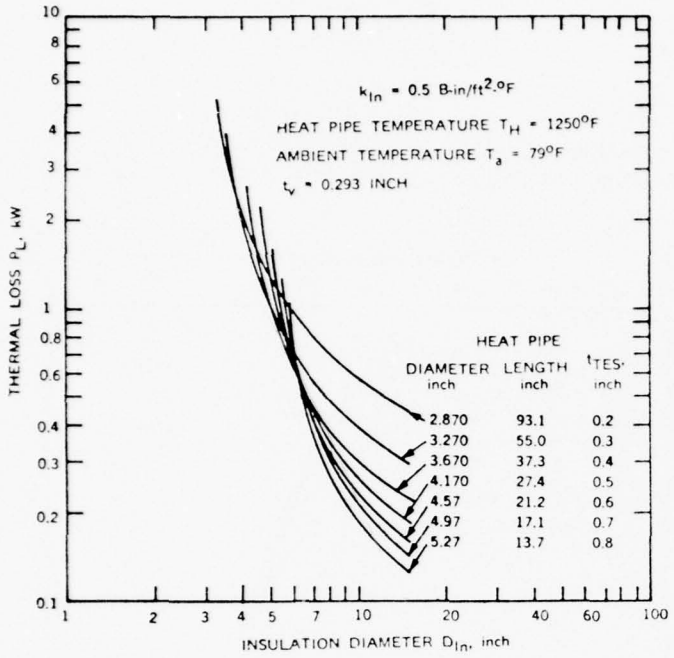



Figure 11. Thermal Losses from Thermal Energy Storage Heat Pipe (0.125-inch Dia. Heater)

56704 A

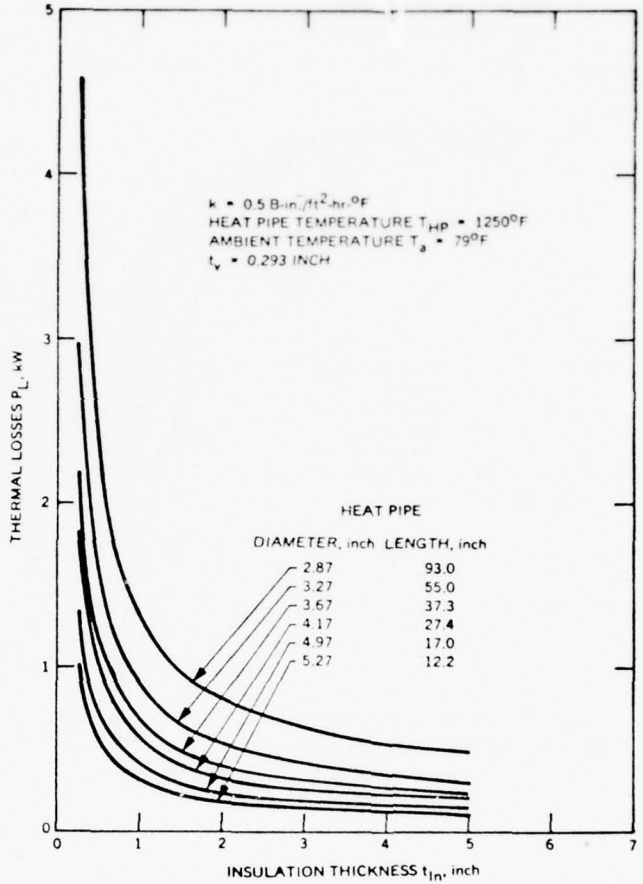



Figure 12. Power Losses from Thermal Energy Storage Heat Pipe (0.125-inch Dia. Heater)

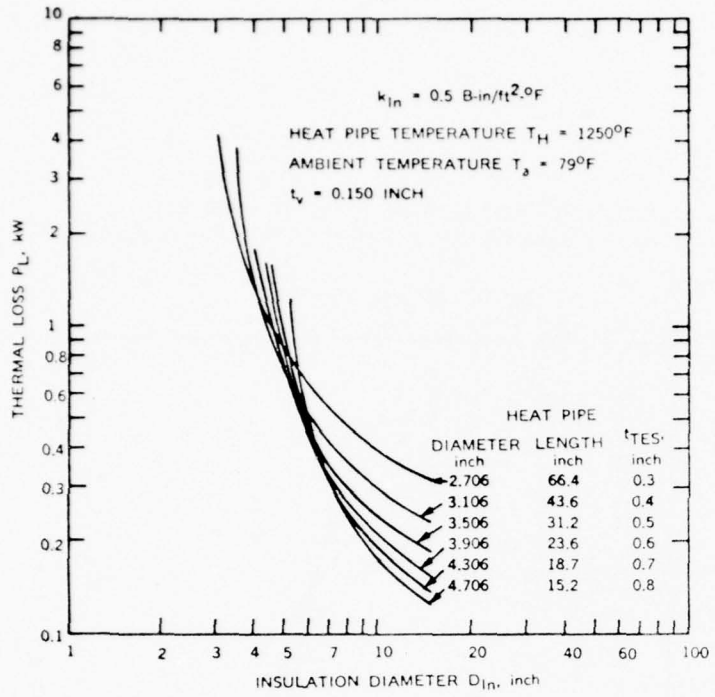



Figure 13. Thermal Losses from Thermal Energy Storage Heat Pipe (0.125-inch Dia. Heater)

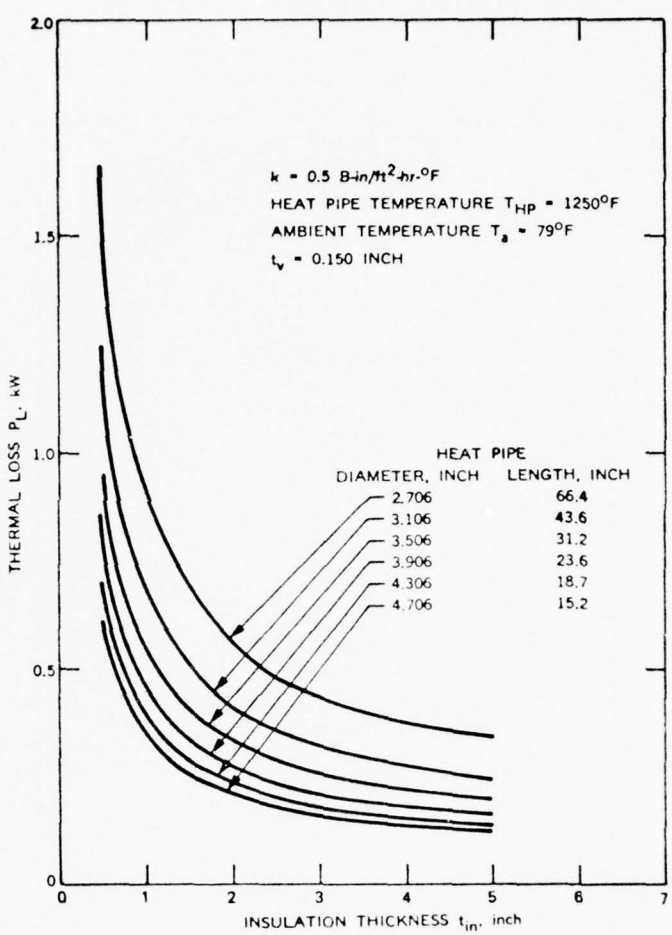



Figure 14. Power Loss from Thermal Energy Storage Heat Pipe (0.125-inch Dia. Heater)

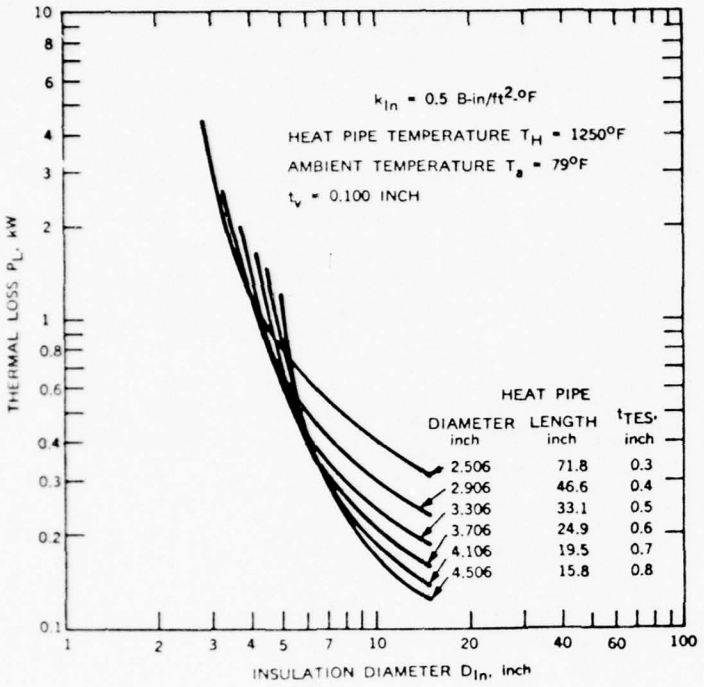



Figure 15. Thermal Losses from Thermal Energy Storage Heat Pipe (0.125-inch Dia. Heater)

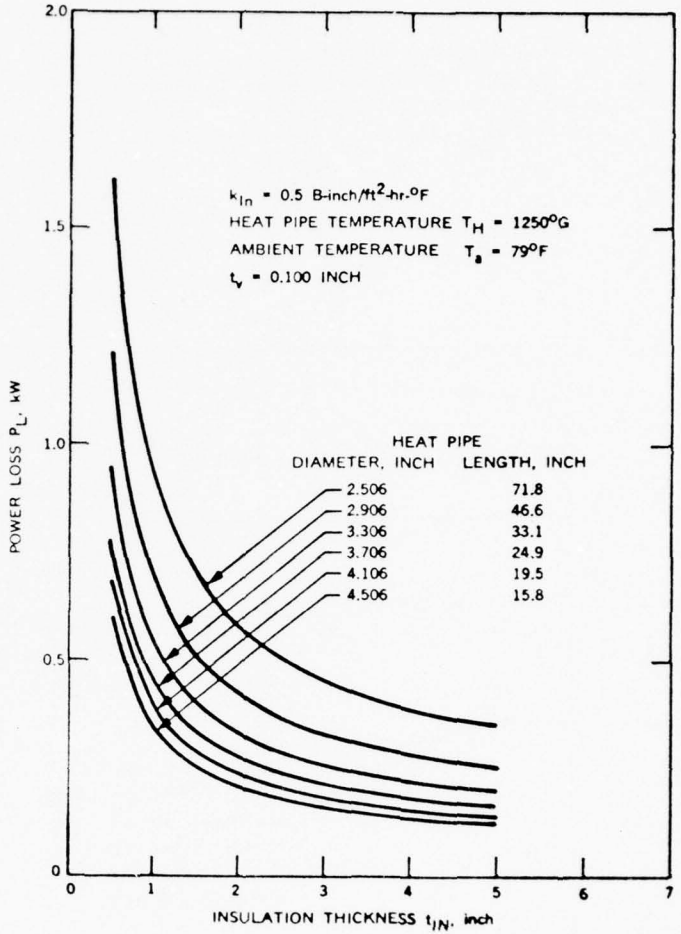



Figure 16. Power Loss from Thermal Energy Storage Heat Pipe (0.125-inch Dia. Heater)

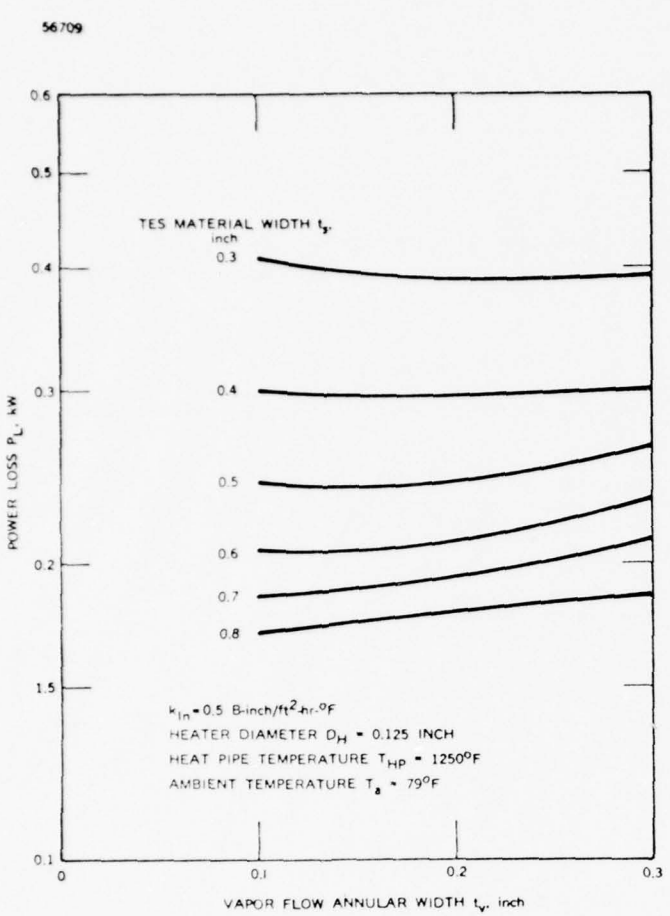



Figure 17. Effect of Vapor Flow Annular Width and Thermal Energy Storage Material Thickness on Thermal Loss of the Thermal Energy Storage Unit (Insulation Diameter $D_{In}$ = 10 Inch)

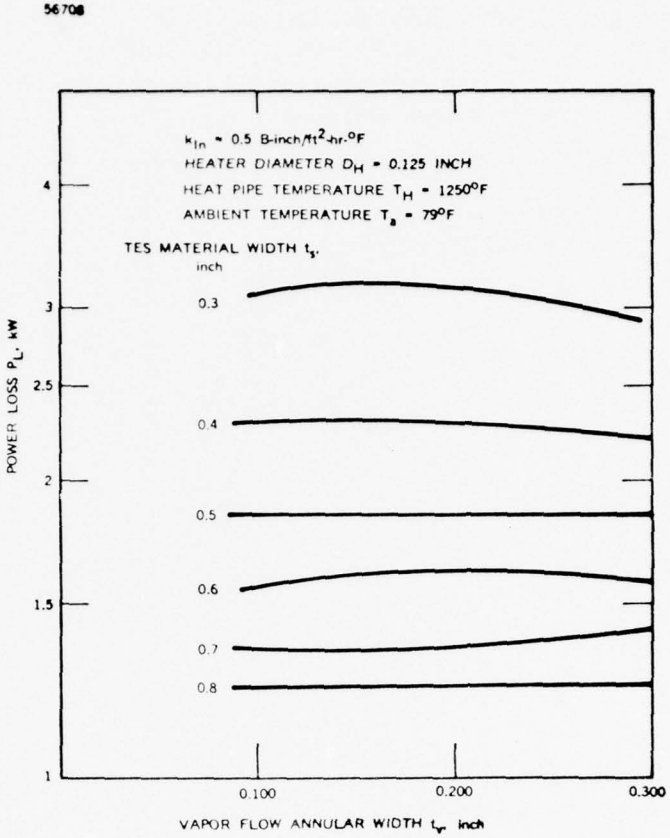
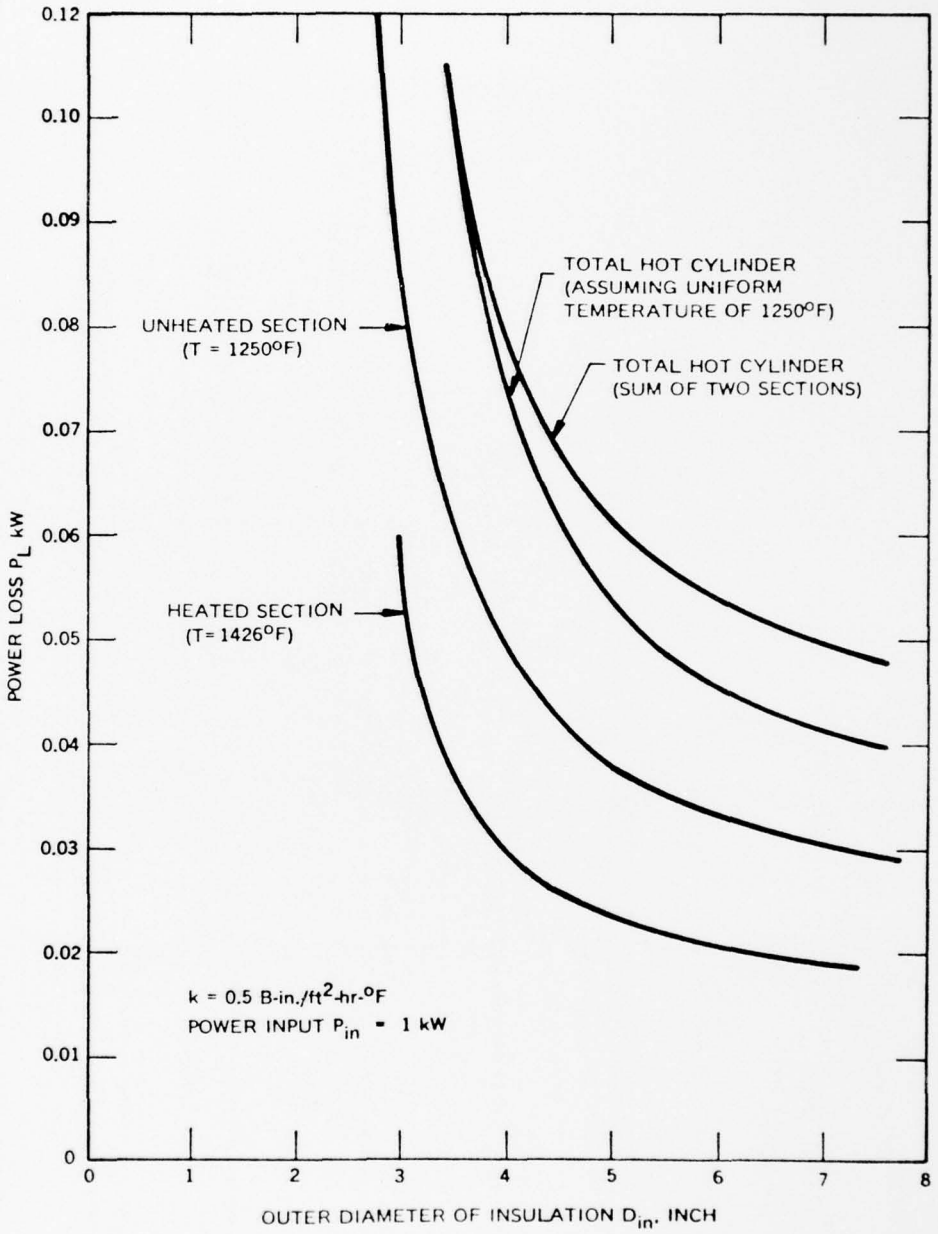



Figure 18. Effect of Vapor Flow Annular Width and Thermal Energy Storage Material Thickness on Thermal Loss of the Thermal Energy Storage Unit (Insulation Diameter $D_{In}$ = 15 Inch)




56714

Figure 19. Power Losses from Hot Cylinder of VM Cooler

56721

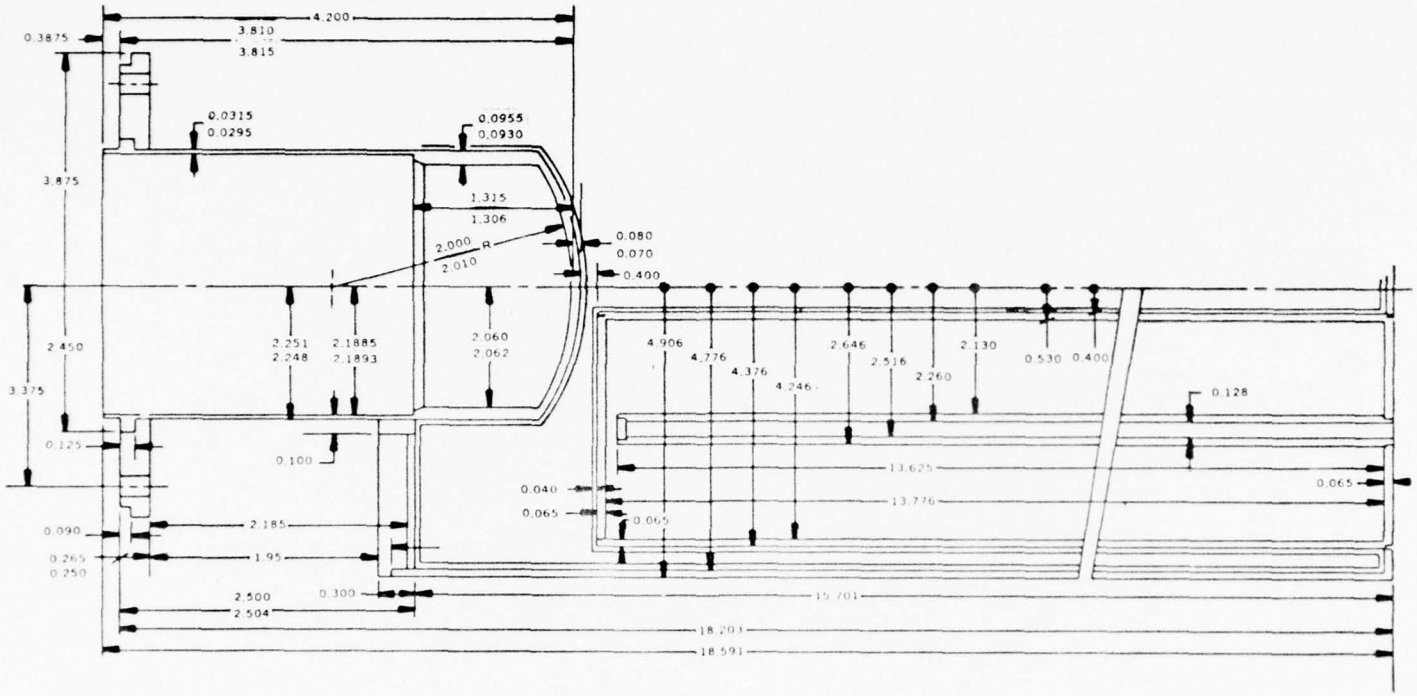



Figure 20. Optimum Design for a 1-kW-Hr Thermal Energy Storage Unit

For the final design of the thermal energy storage unit, the thermal losses as a function of insulation thickness and outer insulation diameter are shown in Figure 21. The temperature distribution through the insulation for three insulation thicknesses are presented in Figure 22. Based on these parametric studies, the amount of insulation material for each type and the total insulation weight were calculated as shown in Figure 23.

2.2.2.3 Heat Pipe Design

With the basic dimensions of the thermal energy storage unit established, the heat pipe parameters had to be determined. The analysis and heat pipe computer program that had been developed for the design of the 15-ft long heat pipe could not be used because of the substantial differences between the thermal energy storage unit and the heat pipe with respect to design and operation. The 15-ft long heat pipe had a distinct evaporator and condenser section which were separated by a relatively long adiabatic section. In the thermal energy storage unit, the adiabatic section is missing. Since the evaporator section constitutes the heat pipe, the flow rate of the vapor as well as of the fluid in the wick vary along the heat pipe. Furthermore, the vapor flow area of the TES unit is the combination of an annulus and a pipe, thus having a completely different hydraulic diameter than the 15-ft heat pipe. The vapor flow in the thermal energy storage unit has to account for "blowing," while the flow in the wick has to consider suction flow.

In Figures 24, 25, and 26, the pressure drops for three different vapor flow area designs are presented. In order for the heat pipe to operate satisfactorily, the total pressure drop cannot be larger than the capillary pressure or suction pressure available from the wick structure. In all three designs the elevation pressure drop is the highest while the pressure drop in the wick is the lowest. The elevation pressure drop is the dominating pressure drop and is entirely determined by the diameter of the thermal energy storage unit. As was indicated earlier, the diameter of the

56972

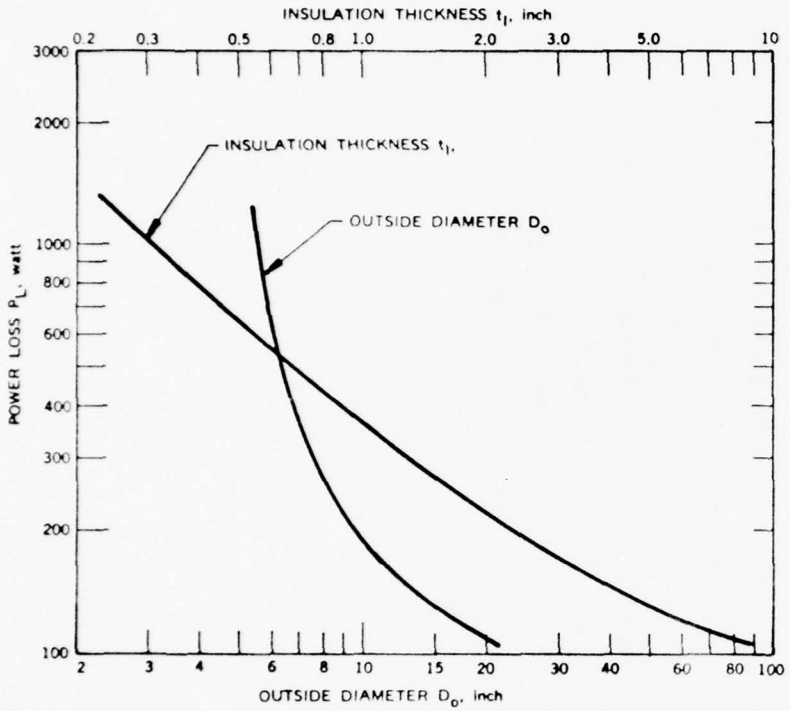



Figure 21. Power Loss as Function of Insulation Thickness of Final Thermal Energy Storage Demonstration Unit Design

56973

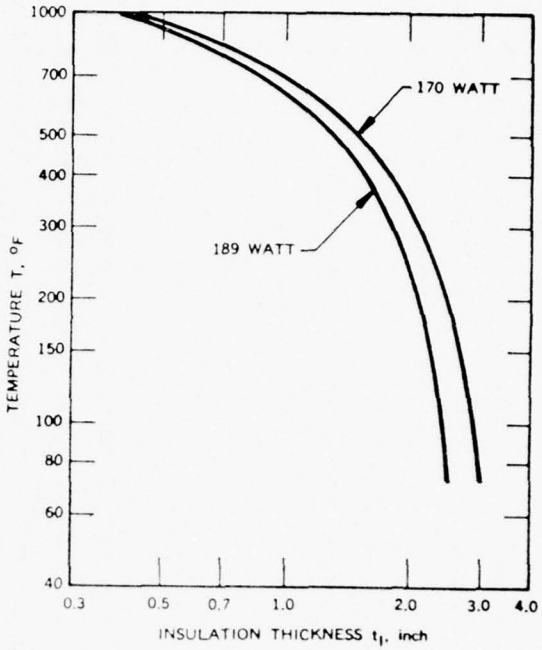



Figure 22. Temperature Distribution in Thermal Insulation of Thermal Energy Storage Demonstration Unit

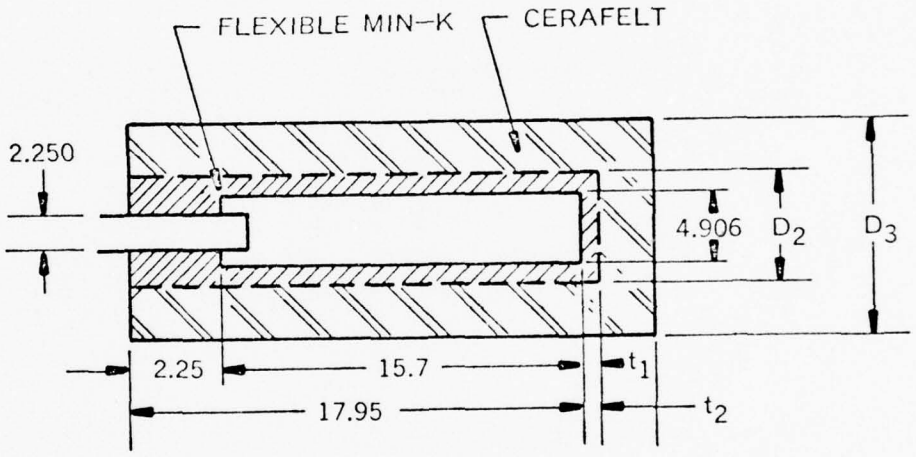



Figure 23. Insulation Design of Thermal Energy Storage Unit

56710

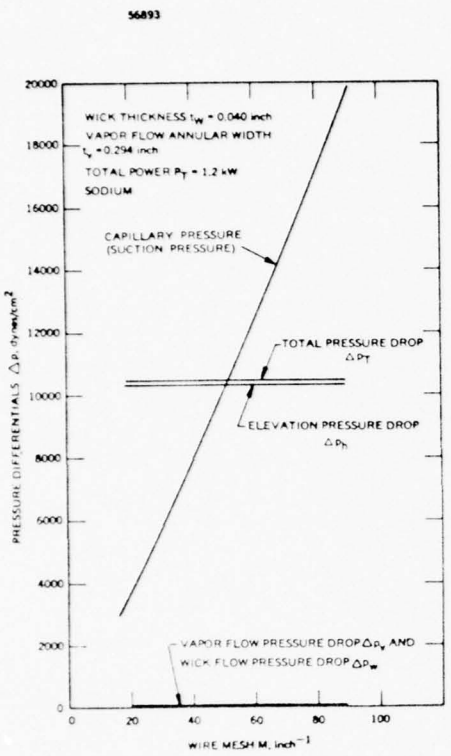



Figure 24. Pressure Drops and Available Suction Pressure for Various Wire Screens

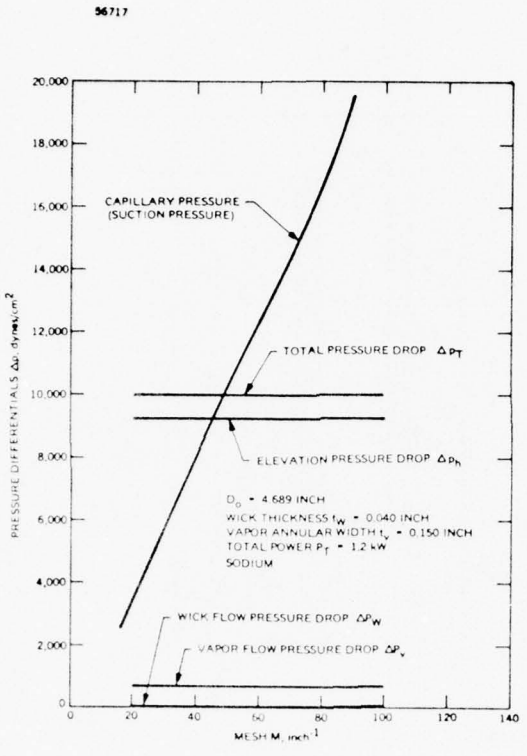



Figure 25. Pressure Drops and Available Suction Pressure for Various Wire Screens

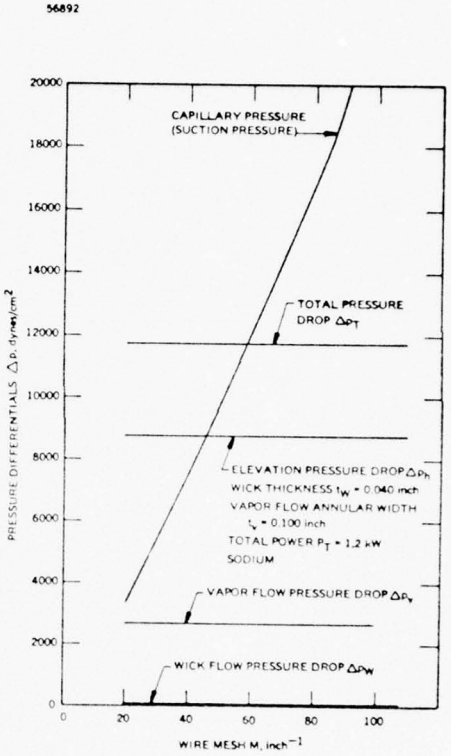



Figure 26. Pressure Drops and Available Suction Pressure for Various Wire Screens

unit was predicated on the lowest thermal losses from the unit. The optimum wick design was based on the calculations shown in Figure 27.

A bolting cloth with Mesh 70 was selected for the wick structure. This design would generate a suction pressure about 37 percent above that required. As indicated by the calculations, a finer mesh bolting cloth would apparently provide a larger safety margin. There is, however, an uncertainty whether the higher safety margin can actually be achieved because of limitations in maintaining a consistent wick structure with effective small pore sizes between the layers during the manufacturing process.

2.2.2.4 Total Weight of Optimum Thermal Energy Storage Unit

The total weight of the thermal energy storage unit is comprised of the weight of: (1) the container material, Inconel 600; (2) the wick filled with the sodium working fluid; (3) the insulation; and (4) the thermal energy storage material.

Container (Inconel 600)

| | |
|---|---|
| Total Volume | 47.48 $inch^3$ |
| Specific Weight | 0.302 $lb/inch^3$ |
| Weight | 14.34 lb |

Wick with Sodium

| | |
|---|---|
| Total Volume | 18.70 $inch^3$ |
| Wick Material | $M = 70\ inch^{-1}$, $D_W = 0.00375$ inch |
| Specific Weight of Wick Material | 0.302 $lb/inch^3$ |
| Effective Volume Density | 20.33 percent |
| Specific Weight of Sodium | 0.0279 $lb/inch^3$ |

TES PROGRAM T3 K=1.62X10-3XM-.797 CM2

PROGRAM 2340-002-000
PARAMETRIC STUDY OF TES HEAT PIPE 22 JULY 1975

| | | | |
|---|---|---|---|
| WORKING FLUID SODIUM, | 22.991 GRAM/MOL | | |
| OPERATING TEMPERATURE | 1250.000 DEG.F | | |
| POWER | 1200.00 WATT | | |
| HEAT PIPE DIAMETERS | 4.776 INCH | 4.376 INCH | .400 INCH |
| WICK LENGTH | 14.620 INCH | | |

PROPERTIES

| | FLUID | VAPOR |
|---|---|---|
| LATENT HEAT,JOULES/G | .401E 04 | |
| SURFACE TENSION,DYN/CM | .134E 03 | |
| VISCOSITY,G/SEC-CM | .195E-02 | .106E-03 |
| SPECIFIC GRAVITY,G/SEC3 | .789E 00 | .328E-04 |
| PARTIAL PRESSURE,DYN/CM2 | | .112E 06 |
| SONIC VELOCITY,CM/SEC | | 75656.06 |

WALL WICK THICKNESS .040 INCH

WICK AREA 3.871 CM2, VAPOR AREA 11.646 CM2, AREA RATIO 3.008
ELEVATION PRESSURE 9386.91 DYN/CM2, VELOCITY 784.044 CM/SEC

| MESH IN-1,INCH | WIRE | PERMEABILITY CM2 | SUCTION DYN/CM2 | DELP W DYN/CM2 | DELP V DYN/CM2 | DELP T DYN/CM2 | SAFETY PERC. |
|---|---|---|---|---|---|---|---|
| 20 | .0090 | .148E-03 | 3630. | 24. | 836. | 10247. | -64.57 |
| 30 | .0065 | .107E-03 | 5547. | 33. | 836. | 10256. | -45.91 |
| 40 | .0065 | .854E-04 | 8046. | 42. | 836. | 10264. | -21.61 |
| 50 | .0055 | .715E-04 | 10265. | 50. | 836. | 10272. | -.07 |
| 60 | .0045 | .618E-04 | 12234. | 57. | 836. | 10280. | 19.01 |
| 70 | .0037 | .547E-04 | 14061. | 65. | 836. | 10288. | 36.68 |
| 80 | .0037 | .492E-04 | 16914. | 72. | 836. | 10295. | 64.30 |
| 90 | .0035 | .448E-04 | 19556. | 79. | 836. | 10302. | 89.83 |

Figure 27. Heat Pipe Design Calculations for Final Design of a 1-kW-Hr Thermal Energy Storage Unit

| | |
|---|---|
| Effective Specific Weight of Wick | 0.0836 lb/inch$^3$ |
| Weight | 1.564 lb |

Thermal Energy Storage Material

| | |
|---|---|
| Material (Molecular) | 65 LiF - 30 $MgF_2$ - 6 KF |
| Material (Weight) | 42.81 LiF - 48.21 $MgF_2$ - 8.99 KF |
| Heat of Fusion | 99.43 watt-hr/lb |
| Specific Weight | 0.0766 lb/inch$^3$ |
| Energy Requirement | 1200 watt-hr |
| Volume | 157.48 inch$^3$ |
| Weight | 12.07 lb |

Insulation

| | |
|---|---|
| Material | Flexible Min-K and Cerafelt |
| Weight | 7.96 lb (189 watt loss) |
| | 8.81 lb (179 watt loss) |
| | 10.59 lb (170 watt loss) |

Based on the above tabulated weight values of the four major components of the thermal energy storage unit, the total weight of the unit and the specific power weights are as shown in Table 2.

TABLE 2. TOTAL WEIGHT OF THERMAL ENERGY STORAGE UNIT

| Total Weight $W_T$ (lb) | Power Loss $P_L$ (watt) | Specific Weight $W_T/E$ (lb/watt-hr) | Specific Energy $E/W_T$ (watt-hr/lb) |
|---|---|---|---|
| 35.93 | 189 | 29.94 | 33.40 |
| 36.78 | 179 | 30.65 | 32.63 |
| 38.56 | 170 | 32.13 | 31.11 |

The weight distribution for the entire thermal energy storage unit is shown in Table 3.

TABLE 3. WEIGHT DISTRIBUTION OF THE THERMAL ENERGY STORAGE UNIT

| | | Weight (lb) | Percent of Total |
|---|---|---|---|
| Thermal storage Material | | 12.07 | 32.82 |
| Container Material | | 14.34 | 38.99 |
| Wick | | | |
| Screen | 1.148 lb | | |
| Sodium | 0.416 lb | | |
| | | 1.56 | 4.24 |
| Insulation | | 8.81 | 23.95 |
| | Total | 36.78 | 100.00 |

The values in Table 3 indicate that the greatest impact on the weight of the thermal energy storage unit could be achieved by a reduction in the container weight. The container weight is primarily determined by the thickness of the walls, which in the optimized design was t = 0.065 inch. If by further investigation it could be established that thinner walls would be safe for containing the thermal energy storage material and the working fluid of the heat pipe, considerable savings in overall TES unit weight could be achieved.

The wick of the heat pipe contributes a surprisingly low value to the overall weight. Only 4.24 percent of the total weight is attributed to the wick, and the wick structure itself adds only 3.12 percent to the weight. The insulation material contributes a substantial amount to the overall weight, despite the fact that it has already been optimized by using two different materials according to the temperature distribution in the insulation. The effect of superinsulation on heat losses and weight is discussed in the next section.

2.2.2.5 Alternate Insulation

For practical reasons it was decided to employ Flexible Min-K insulation with a layer of Cerafelt for testing the thermal energy storage demonstration unit. The weight evaluation indicated that the insulation contributed about 24 percent to the total weight of the thermal energy storage unit. It was concluded that the weight of the unit and the thermal losses could be lowered by employing the insulating technique used for achieving the lowest heat losses from a resistojet.

The properties of high temperature thermal insulation materials as they have been reported in the literature are presented in Table 4. During the development of ion engines at XEOS, in-house work on the improvement of the insulation of ionizers was carried out. This brought about the results plotted in Figure 28. The performance of an insulation system, which was called Linde Super Insulation and was reported in the literature, has a characteristic shown in Figure 29. This insulation system is compared with a system which was applied to the ion engine and to a resistojet in a slightly different and easier applicable form. The construction of this insulation employs a nominal 0.020 inch thick Fiberfrax paper separated by 0.001 inch thick molybdenum foil. For this construction the Fiberfrax paper had an effective thickness of only 0.016 inch. Fiberfrax is an alumina-silica fiber composition which is processed to the Fiberfrax paper with a binder.

Using the thermal conductivity value determined from the apparent thermal losses of the resistojet, the thermal losses from the thermal energy storage unit were calculated as shown in Table 5 and plotted in Figure 30. For comparison, the thermal losses have also been calculated for an insulation with a thermal conductivity of only $9.7 \times 10^{-3}$ B-inch/ft$^2$-hr-$^{o}$F. This insulation was mentioned in a paper as being available. The weight of the insulation as a function of the total thermal losses from the thermal energy storage unit are presented in Figure 31 with the weight of the

TABLE 4. PROPERTIES OF HIGH-TEMPERATURE THERMAL INSULATION MATERIALS

| Insulating Material | Maximum Service Temperature ($^{o}F$) | Density ($lb/ft^3$) | Thermal Conductivity at $1250^{o}F$ ($Btu/hr\text{-}ft\ ^{o}F$) |
|---|---|---|---|
| Thermoflex Refractory Fiber Felt | 2300 | 3.0 | $1.4 \times 10^{-1}$ |
| | | 24.0 | $6.4 \times 10^{-2}$ |
| Micro-Quartz Felt | 2000 | 3.0 | $9.5 \times 10^{-2}$ |
| | | 6.0 | $6.9 \times 10^{-2}$ |
| Dyna-Quartz Felt | 2750 | 4.5 | $7.3 \times 10^{-2}$ |
| | | 10.0 | $6.3 \times 10^{-2}$ |
| Min-K 2000 (molded) | 1800 | 20.0 | $2.9 \times 10^{-2}$ |
| Copper flakes dispersed in fibrous quartz | 1400 | - | $5 \times 10^{-3}$ |
| Nickel flakes dispersed in fibrous quartz | 1700 | - | $5 \times 10^{-3}$ |
| Copper foil spaced by fibrous quartz paper | 1400 | - | $5 \times 10^{-4}$ |
| Nickel foil spaced by fibrous quartz paper | 1700 | - | $5 \times 10^{-4}$ |
| Stainless steel spaced by $ZrO_2$ | 2000 | - | $3 \times 10^{-4}$ |
| Titanium spaced by $ZrO_2$ particles | 2000 | - | $3 \times 10^{-4}$ |

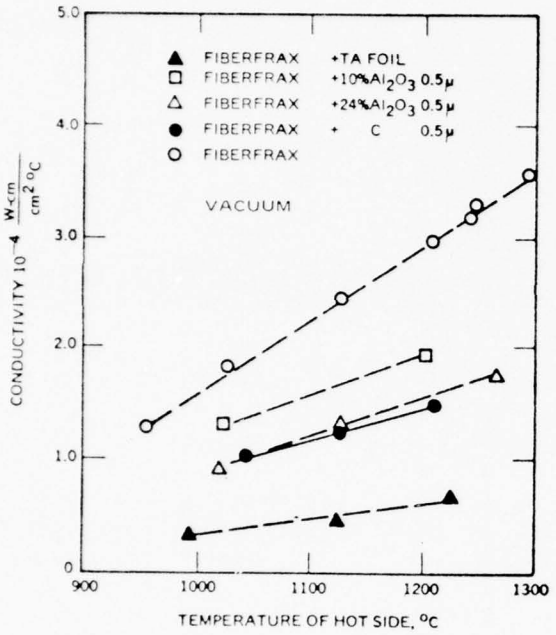



Figure 28. Conductivity of Various Combinations of Fiberfrax

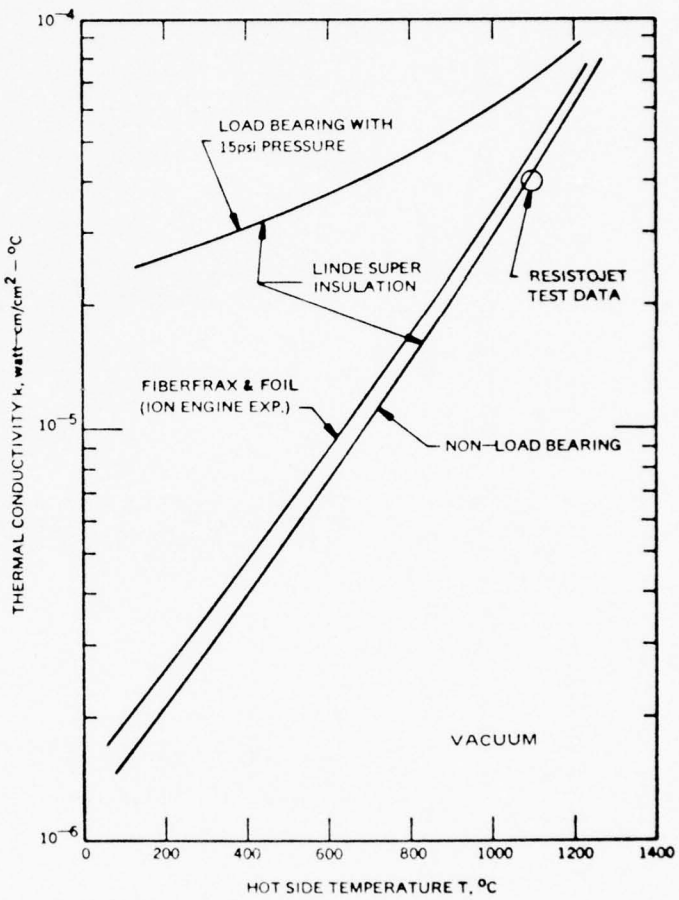



Figure 29. Thermal Conductivity of Super Insulation

TABLE 5. THERMAL LOSSES AS FUNCTION OF THERMAL CONDUCTIVITY OF INSULATION MATERIAL AND INSULATION THICKNESS

| INNER DIAMETER D INCH | LENGTH L INCH | TEMPERATURE DIFFERENCE DELT DEGREE F |
|---|---|---|
| 4.906 | 15.701 | 1171.00 |

HEAT TRANSFER COEFFICIENT,B-INCH/FT2-HR-DEG.F 9.71E-03

| OUTER DIAMETER INCH | THICKNESS TI INCH | POWER LOSS KW |
|---|---|---|
| 5.406 | .250 | .024 |
| 5.906 | .500 | .013 |
| 6.406 | .750 | .009 |
| 6.906 | 1.000 | .007 |
| 7.406 | 1.250 | .006 |
| 7.906 | 1.500 | .005 |
| 8.406 | 1.750 | .005 |
| 8.906 | 2.000 | .004 |
| 9.406 | 2.250 | .004 |
| 9.906 | 2.500 | .004 |
| 10.406 | 2.750 | .003 |
| 10.906 | 3.000 | .003 |
| 11.406 | 3.250 | .003 |
| 11.906 | 3.500 | .003 |
| 12.406 | 3.750 | .003 |

| INNER DIAMETER D INCH | LENGTH L INCH | TEMPERATURE DIFFERENCE DELT DEGREE F |
|---|---|---|
| 4.906 | 15.701 | 1171.00 |

HEAT TRANSFER COEFFICIENT,B-INCH/FT2-HR-DEG.F 2.78E-02

| OUTER DIAMETER INCH | THICKNESS TI INCH | POWER LOSS KW |
|---|---|---|
| 5.406 | .250 | .069 |
| 5.906 | .500 | .036 |
| 6.406 | .750 | .026 |
| 6.906 | 1.000 | .020 |
| 7.406 | 1.250 | .017 |
| 7.906 | 1.500 | .015 |
| 8.406 | 1.750 | .013 |
| 8.906 | 2.000 | .012 |
| 9.406 | 2.250 | .011 |
| 9.906 | 2.500 | .011 |
| 10.406 | 2.750 | .010 |
| 10.906 | 3.000 | .009 |
| 11.406 | 3.250 | .009 |
| 11.906 | 3.500 | .009 |
| 12.406 | 3.750 | .008 |

BEST AVAILABLE COPY

TABLE 5. THERMAL LOSSES AS FUNCTION OF THERMAL CONDUCTIVITY OF INSULATION MATERIAL AND INSULATION THICKNESS (Cont'd)

| INNER DIAMETER D INCH | LENGTH L INCH | TEMPERATURE DIFFERENCE DELT DEGREE F |
|---|---|---|
| 4.906 | 15.701 | 1171.00 |

HEAT TRANSFER COEFFICIENT,B-INCH/FT2-HR-DEG.F 5.00E-01

| OUTER DIAMETER INCH | THICKNESS TI INCH | POWER LOSS KW |
|---|---|---|
| 5.406 | .250 | 1.229 |
| 5.906 | .500 | .653 |
| 6.406 | .750 | .460 |
| 6.906 | 1.000 | .364 |
| 7.406 | 1.250 | .306 |
| 7.906 | 1.500 | .267 |
| 8.406 | 1.750 | .239 |
| 8.906 | 2.000 | .219 |
| 9.406 | 2.250 | .202 |
| 9.906 | 2.500 | .189 |
| 10.406 | 2.750 | .179 |
| 10.906 | 3.000 | .170 |
| 11.406 | 3.250 | .162 |
| 11.906 | 3.500 | .156 |
| 12.406 | 3.750 | .150 |

```
*STOP* 0

!EDIT DCUN
EDIT PERE
*TY 1-9
   1.000 4.906,15.701,1171.,
   2.000 .25,15,
   3.000 0.00971,
   4.000 4.906,15.701,1171.,
   5.000 .25,15,
   6.000 .0278,
   7.000 4.906,15.701,1171.,
   8.000 .25,15,
   9.000 .5,
*
```

BEST AVAILABLE COPY

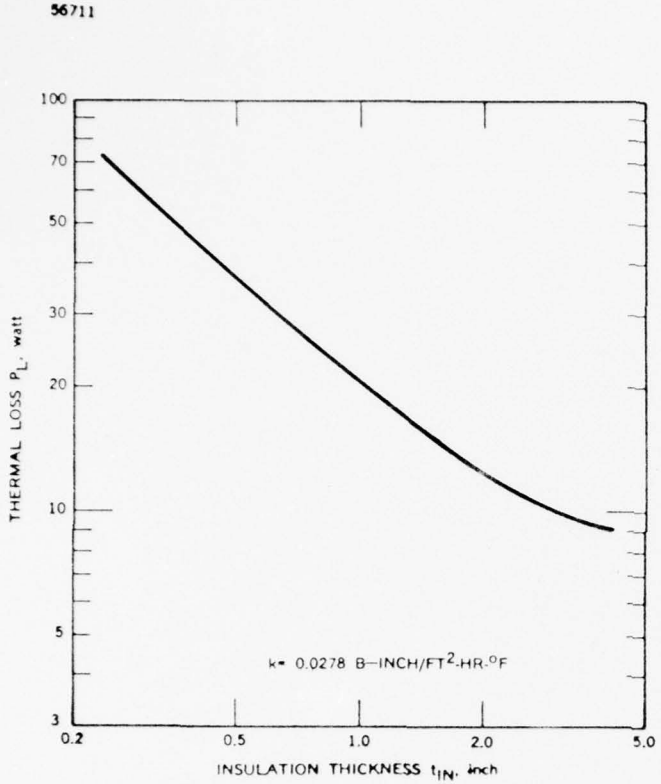



Figure 30. Effect of Insulation Thickness on the Total Loss of Thermal Energy from the Thermal Energy Storage Unit (Fiberfrax with Molybdenum Foil)

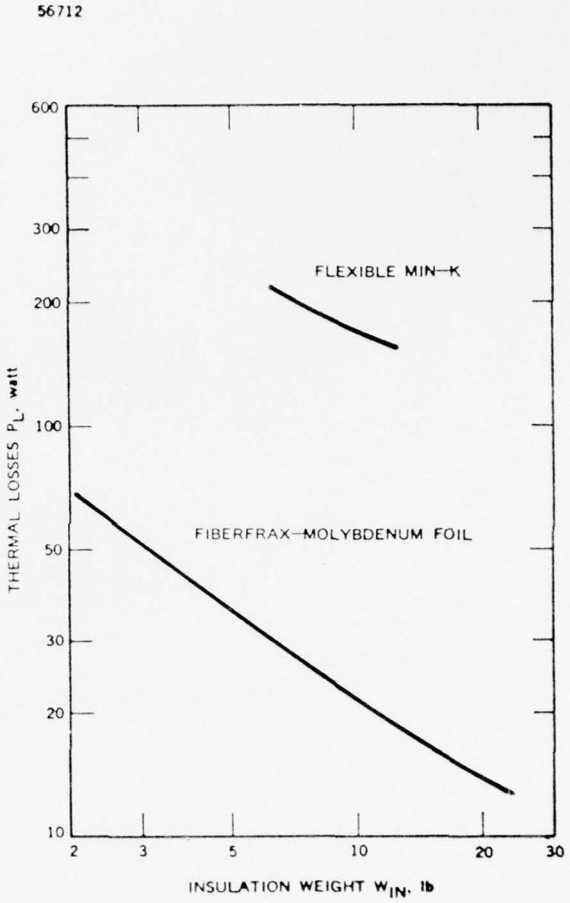



Figure 31. Thermal Losses as Affected by the Amount of Insulation

insulation composed of Flexible Min-K. While the losses are close to 200 watts for 8 pounds of Flexible Min-K, the Fiberfrax-Molybdenum foil system reduces the loss to less than 30 watts for the same weight.

The application of the Fiberfrax-Molybdenum foil system is much more costly. As the insulation has to be designed to minimize the heat flux along the metal foil, the seams of the insulation cannot be permitted to run perpendicular to the surfaces. Therefore, the insulation has to be cut to different widths for each layer, which has to be wrapped individually over the thermal energy storage unit. The use of this type of insulation would have contributed little to the demonstration of the thermal energy storage unit concept. In the discussion on the testing of the TES demonstration unit it will become clear that the relatively high thermal loss helped to produce a consistent and repeatable test condition for determining the operation of the TES unit.

### 2.2.3 FINAL THERMAL ENERGY STORAGE DEMONSTRATION UNIT DESIGN

When placing the order for the fabrication of the components of the optimized thermal energy storage demonstration unit, it was impossible to locate a vendor who was willing to fabricate the tubes to the design dimensions. The vendor who had formed the tubes for the 15-foot heat pipe was not able to manufacture the smallest of the five tubes, which has an inner diameter of 0.493 inch. He stated that his manpower was no longer available to perform this work, although he was willing to undertake the forming of the other four tubes. No other vendor could be found to even respond to the request for quote.

Because of the unexpected difficulties in locating a vendor for manufacturing the tubes, it became obvious that the thermal energy storage demonstration unit would have to be designed around standard tubes or pipes made of Inconel 600. In Figure 32 the available Inconel 600 pipes are shown. Pipes were selected from this stock sheet that permitted the

BEST AVAILABLE COPY

| PIPE SIZE | O.D. IN INCHES | PIPE SCHEDULES | | | | | | | | | | | | |
|---|---|---|---|---|---|---|---|---|---|---|---|---|---|---|
| | | 5 | 10 | 20 | 30 | STD. | 40 | 60 | E.H. | 80 | 100 | 120 | 140 | 160 | DBLE. E.H. |
| ⅛ | | .035<br>.1383 | .049<br>.1863 | | | .068 | .068<br>.2447 | | .095 | .095<br>.3145 | | | | | |
| ¼ | | .049<br>.2570 | .065<br>.3297 | | | .088 | .088<br>.4248 | | .119 | .119<br>.5351 | | | | | |
| ⅜ | | .049<br>.3276 | .065<br>.4235 | | | .091 | .091<br>.5676 | | .126 | .126<br>.7388 | | | | | |
| ½ | | .065<br>.5380 | .083<br>.6710 | | | .109 | .109<br>.8510 | | .147 | .147<br>1.088 | | | | .187<br>1.304 | .294 |
| ¾ | | .065<br>.6838 | .083<br>.8572 | | | .113 | .113<br>1.131 | | .154 | .154<br>1.474 | | | | .218<br>1.937 | .308 |
| 1 | | .065<br>.8678 | .109<br>1.404 | | | .133 | .133<br>1.679 | | .179 | .179<br>2.172 | | | | .250<br>2.844 | .358 |
| 1¼ | | .065<br>1.107 | .109<br>1.806 | | | .140 | .140<br>2.273 | | .191 | .191<br>2.997 | | | | .250<br>3.765 | .382 |
| 1½ | | .065<br>1.274 | .109<br>2.085 | | | .145 | .145<br>2.718 | | .200 | .200<br>3.631 | | | | .281<br>4.859 | .400 |
| 2 | | .065<br>1.604 | .109<br>2.638 | | | .154 | .154<br>3.653 | | .218 | .218<br>5.027 | | | | .343<br>7.444 | .436 |
| 2½ | | .083<br>2.475 | .120<br>3.531 | | | .203 | .203<br>5.793 | | .276 | .276<br>7.661 | | | | .375<br>10.01 | .552 |
| 3 | | .083<br>3.029 | .120<br>4.332 | | | .216 | .216<br>7.576 | | .300 | .300<br>10.25 | | | | .438<br>14.32 | .600 |
| 3½ | | .083<br>3.472 | .120<br>4.973 | | | .226 | .226<br>9.109 | | .318 | .318<br>12.50 | | | | | .636 |
| 4 | | .083<br>3.915 | .120<br>5.613 | | | .237 | .237<br>10.79 | .281<br>12.66 | .337 | .337<br>14.98 | | .438<br>19.00 | | .531<br>22.51 | .674 |
| 4½ | | | | | | .247 | | | .355 | | | | | | .710 |
| 5 | | .109<br>6.349 | .134<br>7.770 | | | .258 | .258<br>14.62 | | .375 | .375<br>20.78 | | .500<br>27.04 | | .625<br>32.96 | .750 |
| 6 | | .109<br>7.585 | .134<br>9.289 | | .250<br>17.02 | .280 | .280<br>18.97 | | .432 | .432<br>28.57 | | .562<br>36.39 | | .718<br>45.30 | .864 |
| 7 | | | | | | .301 | | | .500 | | | | | | .875 |
| 8 | | .109<br>9.914 | .148<br>13.40 | .250<br>22.36 | .277<br>24.70 | .322 | .322<br>28.55 | .406<br>35.64 | .500 | .500<br>43.39 | .593<br>50.87 | .718<br>60.63 | .812<br>67.76 | .906<br>74.69 | .875 |
| 9 | | | | | | .342 | | | .500 | | | | | | |
| 10 | | .134<br>15.19 | .165<br>18.70 | .250<br>28.04 | .307<br>34.24 | .365 | .365<br>40.48 | .500<br>54.74 | .500 | .593*<br>64.33 | .718<br>76.93 | .843<br>89.20 | 1.000<br>104.1 | 1.125<br>115.6 | |
| 11 | | | | | | .375 | | | .500 | | | | | | |
| 12 | | .165<br>22.18 | .180<br>24.16 | .250<br>33.38 | .330<br>43.77 | .375 | .406*<br>53.52 | .562<br>73.15 | .500 | .687*<br>88.51 | .843<br>107.2 | 1.000<br>125.5 | 1.125<br>139.7 | 1.312<br>160.3 | |
| 14 | | | .250<br>36.71 | .312<br>45.68 | .375<br>54.57 | .375 | .438<br>63.37 | .593<br>84.91 | .500 | .750<br>106.1 | .937<br>130.7 | 1.093<br>150.7 | 1.250<br>170.2 | 1.406<br>189.1 | |
| 16 | | | .250<br>42.05 | .312<br>52.36 | .375<br>62.58 | .375 | .500<br>82.77 | .656<br>107.5 | .500 | .843<br>136.5 | 1.031<br>164.8 | 1.218<br>192.3 | 1.437<br>223.5 | 1.593<br>245.1 | |
| 18 | | | .250<br>47.39 | .312<br>59.03 | .437<br>82.06 | .375 | .562<br>104.8 | .750<br>138.2 | .500 | .937<br>170.8 | 1.156<br>208.0 | 1.375<br>244.1 | 1.562<br>274.2 | 1.781<br>308.5 | |
| 20 | | | .250<br>52.73 | .375<br>78.60 | .500<br>104.1 | .375 | .593<br>122.9 | .812<br>166.4 | .500 | 1.031<br>208.9 | 1.280<br>256.1 | 1.500<br>296.4 | 1.750<br>341.1 | 1.968<br>379.0 | |
| 24 | | | .250<br>63.41 | .375<br>94.62 | .562<br>140.8 | .375 | .687<br>171.2 | .968<br>238.1 | .500 | 1.218<br>296.4 | 1.531<br>367.4 | 1.812<br>429.4 | 2.062<br>483.1 | 2.343<br>541.9 | |

UPPER FIGURES
Wall Thickness
in inches

LOWER FIGURES
Wt. per Ft.
in pounds

*12"—Sch. 40S: .375 WALL
49.56 WT. PER FT.

*10"—Sch. 80S: .500 WALL
54.74 WT. PER FT.

*12"—Sch. 80S: .500 WALL
65.42 WT. PER FT.

007636

Figure 32. Available Inconel 600 Pipes

manufacture of the thermal energy storage demonstration unit with some small variations in the optimum design. The most appropriate pipe sizes for satisfying the design requirements were:

| | |
|---|---|
| 3/8" nominal | 0.674" O.D. x 0.091" wall |
| 2" nominal | 2.375" O.D. x 0.154" wall |
| 2-1/2" nominal | 2.875" O.D. x 0.302" wall |
| 4" nominal | 4.500" O.D. x 0.237" wall |

Since a replacement pipe for the largest of the five tubes was not available, it still had to be fabricated from available sheet metal.

Figure 33 shows the modified design that evolved from incorporating standard pipes. This design can be compared with the original design which was shown in Figure 20. Because the smallest pipe had a larger internal diameter than in the original design, the vapor flow passage in the center of the TES unit was larger than required. This displaced some of the TES material which had to be compensated for by lengthening the unit approximately 2 inches. The lengthening of the unit resulted in a 3 percent increase in total weight as given in the following weight distribution:

| Design | | Weight, lb | Percent |
|---|---|---|---|
| Original | | | |
| TES material | | 12.07 | 32.82 |
| Container material | | 14.34 | 38.99 |
| Wick - screen material | 1.15 lb | | |
| - sodium | 0.42 lb | | |
| Insulation | | 8.81 | 23.95 |
| Total | | 36.79 | 100.00 |

56721 A

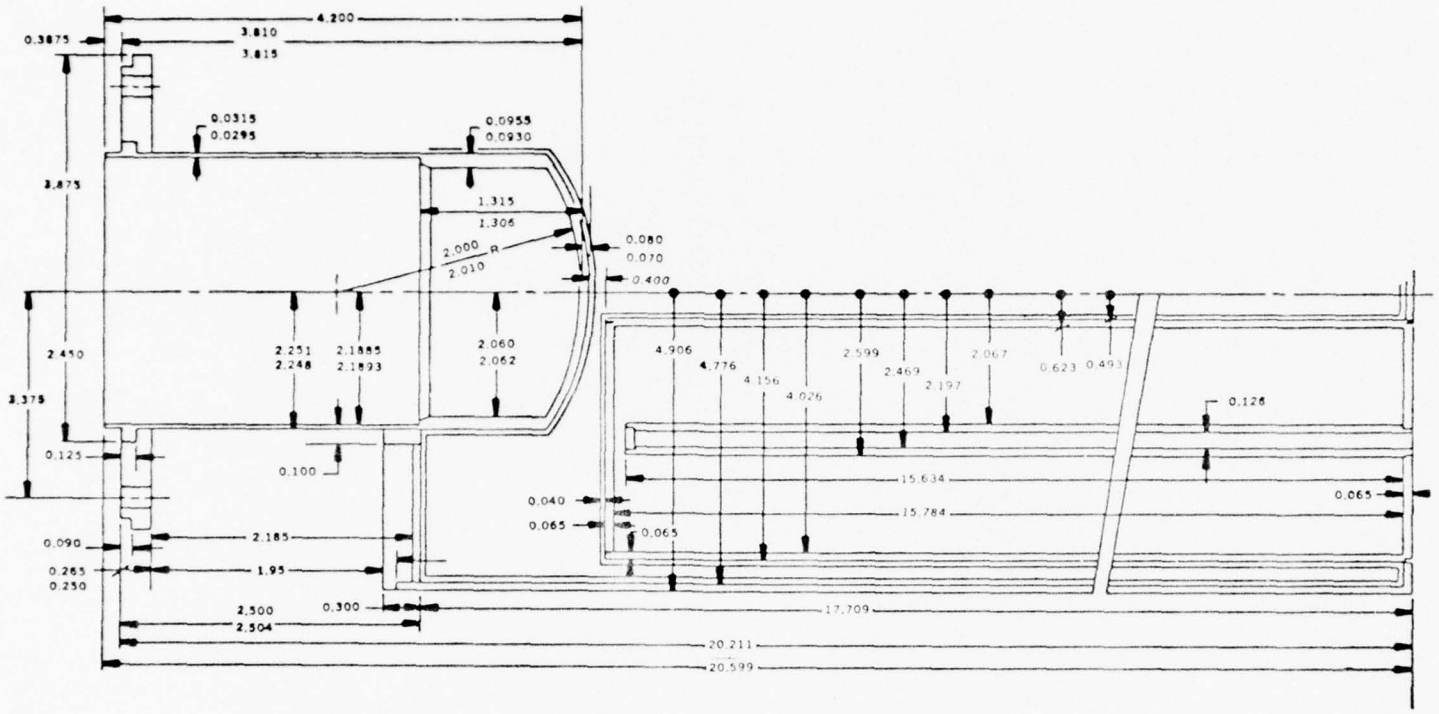



Figure 33. Final Design for a 1-kW-Hr Thermal Energy Storage Unit

| | | | |
|---|---|---|---|
| Modified | | | |
| TES material | | 12.07 | 31.89 |
| Container material | | 15.17 | 40.08 |
| Wick - screen material | 1.32 lb | | |
| - sodium | 0.48 lb | | |
| Insulation | | 8.84 | 23.28 |
| Total | | 37.88 | 100.00 |

The heater well in the modified design had a slightly larger width. The original design called for a gap of only 0.128 inch. The modified design resulted in a gap of 0.136 inch. With the maximum heater diameter of 0.130 inch, this design was expected to operate in the radiation heat transfer mode. Heat transfer from the heater to the walls of the well solely by radiation heat transfer had been assumed in the original heat transfer calculations and in the selection and sizing of the heaters. Any heat transfer by conduction had been considered a bonus in the operation of the heater, as it would slightly decrease the heater operating temperature.

When compared with the original design, the modified design resulted in a 3 percent increase in weight. The heater surface was slightly larger because of the greater length of the unit. The design modification required for using standard - though still not easily available -Inconel 600 tubes for the fabrication of the TES unit appeared to be acceptable.

### 2.2.4 HOT CYLINDER DESIGN

Prior to machining of the hot cylinder, the design was evaluated for maximum stresses and their location. This was deemed important as the hot cylinder was to become an integral part of the thermal energy storage unit. The pertinent dimensions and tolerances of the hot cylinder, as shown in Hughes Aircraft Company Drawing X3180095, are repeated in Figure 34. When using the relations given in Roark: Formulas for Stress and Strain, and the stress concentration factors given by Peterson: Stress Concentration

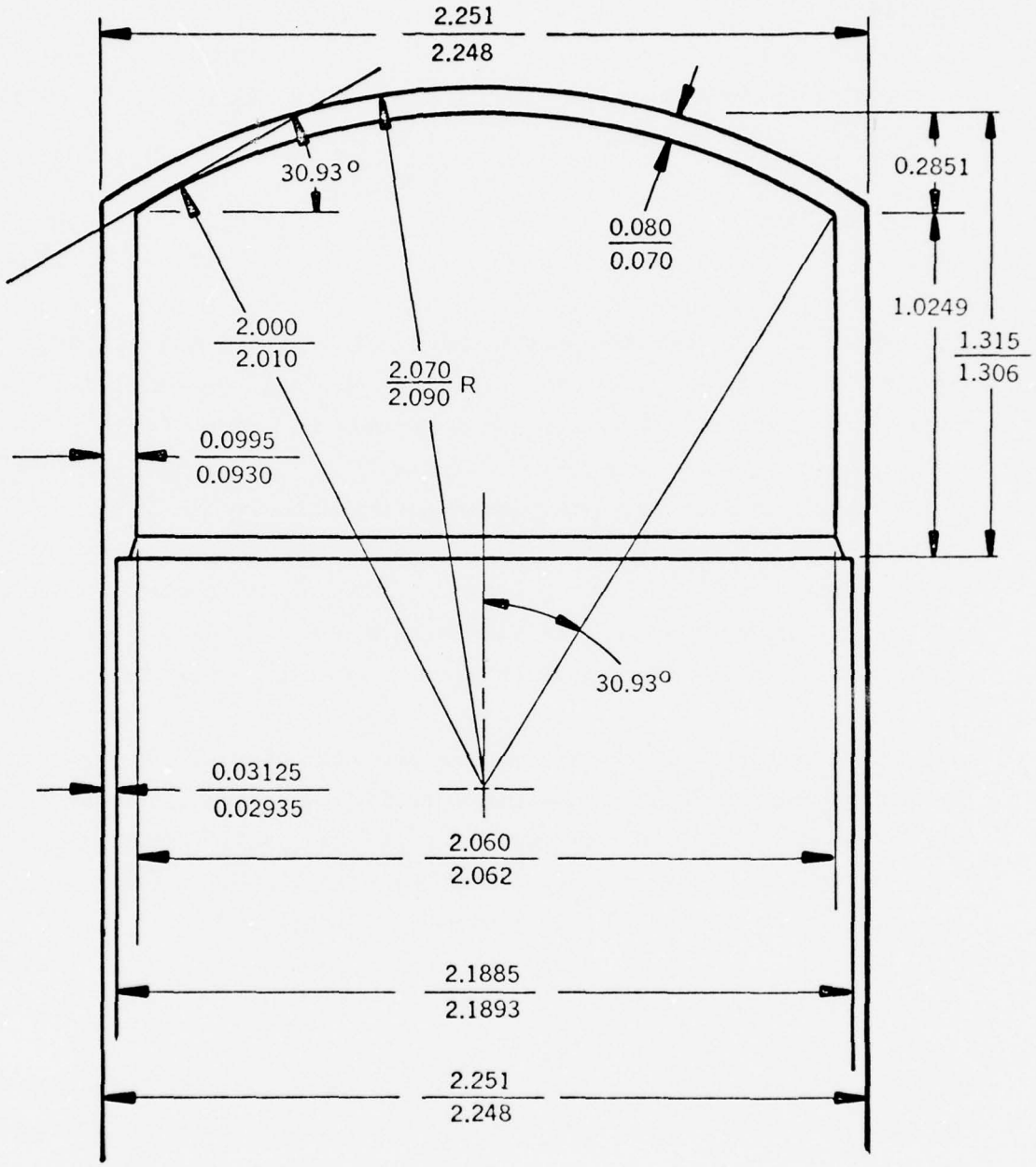



Figure 34. Original Hot Cylinder Design

56694

Factors, stresses as high as 157,000 psi with the lower limit of the plate thickness of 0.070 inch were calculated. The calculations took into account the curvature of the end plate which attaches to the cylinder under an angle of 30.93 degrees as shown in Figure 34. When using a simplified approach for calculating maximum stresses by matching of moments and deflections of a curved plate with a cylinder, stresses as high as 132,000 psi were calculated.

Data given by the Carpenter Technology Corporation for René 41 (Vacumeltrol 41) were correlated with the Larson-Miller parameter

$$P_{L-M} = (460 + T) \times (C + \log_{10} t) \times 10^{-3}$$

where:

T = temperature, $^{o}F$
t = time, hours

The best fit was found by making the constant C equal to 20. The correlation with the original data is shown in Figure 35. For an operating temperature of 1250$^{o}$F and an operating lifetime of 5000 hours and 20,000 hours, the Larson-Miller parameters are 40.53 and 41.55, respectively. Based on the correlation of Figure 35, the maximum allowable stresses for rupture are 55,000 and 69,000 psi, respectively. For structural stability and maximum allowable distortion, the allowable stresses should be kept below these values.

For comparison, the Larson-Miller parameter correlation with the rapture stress for Inconel X750 and Inconel 718 are shown in Figures 36 and 37. The constant C is 17.5 for Inconel alloy X750 and 25 for Inconel alloy 718. The Larson-Miller parameters for the two lifetimes are tabulated below.

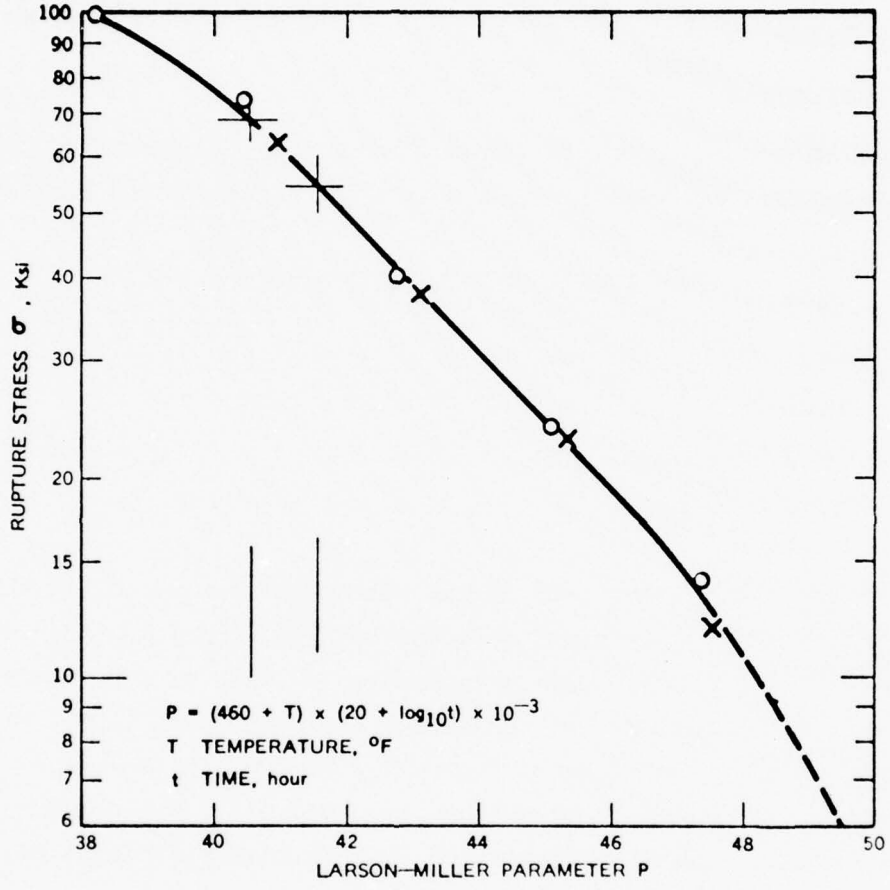



Figure 35. Rupture Stress of René 41 (Carpenter Vacumeltrol 41) (Technical Data, Carpenter Technology Corporation 6/70)

56693

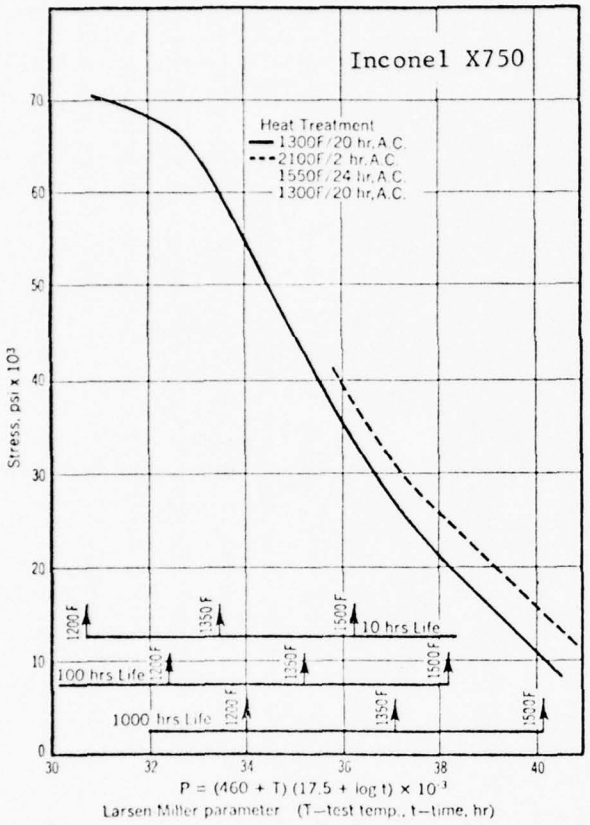



Figure 36. Life of cold-rolled, annealed and aged sheet.

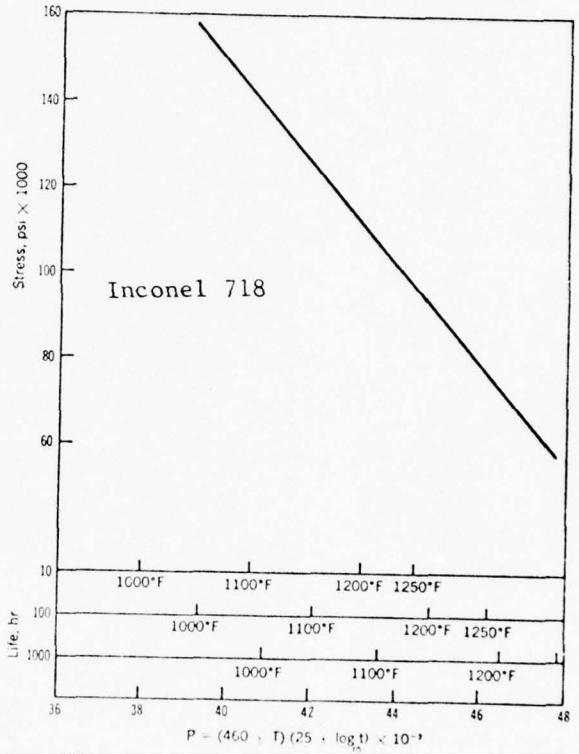



**Figure 37.** Larson-Miller parameter plot of rupture life of cold-rolled sheet, 0.025–0.250-in. (Annealed and aged in accordance with AMS 5596B). In the Larson-Miller parameter, P, T is temperature, °F, and t is time, hr.

Larson-Miller Parameters

| | Inconel X750 | Inconel 718 | René |
|---|---|---|---|
| 5,000 hours | 36.25 | 49.08 | 40.53 |
| 20,000 hours | 37.28 | 50.11 | 41.55 |

The maximum allowable stresses for the various materials are given in the following tabulation.

Maximum Allowable Stresses

| | Inconel X750 | Inconel 718 | René |
|---|---|---|---|
| 5,000 hours | 33,000 psi | 50,000 psi | 69,000 psi |
| 20,000 hours | 24,000 psi | 25,000 psi | 55,000 psi |

When the maximum allowable stresses for rupture (this does not consider the maximum allowable stresses for structural stability) were compared with the calculated maximum stresses in the hot cylinder under the stated operating conditions, it was felt that it would be of value to ascertain whether modifications could be made in the design without affecting the operating characteristic of the hot cylinder.

The most obvious improvement was the increase in the plate thickness and the tightening of its tolerance. The results of the parametric study are shown in Figure 38. It is interesting to note that just the tolerance of the plate thickness permits the maximum stress to vary between 130,000 and 96,000 psi. Without increasing the cylinder wall thickness, which was 0.0955 inch in the original design, the plate thickness should be at least 0.092 inch. With this plate thickness, the maximum stresses are equal at 68,000 psi. A slight increase of the cylinder wall thickness would bring the maximum stresses down to the allowable stress for 20,000 hour operation with René 41.

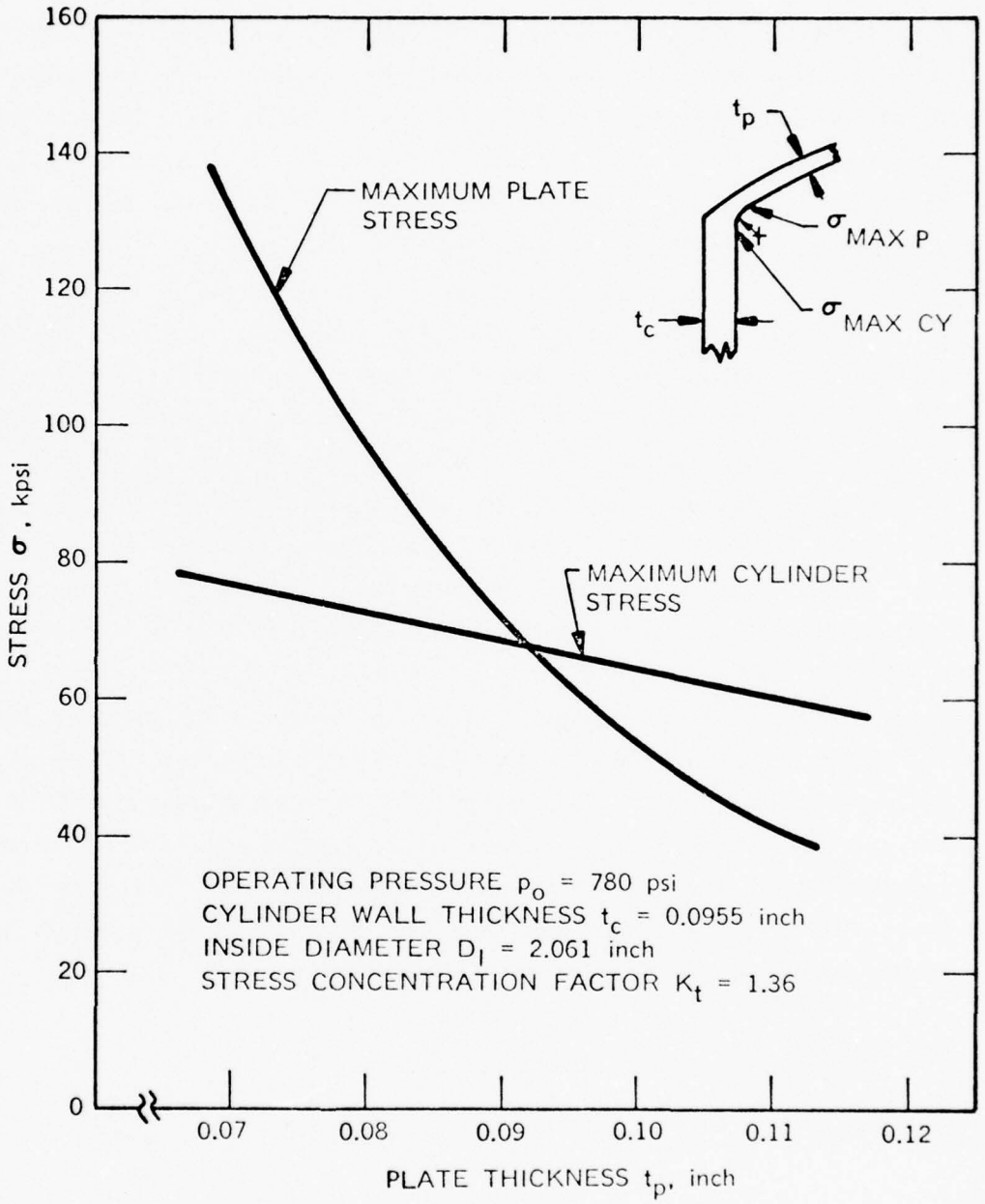



Figure 38. Effect of Plate Thickness on the Maximum Stresses in the Hot Cylinder of the AFLIR Vuilleumier Cooler

56691

When the manufacture of the hot cylinder was investigated, it became apparent that the availability of material in the most desirable sizes was very limited and that the cost of the material was relatively high. Since the difficulties in obtaining the material increase with the diameter, it became obvious that the hot cylinder should be designed for the smallest bar diameter. The original design called for a bar stock diameter of at least 3.875 inches. This size was needed for machining the hot cylinder with the mounting flange as a single unit.

A considerable saving in material and machining could be achieved by designing the hot cylinder with the smallest mounting flange possible. Calculations indicated that, for a very conservative allowable bearing stress of 20,000 psi and a shear stress of 15,000 psi, the flange diameter had not to be larger than 2.292 inches, and the thickness of the flange not more than 0.029 inch. A hold-down ring with the diameter equal to that of the original flange, made of plate material, could be used for securing the hot cylinder to the cooler body. Such design modification appeared to be especially useful if René 41 was to be used, as the machinability of that material is considered extremely poor. The proposed and accepted design of the hot cylinder is presented in Figure 39 with the detailed design of the TES demonstration unit. This change did not require modifications to the cooler. All design changes assured better dimensional stability and easier fabrication of the hot cylinder. Furthermore, the material selection became less critical and made the use of Inconel 718 possible without reservations for the present application.

## 2.3 SPECIAL HEAT TRANSFER CONSIDERATIONS

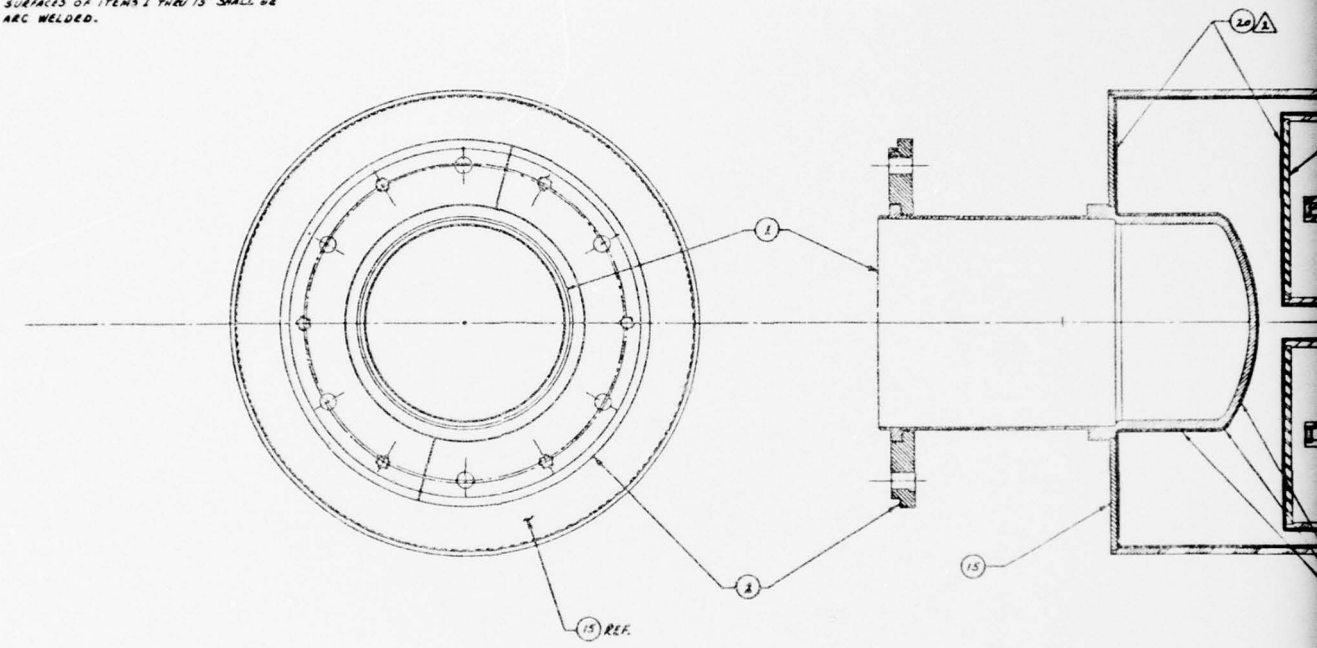
### 2.3.1 EFFECT OF VOLUMETRIC CHANGE OF THERMAL ENERGY STORAGE MATERIAL

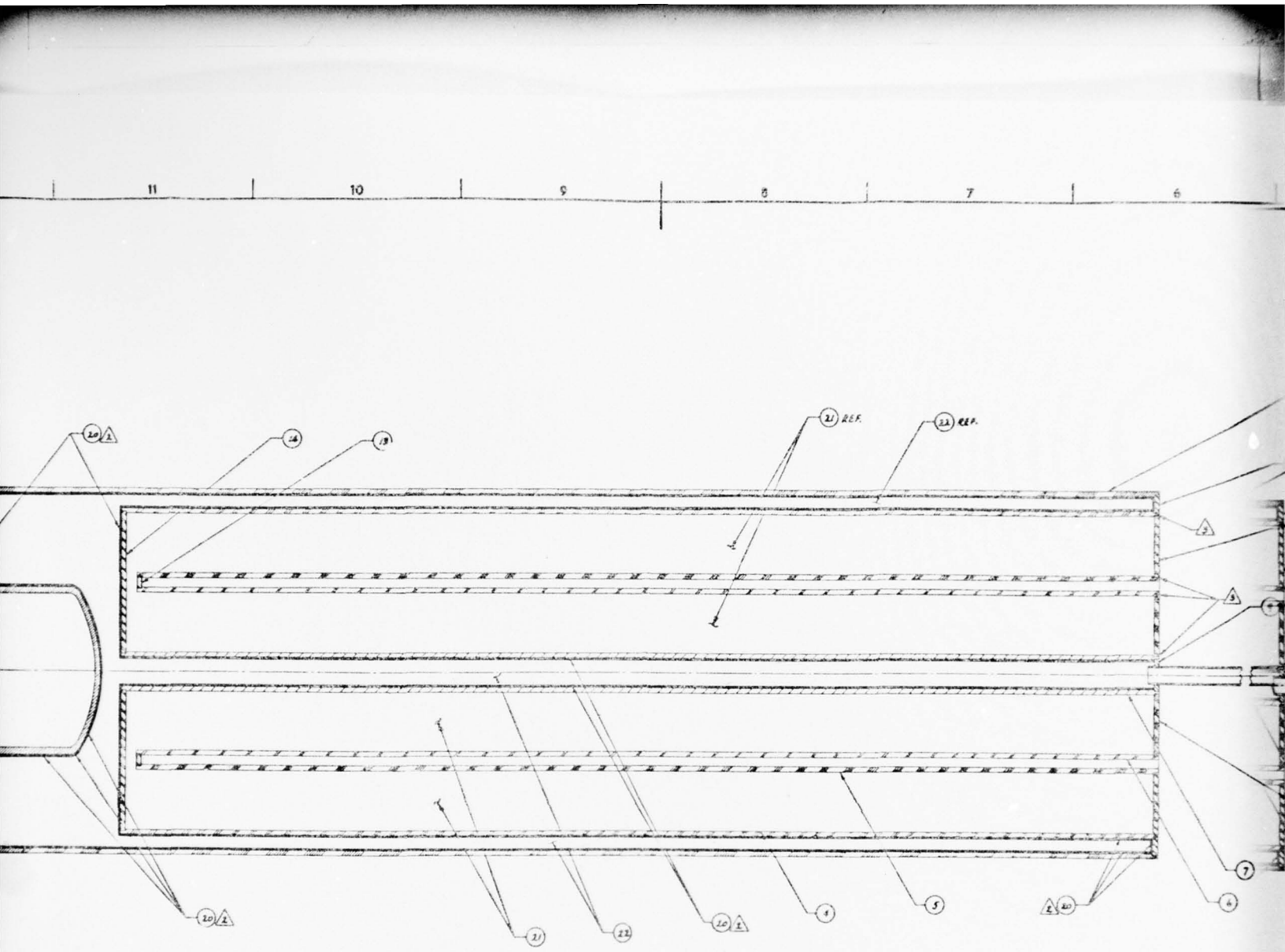
With the specific design of the thermal energy storage demonstration unit established, the secondary effect associated with the volumetric change of the thermal energy storage material during melting and solidification was

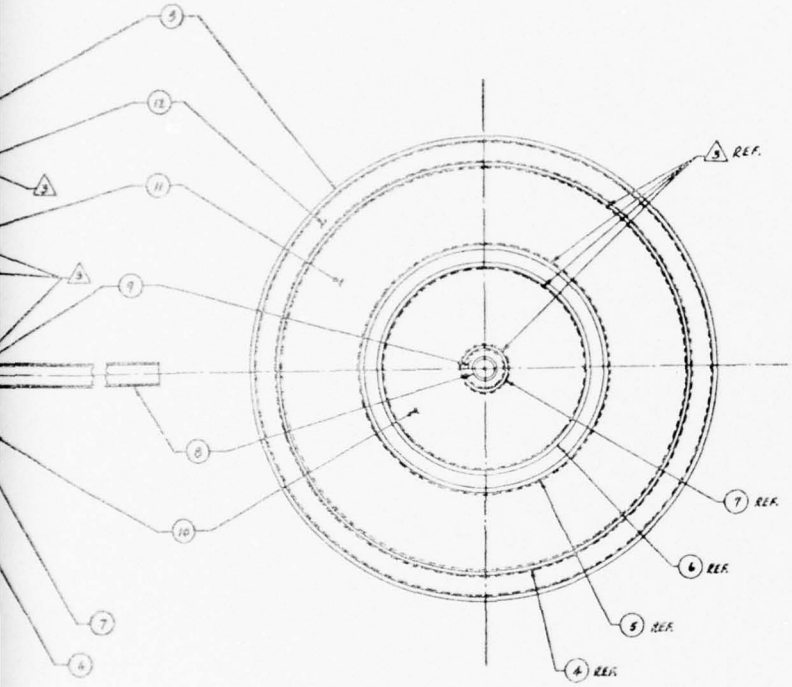
SECURITY CLASSIFICATION

NOTES: UNLESS OTHERWISE SPECIFIED

1. REMOVE ALL BURRS AND SHARP EDGES.
2. SPOTWELD 4 LAYERS OF ITEM 16 - BOLTING CLOTH - TO ALL INDICATED SURFACES. LOCATIONS AND NUMBER OF SPOTWELDS AS REQUIRED.
3. ALL INDICATED FAYING SURFACES OF ITEMS 4, 5, 6, 7, 10 AND 11 SHALL BE ELECTRON BEAM WELDED AFTER INSTALLATION OF ITEM 21 - THERMAL ENERGY STORAGE SALT. ALL OTHER FAYING SURFACES OF ITEMS 1 THRU 15 SHALL BE INERT ARC WELDED.




11
10
9
8
7
6
21 REF.
22 REF.
20
1
14
13
2
3
4
7
6
5
707485




| ITEM NO. | ZONE | NOT REQ'D | MATERIAL | SPECIFICATION | DESCRIPTION | PART OR IDENTIFYING NO. | CODE IDENT | SYM | QTY REQD |
|---|---|---|---|---|---|---|---|---|---|
| 22 | | | Na | | SODIUM | | | | AR |
| 21 | | | LiF-MgF$_2$-KF | | THERMAL ENERGY STORAGE SALT | | | | AR |
| 20 | | | CRES. | | BOLTING CLOTH - MESH 20 | | | | AR |
| 19 | | | | | | | | | |
| 18 | | | | | | | | | |
| 17 | | | | | | | | | |
| 16 | | | | | | | | | |
| 15 | | | INCONEL 617 | | RING No. 7 | 707483-31 | | | 1 |
| 14 | | | INCONEL 617 | | RING No. 6 | -29 | | | 1 |
| 13 | | | INCONEL 617 | | RING No. 5 | -27 | | | 1 |
| 12 | | | INCONEL 617 | | RING No. 4 | -25 | | | 1 |
| 11 | | | INCONEL 617 | | RING No. 3 | -23 | | | 1 |
| 10 | | | INCONEL 617 | | RING No. 2 | -21 | | | 1 |
| 9 | | | INCONEL 617 | | RING No. 1 | -19 | | | 1 |
| 8 | | | INCONEL 600 | | FILL TUBE | -17 | | | 1 |
| 7 | | | INCONEL 617 | | TUBE No. 5 | -15 | | | 1 |
| 6 | | | INCONEL 617 | | TUBE No. 4 | -13 | | | 1 |
| 5 | | | INCONEL 617 | | TUBE No. 3 | -11 | | | 1 |
| 4 | | | INCONEL 617 | | TUBE No. 2 | -9 | | | 1 |
| 3 | | | INCONEL 617 | | TUBE No. 1 | -7 | | | 1 |
| 2 | | | CRES - TYPE 304 | 60.5-763 CL410-304 | FLANGE - HOLD DOWN | -5 | | | 1 |
| 1 | | | INCONEL X-750 | | HOT CYLINDER | 707483-3 | | | 1 |

LIST OF MATERIALS

UNLESS OTHERWISE NOTED
LINEAR DIMS. IN INCHES
TOLERANCES
DECIMAL
DO NOT SCALE
MATERIAL
TREATMENT FINISH
NEXT ASSY
APPLICATION
DRAWING LEVEL
CONTRACT NO.
DRAWN
CHECK
DETAIL
ENGR APPV'D
MFG APPV'D
CUSTOMER APPV'D
ENGINEER
MATL MGR
PROJ MGR
CUSTOMER

ELECTRO-OPTICAL SYSTEMS, INC.
A XEROX COMPANY

TITLE: THERMAL ENERGY STORAGE DEMONSTRATION UNIT - ASSEMBLY -

SIZE J | CODE IDENT NO. 12705 | DWG NO. 707485

SCALE 3/8 | RELEASE DATE | SHEET 1 OF 3

ON THRU
EFFECTIVE SERIAL NO.
USAGE DATA

REVISIONS

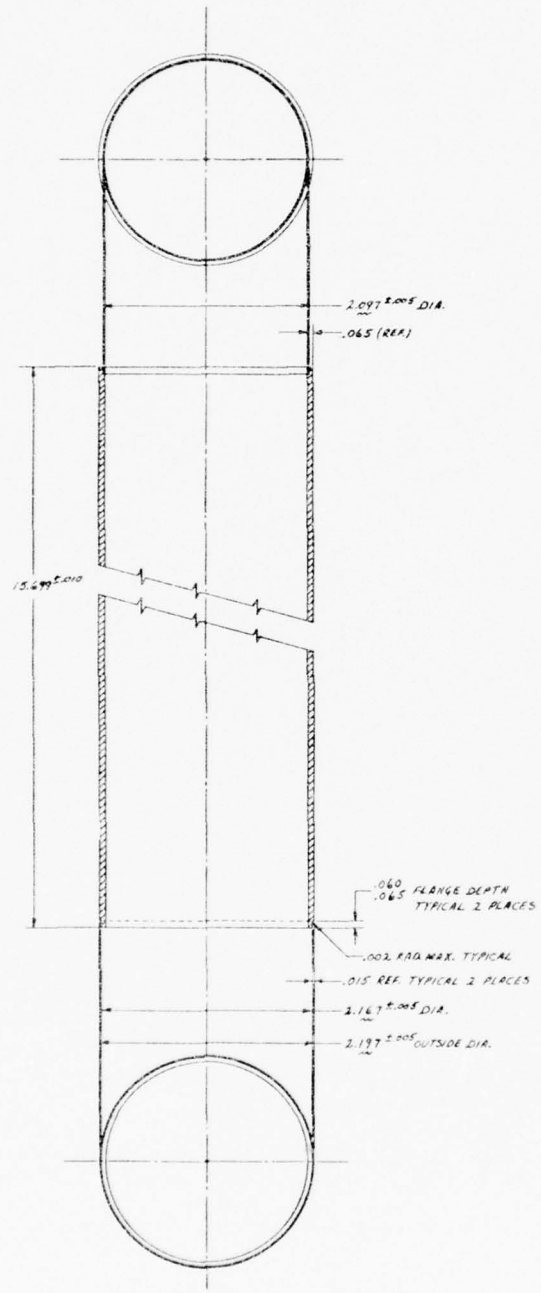
| ZONE | LTR | DESCRIPTION | DATE | APPROVED |
|---|---|---|---|---|

BEST AVAILABLE COPY

Figure 39. (Sheet 1 of 3) 57/58

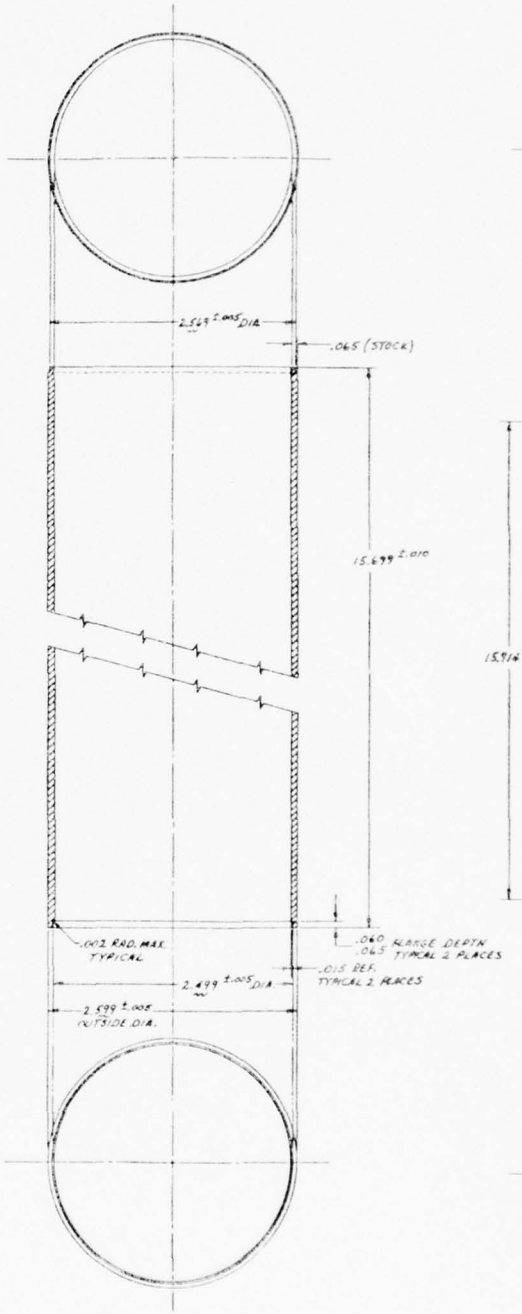
SECURITY CLASSIFICATION

NOTES: UNLESS OTHERWISE SPECIFIED



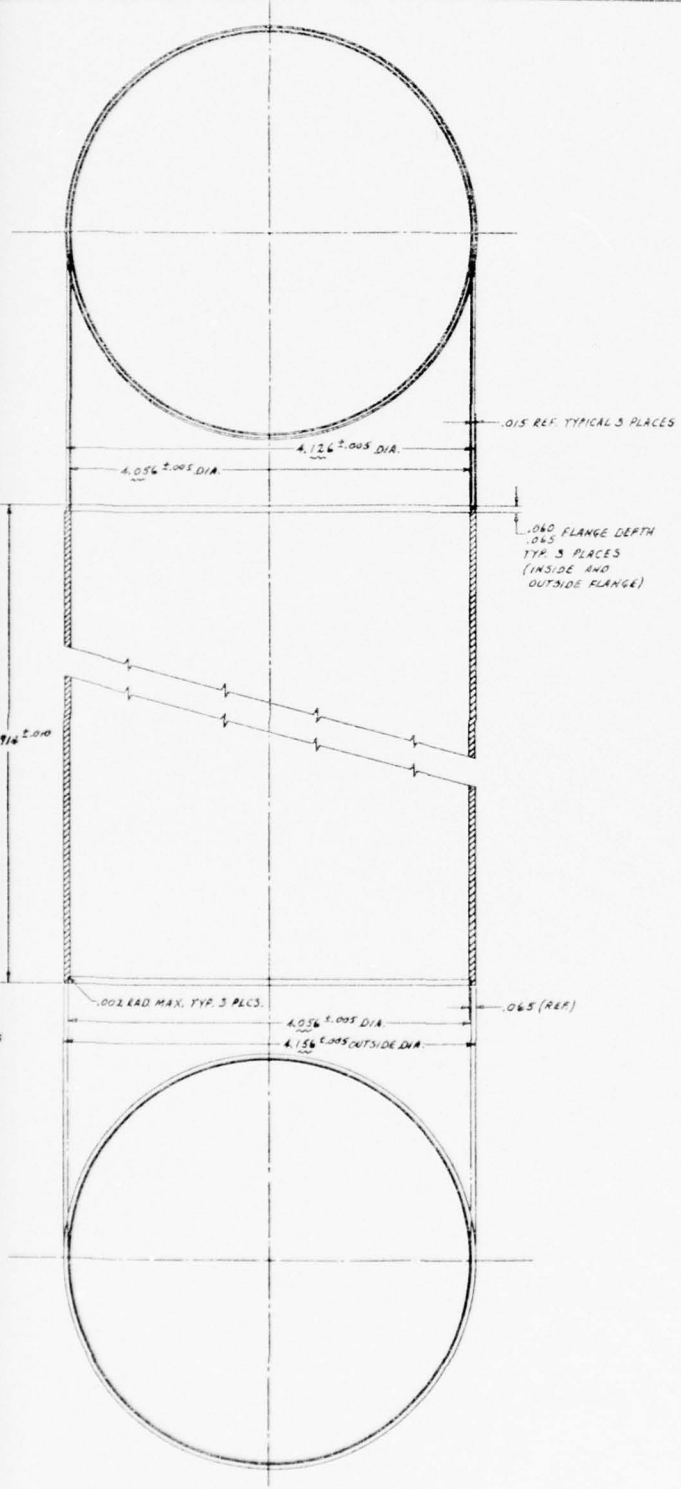

ITEM 6 - TUBE NO. 4 - ONE REQ'D. /1

MAT'L. REF: INCONEL 600

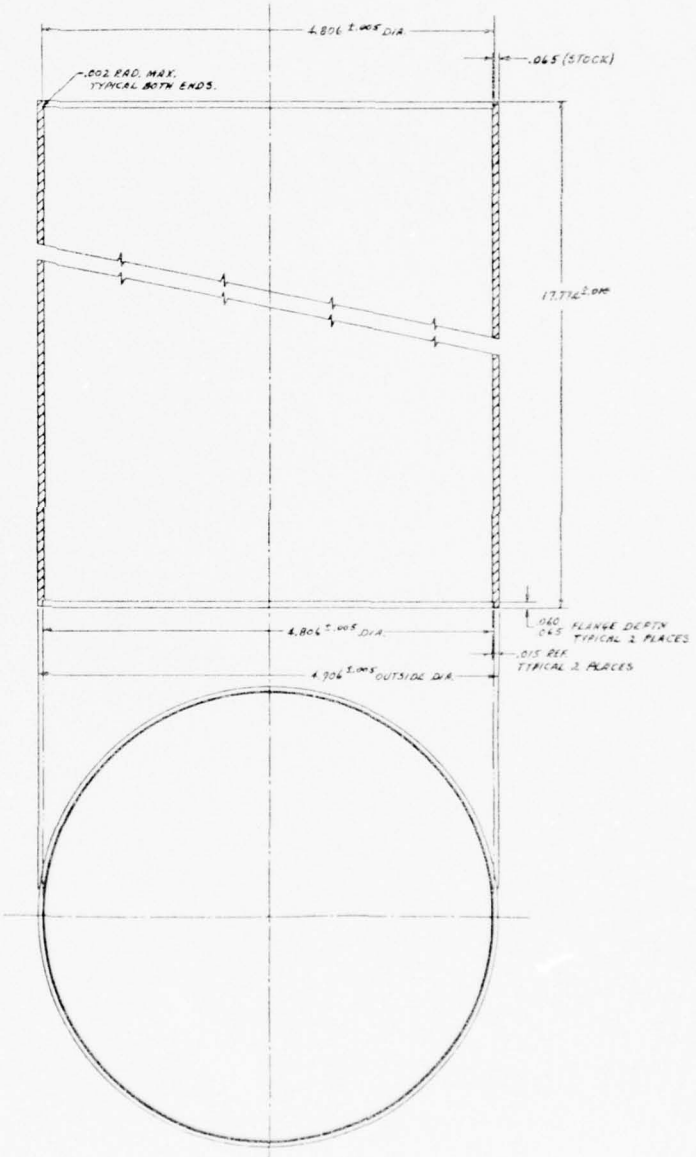



ITEM 5 - TUBE NO. 3 - ONE REQ'D. /1

MAT'L. REF: INCONEL 600




ITEM 4 - TUBE NO. 2 - ONE REQ'D.
MAT'L. REF: INCONEL 600




ITEM 3 - TUBE NO. 1 - ONE REQD.
MAT'L. REF: INCONEL 617

707485

BEST AVAILABLE COPY

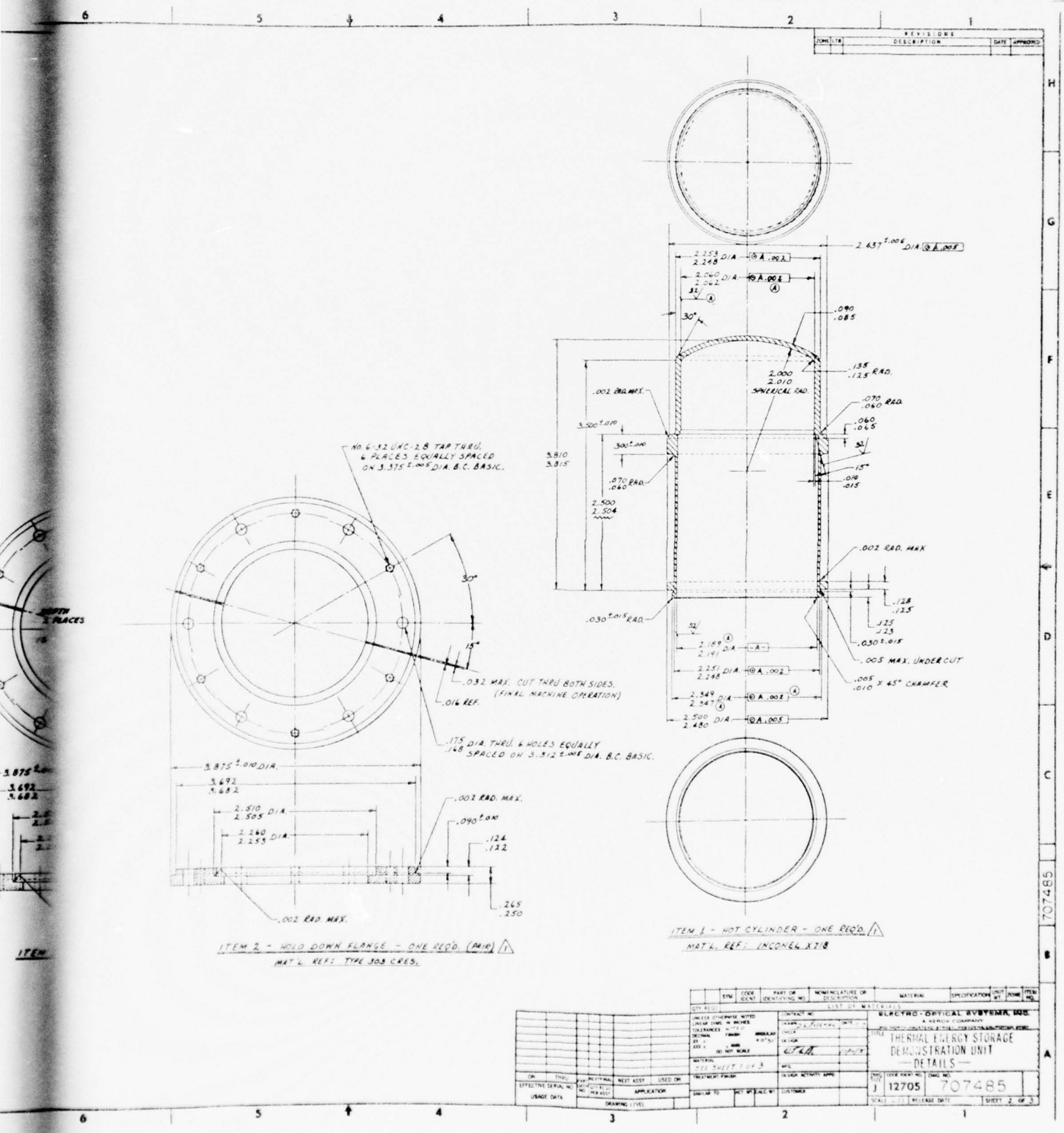
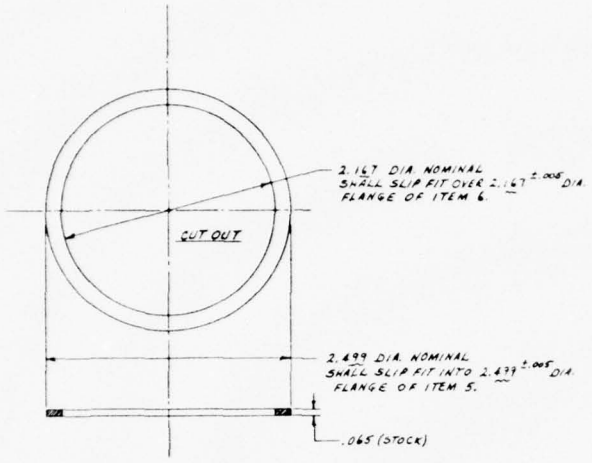



Figure 39. (Sheet 2 of 3) 59/60

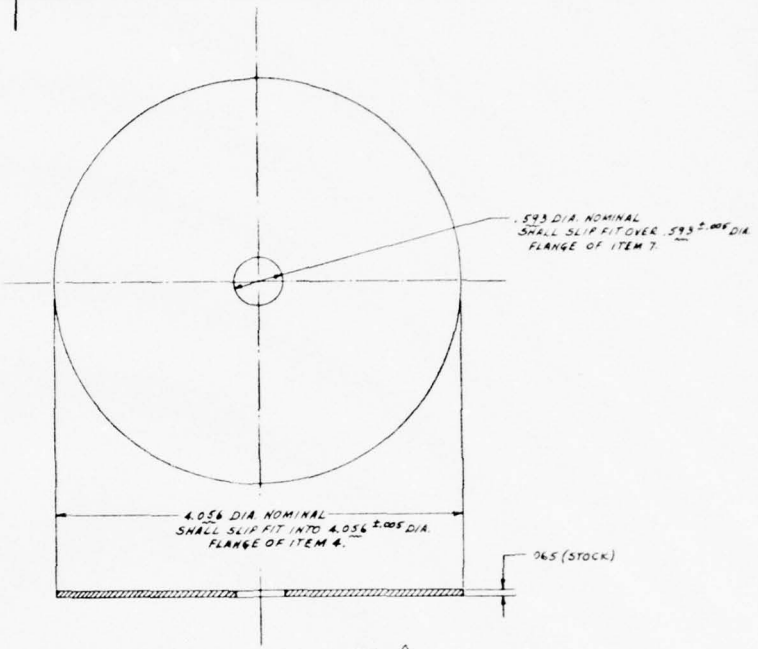
SECURITY CLASSIFICATION

NOTES: UNLESS OTHERWISE SPECIFIED



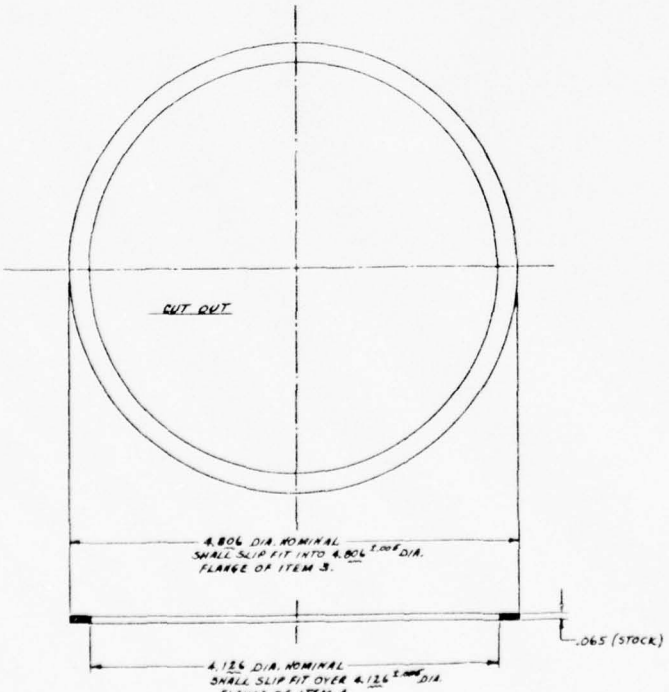

ITEM 13 - RING NO. 5 - ONE REQ'D. (1)

MAT'L REF: INCONEL 617



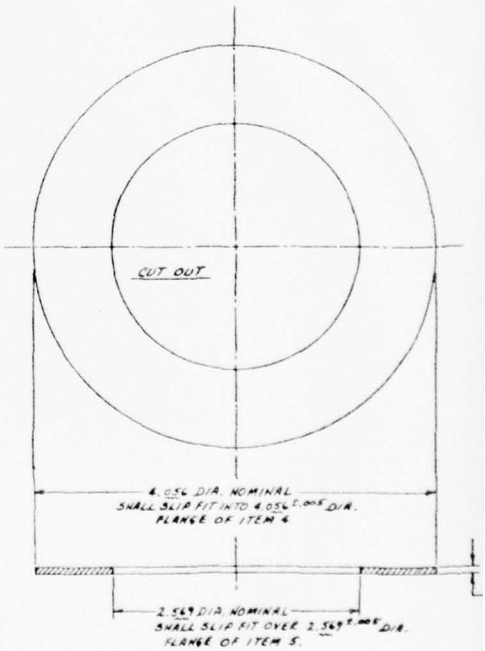

ITEM 14 - RING NO. 6 - ONE REQ'D. (1)

MAT'L REF: INCONEL 617




ITEM 12 - RING NO. 4 - ONE REQ'D. (1)

MAT'L REF: INCONEL 617




ITEM 11 - RING NO. 3 - ONE REQ'D. (1)

MAT'L REF: INCONEL 617

Figure 39. S
F

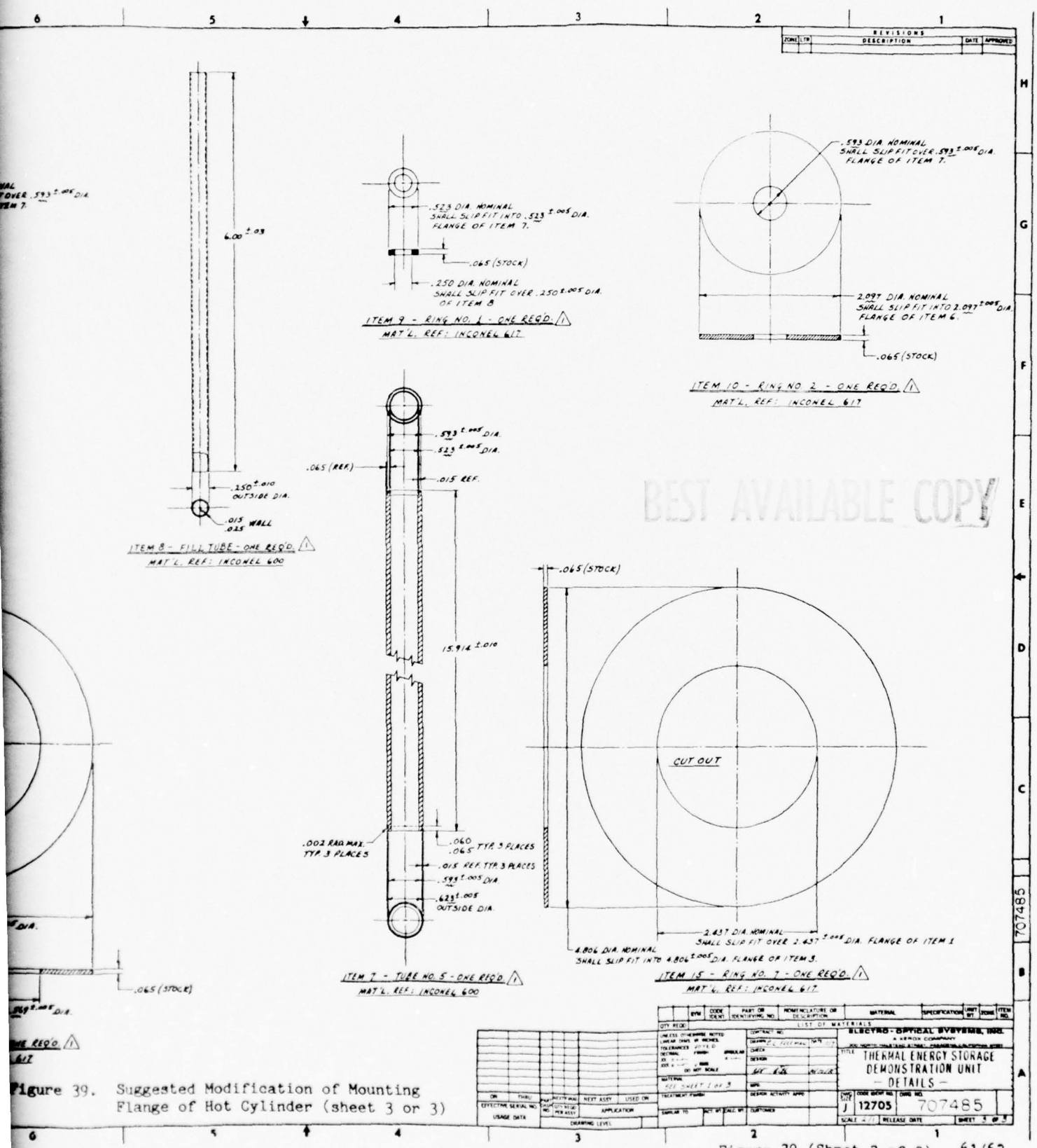



**Figure 39.** Suggested Modification of Mounting Flange of Hot Cylinder (sheet 3 or 3)

Figure 39.(Sheet 3 of 3) 61/62

3

investigated. In the solid state the thermal energy storage material occupies only 76.1 percent of the liquid volume. The container volume of the thermal energy storage unit had to be designed for the largest volume, i.e., the volume of the liquid material. During extraction of the stored thermal energy, the salt contracts and voids form at that time, so that the TES material will no longer be in contact with the entire container wall as shown in Figures 40, 41, and 42. For a 24 percent volumetric void, a 20 percent surface detachment will occur. In the worst case the temperature drop across the thernal energy salt could increase by about 20 percent for a total of $\Delta T = 50^{\circ}F$. Even with this temperature drop the operating temperature of the hot cylinder would still be above $1200^{\circ}F$.

### 2.3.2 COOLING OF HOT CYLINDER DURING PERFORMANCE TESTING

For evaluating the thermal energy storage demonstration unit performance, the hot cylinder was cooled with a flow of air simulating the heat extraction from the hot cylinder wall by helium during operation of the Vuilleumier cooler. The arrangement for testing the thermal energy storage demonstration unit is shown in Figure 43. A plug shown in Figure 44 was machined from stainless steel that provided a 0.020-inch flow pass along the hot cylinder wall. The predicted heat transfer as function of flow rate is shown in Figures 45 and 46. With the 0.020 inch flow passage, the design power is extracted at a flow rate of $8.2 \times 10^{-3}$ lb/sec (3.72 g/sec). At this flow rate the flow is well in the laminar flow regime, and the heat transfer varies relatively little with flow rate, i.e., the total heat transfer changes by only 5 percent for a flow rate variation of about 24 percent.

The length of the flow gap is L = 1.025 inch. With a flow gap of only t = 0.020 inch, the entrance regime is very short compared to the entire flow length. For evaluating the Nusselt number, the relation given by Eckert and Drake in Heat and Mass Transfer, 2nd Edition, p. 197, is used.

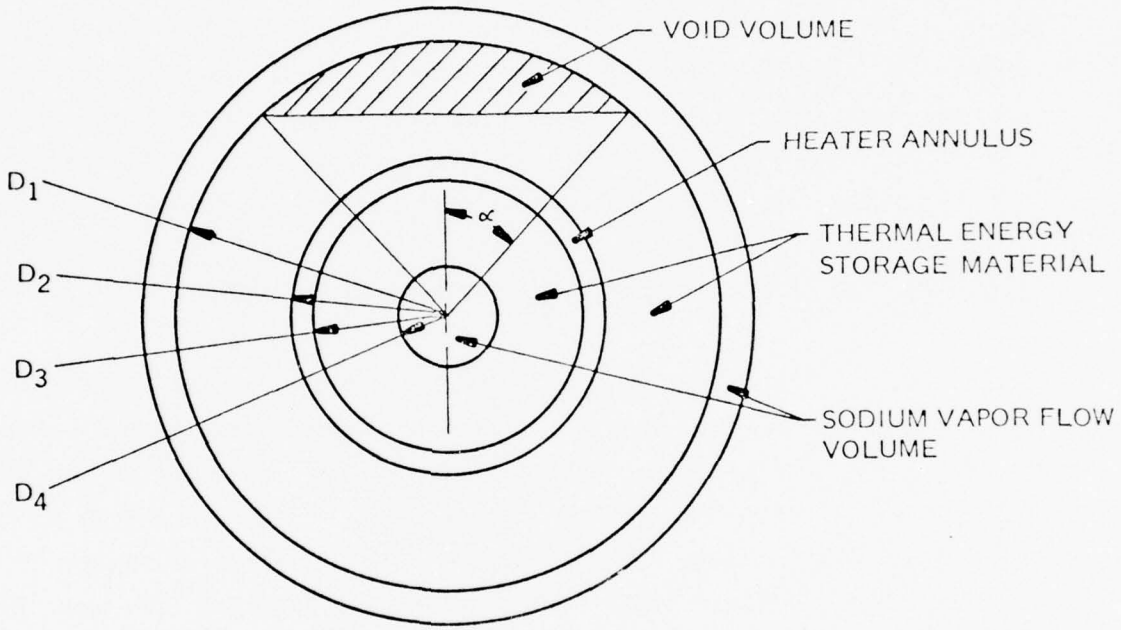



Figure 40. Configuration of Thermal Energy Storage Demonstration Unit

56881

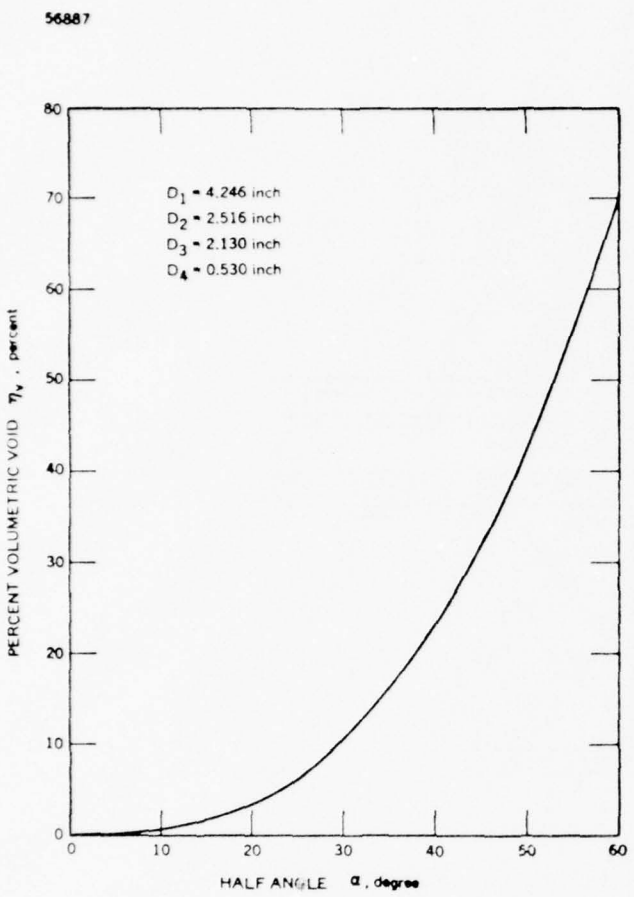



Figure 41. Volumetric Void as a Function of Half Angle for Thermal Energy Storage Demonstration Unit

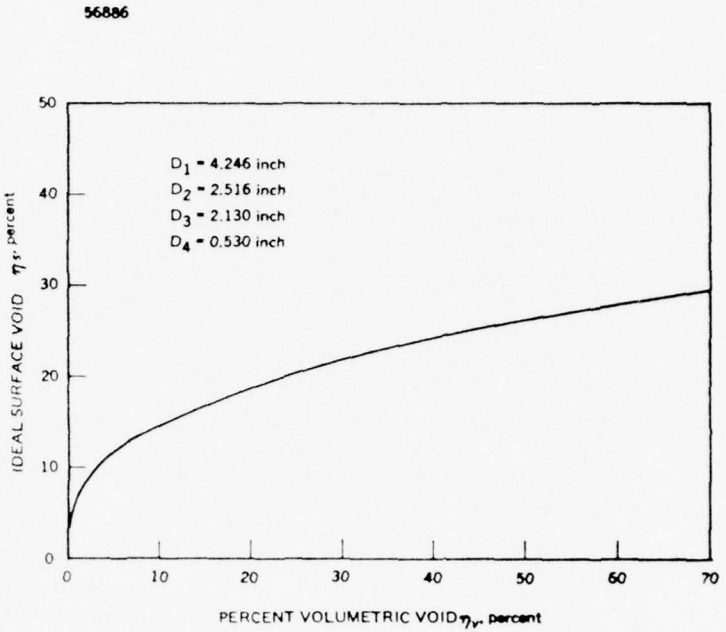



Figure 42. Volumetric Void and Surface Void Relation for Thermal Energy Storage Demonstration Unit

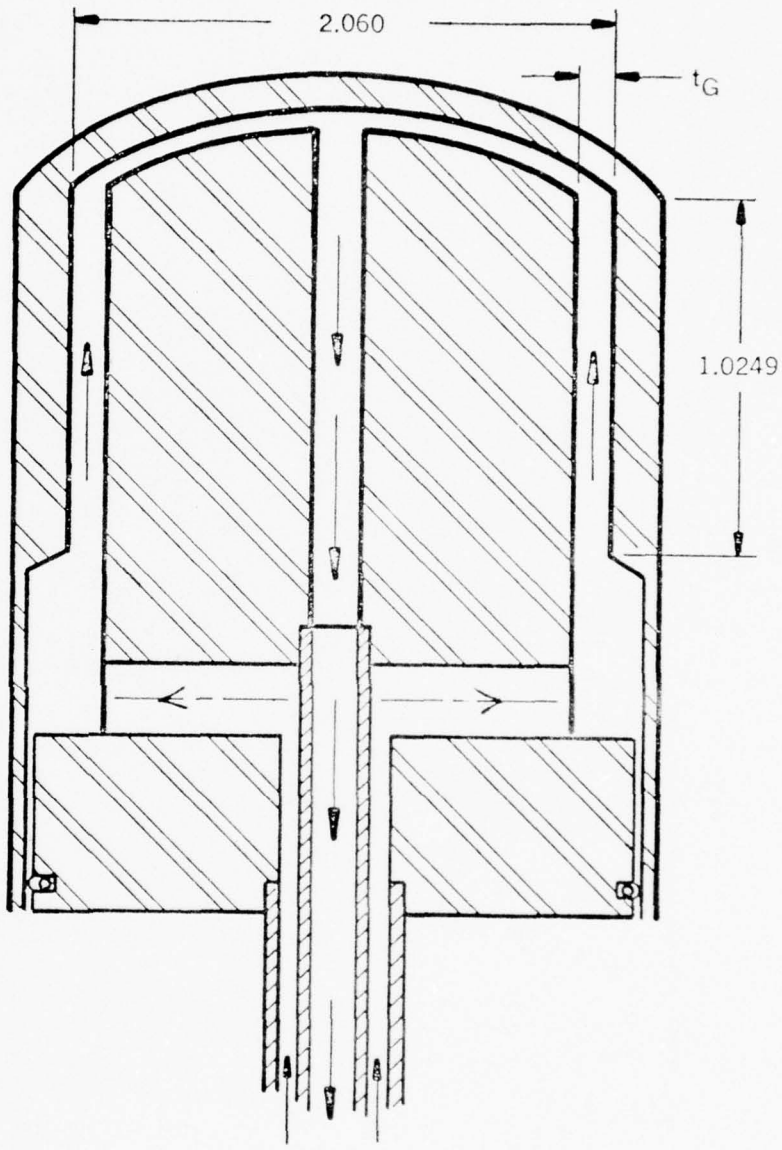



Figure 43. Gas Flow for Performance Testing of Thermal Energy Storage Demonstration Unit

56679

BEST AVAILABLE COPY

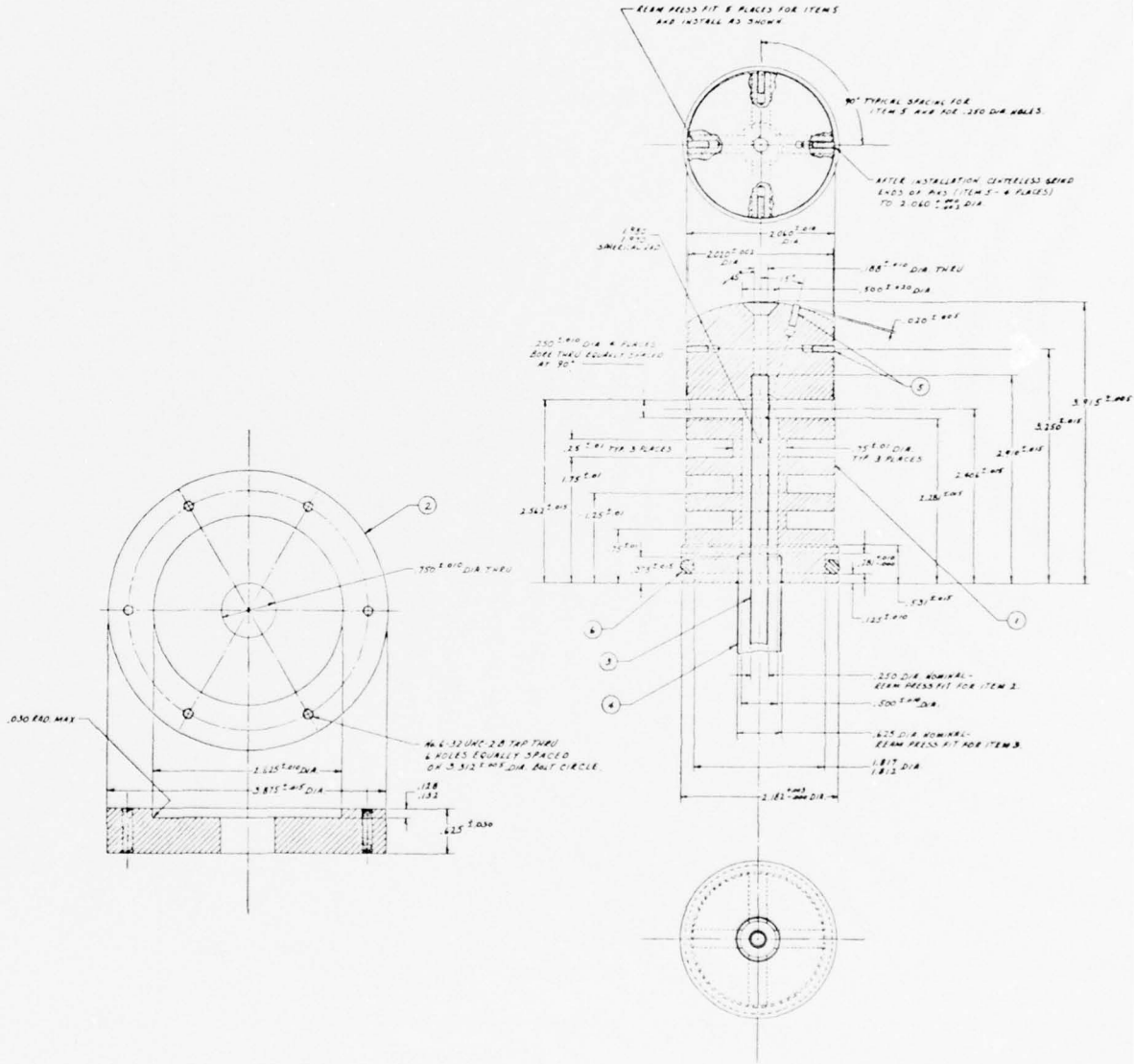
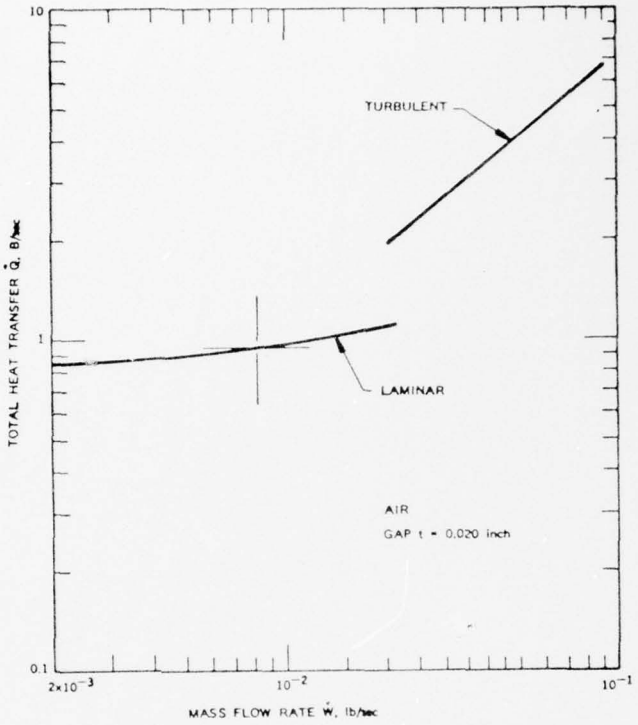
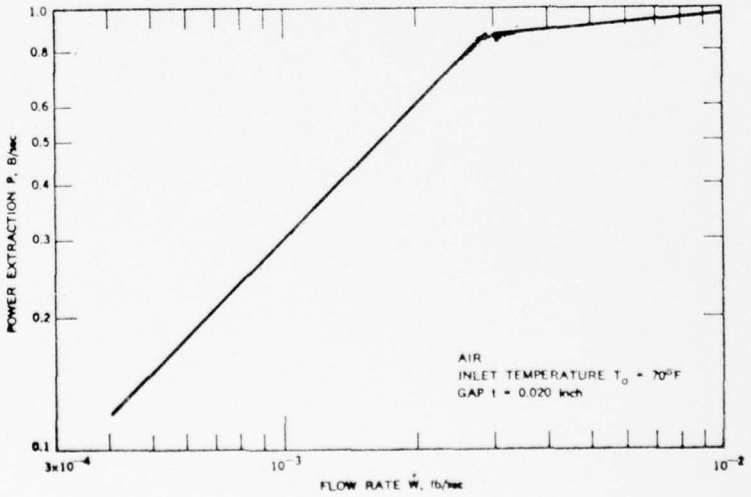



Figure 44. Flow Test Insert - Thermal Energy Storage Demonstration Unit




56683

Figure 45. Total Heat Transfer from the Hot Cylinder to the Cooling Air




56680

Figure 46. Power Extraction from the Hot Cylinder as Function of Flow Rate

The non-dimensional parameter $1/(Re_d\ Pr\ d/x)$ is about 0.05 so that the average effective Nusselt number is about 5 for the case under consideration. As shown by the correlation given by Eckert and Drake, Prandt and various other literature sources, the heat transfer is not entirely dependent on the Nusselt number but is also a function of several additional parameters. Inlet conditions, roughness factors, and surface conditions are contributing parameters which, however, could not be expressed mathematically for inclusion in the heat transfer calculation.

The final temperature of the air that cools the hot cylinder of the Vuilleumier cooler and has an inlet temperature of $70^{\circ}F$, is shown in Figure 47. The calculated pressure drop along the flow pass is shown in Figure 48. With the expected pressure drop being approximately 1 psi, it was possible to arrange the flow metering system to operate in the chocked orifice configuration. With the additional pressure drops in the lines and the fittings leading to and from the flow insert, the total back pressure was estimated to be not higher than 10 psig. The sonic orifice was therefore selected to operate with an upstream pressure of about 50 psia or 35 psig.

For spanning the entire range of flow rates which might be desirable for testing with shop air supply, two sonic orifices were calibrated, No. 55-1 and No. 47. Orifice No. 55-1 permitted lowering the flow rate to less than 0.7 g/sec of air, while with orifice No. 47, the upstream pressure was about 69 psig at the design flow rate of $8.2 \times 10^{-3}$ lb/sec. The orifices were calibrated with a Wet Test Meter (American Meter Company Model AL 22), which has a maximum deviation of $\pm 1$ percent from the calibration, and with a 1/4 percent Bourdon tube type pressure gage (Glassco).

In Figure 46 two regimes are indicated. Below 1.36 g/sec the amount of energy extracted from the hot cylinder will be equal to the heat capacity of the air between the inlet temperature and the operating temperature of

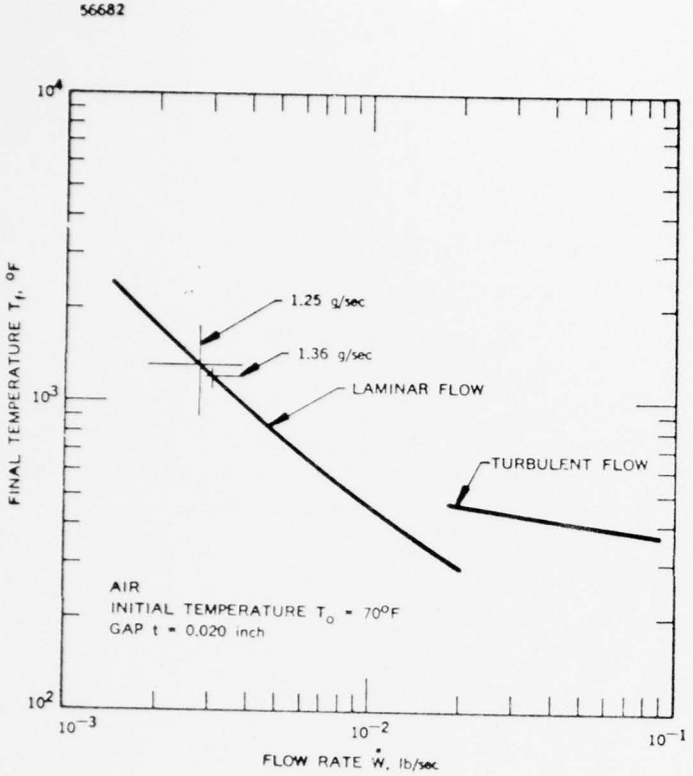



Figure 47. Final Air Temperature as Function of Flow Rate Through the Hot Cylinder

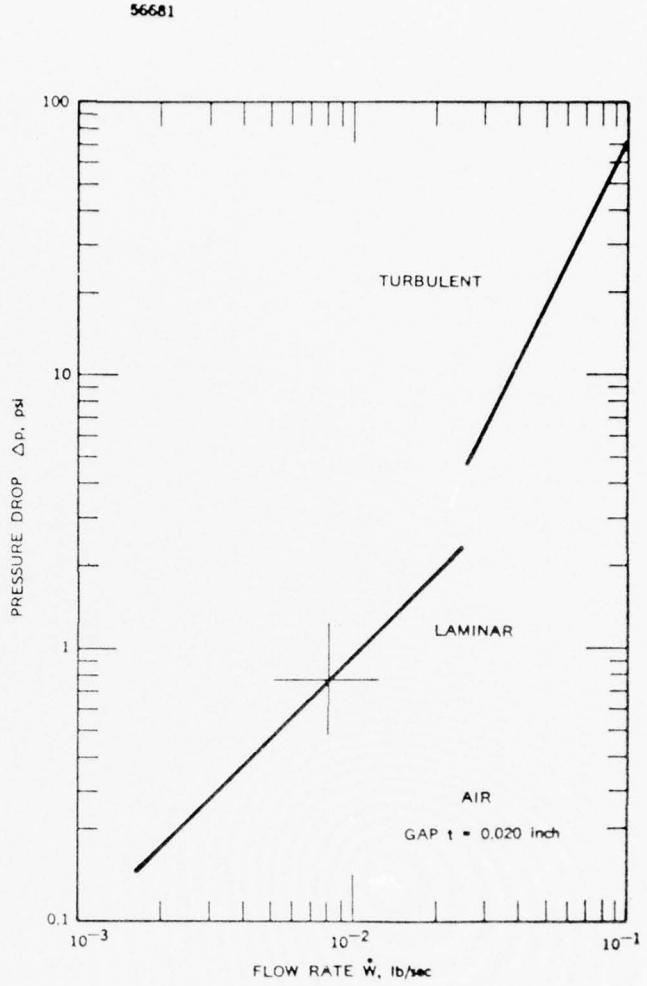



Figure 48. Pressure Drop Along the Heat Transfer Path of the Hot Cylinder of the Vuilleumier Cooler

hot cylinder, as the air will be heated to the operating temperature of the hot cylinder when flowing through the flow gap. Above 1.36 g/sec the cooling air will not reach the operating temperature of the hot cylinder. For this regime the power extraction is determined by the heat transfer to the cooling air under laminar flow conditions.

A testing problem was anticipated for the case when trying to raise the extraction rate to about twice the design rate. As can be seen from Figure 45, a heat transfer rate corresponding to 120 to 200 percent of the design extraction rate lies in a regime in which the flow is unstable for the 0.020-inch gap. Although the 0.020-inch gap is equal to the gap of the hot cylinder when mounted on the Vuilleumier refrigerator, it was anticipated to increase the gap by remachining the flow insert at a later date. This would have permitted testing at heat transfer rates above the design rates for the device. The correlations in Figure 49 indicate that, with a flow gap of 0.100 inch the hot cylinder can be tested from 50 percent of the design heat transfer without change in flow regime; i.e., the entire flow regime is turbulent. Very consistent test data should have been possible with this gap configuration. The pressure drops that were anticipated for that configuration are shown in Figure 50.

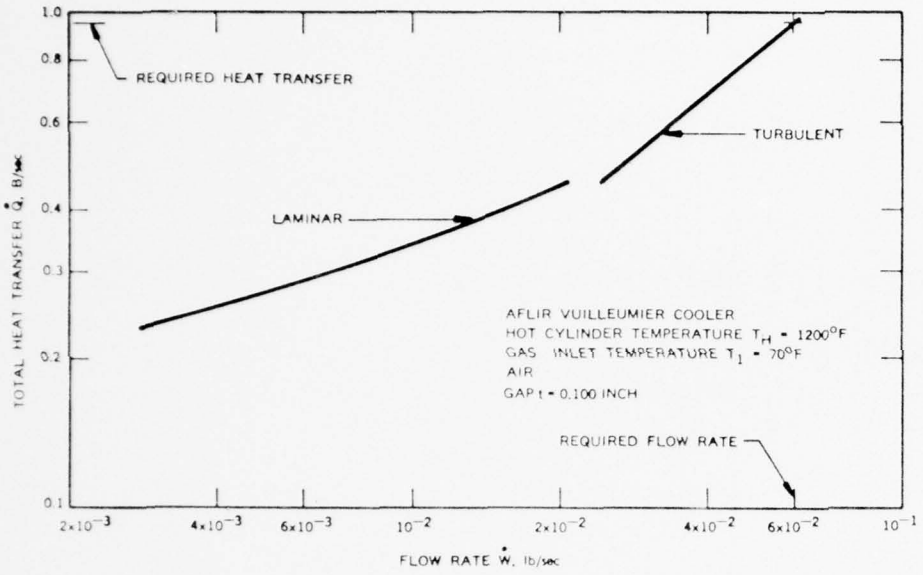



Figure 49. Flow Rate Requirement for Cooling Hot Cylinder of Vuilleumier Cooler During Thermal Energy Storage Unit Performance Test

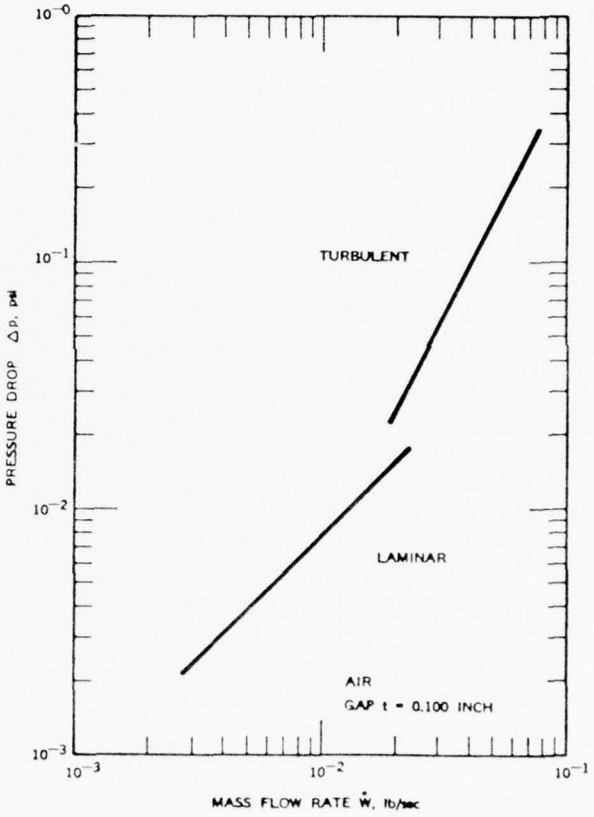



Figure 50. Pressure Drop Along the Heat Transfer Path of the Hot Cylinder of the Vuilleumier Cooler

SECTION III

# FABRICATION OF THERMAL ENERGY STORAGE DEMONSTRATION UNIT

## 3.1 MACHINING AND INITIAL ASSEMBLY

The thermal energy storage unit was fabricated from Inconel 600 sheet metal and Inconel 600 pipes according to the availability of material and the capability of manufacturers to form the required components. Figure 51 shows the machined parts in an exploded view of the thermal energy storage demonstration unit with the hot cylinder and the hold down flange. The four smaller of the five tubes were machined from pipes, while the largest was roled from 0.065-inch Inconel 600 sheet metal. The same material was used for machining the seven flanges shown.

As indicated in a prior section of this report, the original TES design had to be modified to permit manufacture of the tubes from available Inconel 600 pipes because the tube forming vendor did not want to bid on forming the smallest of the five required tubes.

The cost of manufacturing the four tubes from standard pipes instead of from sheet metal was not lower, as one might have expected. Material cost was considerably higher because only thick-walled pipes, Schedule 40, are being manufactured and stocked by the suppliers. The cost of the pipes is based primarily on the material weight of Inconel 600, which is relatively expensive.

The hot cylinder of the Vuilleumier cooler was machined from Inconel 718, $2\frac{1}{2}$-inch diameter bar stock. The inside of the hot cylinder was first rough machined removing the major amount of material. The final dimensions were obtained by the Elox process. The split hold-down flange was fabricated from stainless steel.

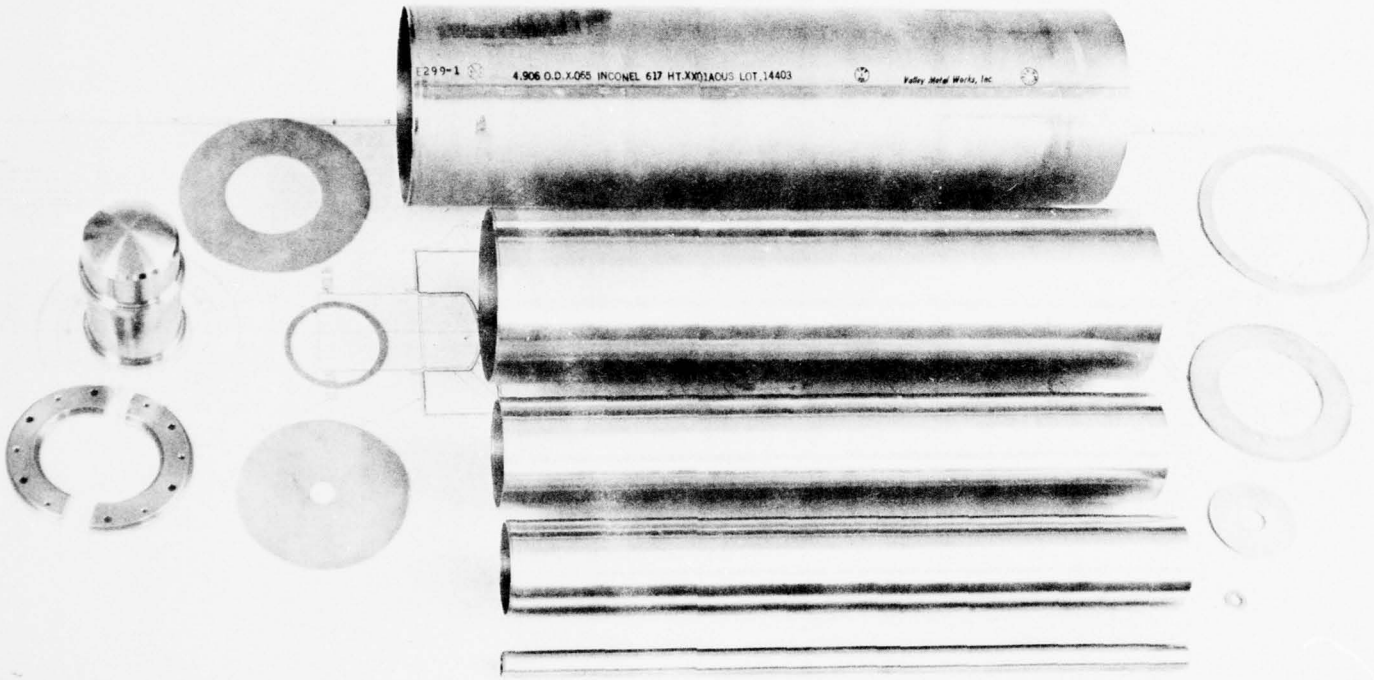



Figure 51. Exploded View of Thermal Energy Storage Demonstration Unit

The assembly of the thermal energy storage unit was initiated by electron beam welding all joints required for forming the container of the thermal energy storage material. Since the heater well walls are part of the thermal energy storage material container, the placement of the six electric heaters had to be included in the initial assembly of the unit. The six electric heaters were first wound tightly over a 2-inch diameter tube and then transferred as a unit over the inner surface of the heater well. The outer tube of the heater well was then slipped over the heaters. The installation of the heaters proved to be more difficult than had been anticipated. The 1/8-inch diameter heaters could not be wound uniformly enough to be easily accommodated even in the 0.132 inch nominal wide well.

With the thermal energy storage material container mechanically assembled and the heaters in place, the remaining welds were completed. At this stage of the assembly, the joints were checked with a helium leak detector. One joint was found faulty and had to be redone. This joint had to be welded with the heaters in place in the heater well. The extensions of the six heaters caused the electron beam to be deflected and to wander away from the joint. During weld repetition, the heater ends were shielded, thus preventing the interaction of the heater ends with the electron beam.

The thermal energy unit as it appeared at this stage of the manufacturing process and prior to its filling with the thermal energy storage material is shown in Figure 52.

## 3.2 LOADING OF THERMAL ENERGY STORAGE UNIT WITH TES MATERIAL

### 3.2.1 EVALUATION OF LOADING PROCEDURES

During the initial design of the thermal energy storage demonstration unit, it was planned to fill the unit with the thermal energy storage salt by first casting it in a casting form made of Mullite tubing. The Mullite tubing was acquired early in the program with the selected tube sizes

37614

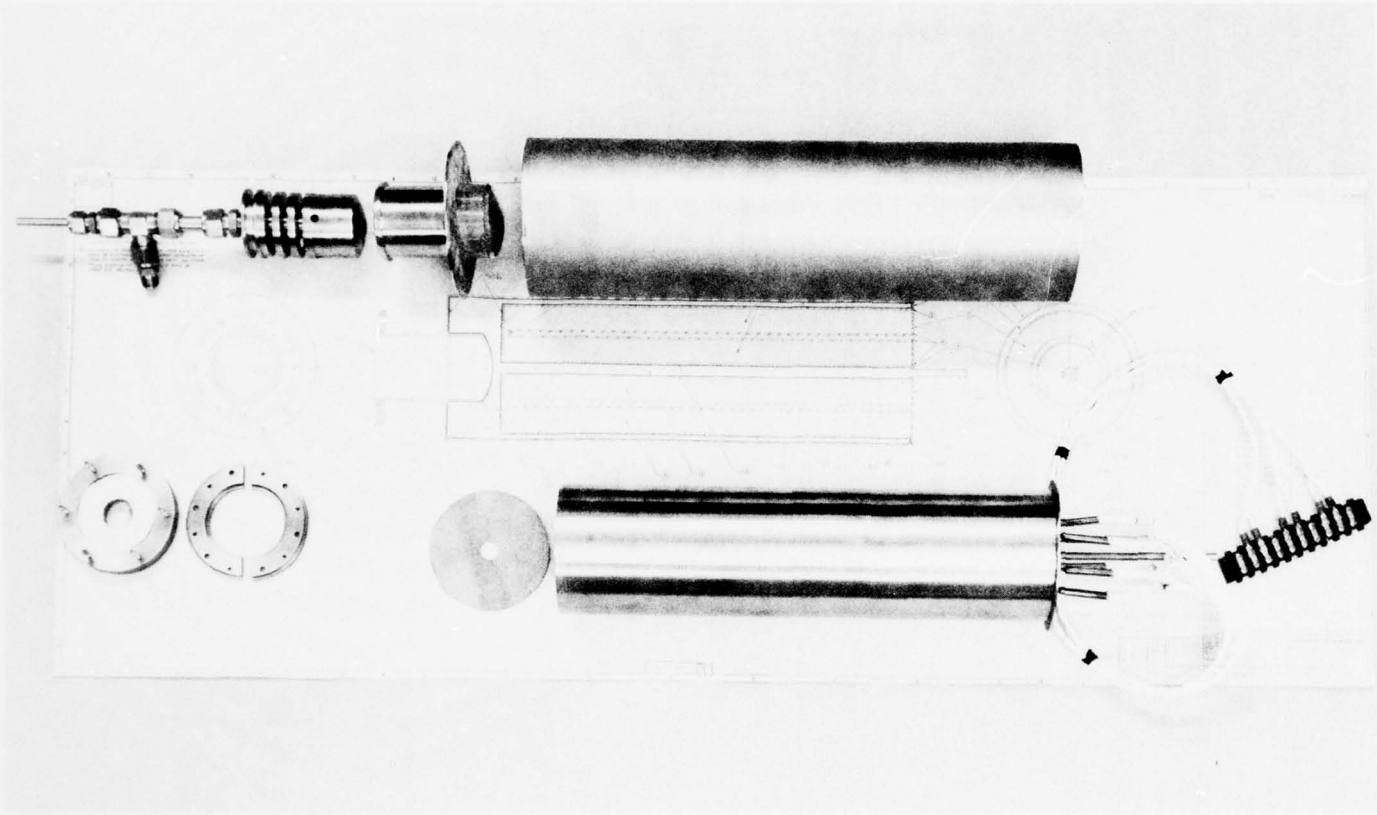


Figure 52. Thermal Energy Storage Unit Prior to Loading with Thermal Energy Storage Material

reflecting the optimum thermal energy storage unit design. When the initial thermal energy storage unit design had to be modified to reflect the availability of material, no standard Mullite tubing could be found that would permit the casting of the thermal energy storage salt to the desired sizes.

When several alternatives to filling the unit with its thermal energy material were considered, the melting of the ternary salt directly in the unit was investigated. The correct amount of the three reagent grade, chemically pure salts, LiF, $MgF_2$, and KF, which are available in powder form would be poured into the unit in their correct combination and the six heaters would be used for melting the mixture directly in the unit.

To evaluate the casting process, a small container was made of Inconel 600 tubing. The volume of the container was sized to hold 100 grams of the eutectic mixture in powder form which occupies about three times the volume of the eutectic in solid form. One hundred grams of the salt mixture in powder form was measured to occupy 92 milliliters.

The container was surrounded by a shell heater which was controlled with a variac. Two thermocouples were placed at the bottom and along the side of the container. The output of the thermocouples was read on a digital voltmeter and also continuously displayed on a chart recorder. The results of a typical melt are shown in Figure 53, indicating the smallest rate of increase in temperature at 1310$^{o}$F during the melting process. After the rate of increase in the temperature had increased again for 6 minutes the heaters were shut off.

After melting the mixture of the three components of the eutectic, LiF, $MgF_2$, and KF, the occupied volume of the container was only one-third of its total volume. Successive additions of the powder mixture to the initial melt should have made it possible to fill the container with

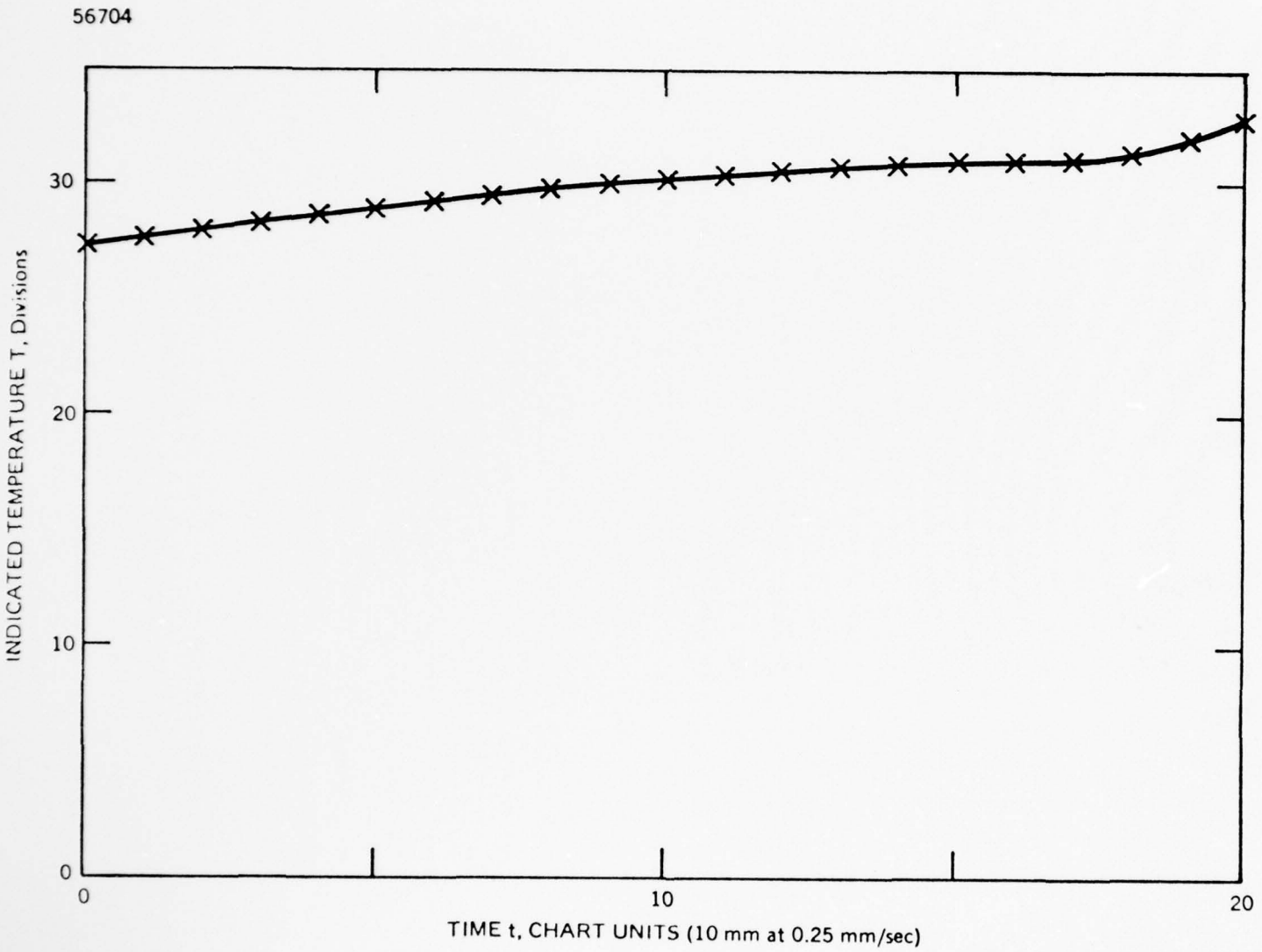



Figure 53. Temperature of Thermal Energy Storage Material Capsule During Melt-down

300 grams of eutectic salt. This proved to be correct. However, dur the filling process, the surfaces of the container at the upper edges w considerably contaminated.

Inspection of those surfaces indicated that if welding would have b intended without danger of inclusion of contaminants remachining wo have been required. The test indicated the need for rework of the TES u after filling with the TES material, if the unit would have been filled casting the material in the unit itself.

As the risk of damaging the hardware by the above outlined filling appro appeared to be high, it was decided to perform the casting in a cast fixture as had originally been intended.

### 3.2.2 CASTING OF TES MATERIAL

For the casting of the thermal energy storage salt, a casting fixture machined from graphite (grade AGSX) which was secured from Union Carb Corporation. The casting fixture was sized for casting one-third of total thermal energy storage salt in each heat in a brazing retort. casting fixture design is shown in Figures 54 and 55, while the fi machined parts of the fixture are shown in Figure 56.

The retort could be heated with an inert gas or in a hydrogen atmosphe An argon atmosphere was selected for the casting to prevent any chemi reaction with the three salts, LiF, $Mg_2F$, and KF. The temperature raised to 1350°F, which is about 40°F above the melting temperature ternary eutectic, and was held at this temperature for about 1 hour ensure full melting.

A total of four casts were made to account for a possible failure of a c and to assure sufficient amount of salt available for filling the TES u

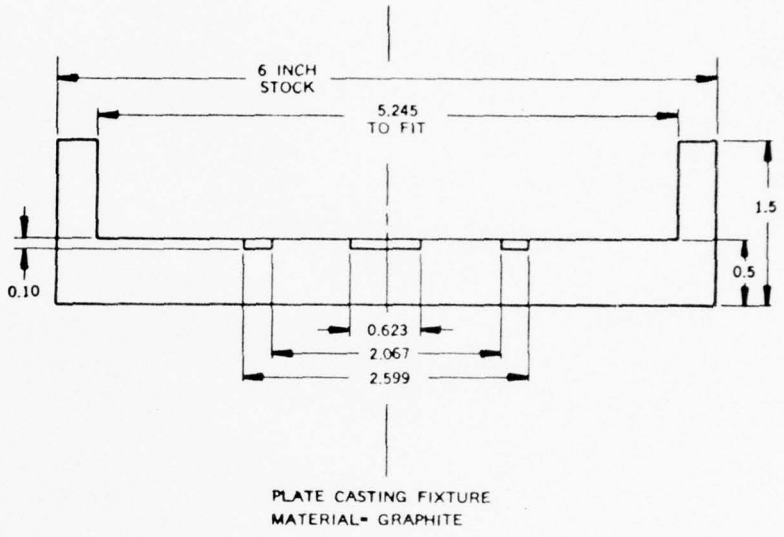



Figure 54. Bottom Plate of Casting Fixture SK2340-004-1
Material: Graphite

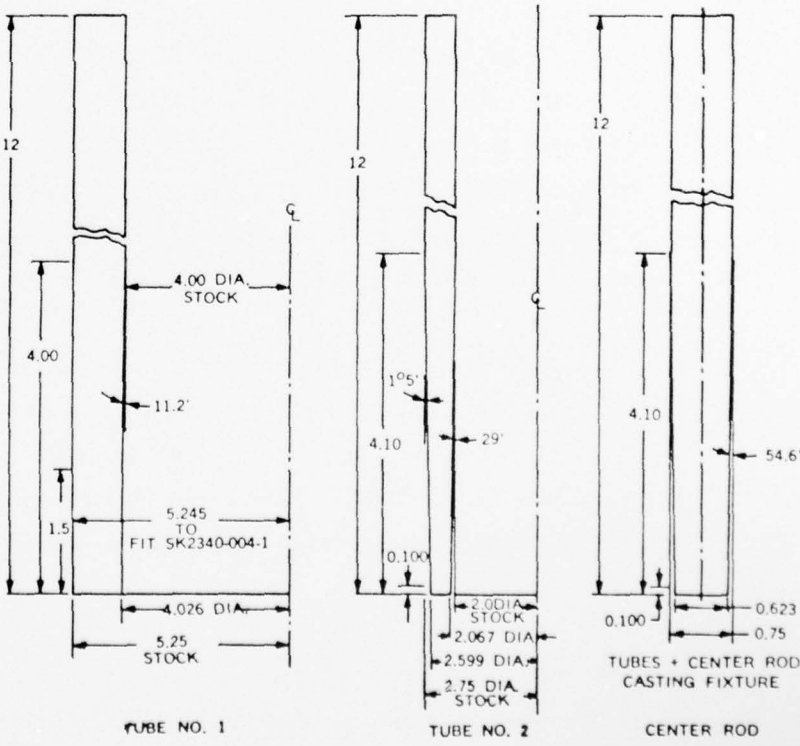



Figure 55. Tubes and Center Rod of Casting Fixture SK2340-004



Figure 56. Casting Fixture (Exploded View)

after the casting. This proved to be a very prudent precaution as cast turned out to be short by several grams. Furthermore, the resu pieces of the salt showed voids in the center. The salt appeared to solidified from the bottom as well as from the top, leaving the c portion full of voids between a large solid bottom piece and a sm solid top piece. This could have been avoided by forcing cooli proceed from the bottom of the cast, which may have been achiev forcing the inert gas around the bottom of the test fixture durin cool-down and by partially insulating the top part by increasing the of the graphite.

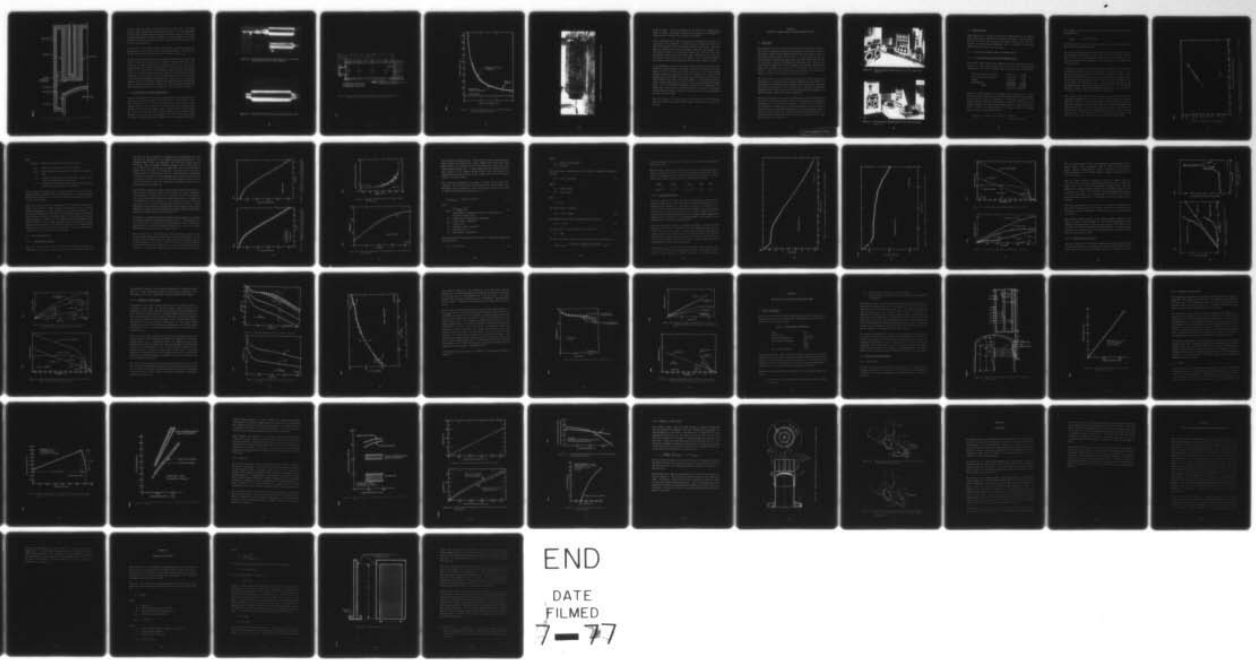
The casting process of the thermal energy storage material in this pr varied from the process used by General Electric in an earlier progra casting single solid pieces. At General Electric, the material was ca a vacuum with shell heaters surrounding the single tube. After the had become molten, the casting fixture was lowered with the he remaining in place. Thus, the lower portion of the fixture was co while the upper portion remained hot and no voids could form. This relatively expensive casting process as a vacuum chamber was contami by the very corrosive vapors of the salt and had to be thoroughly cl after its use.

## 3.3 FINAL ASSEMBLY OF THE THERMAL ENERGY STORAGE DEMONSTRATION UNIT

After the thermal energy storage demonstration unit had been loaded the cast TES material, the final two welds of the container were compl Unfortunately, at this stage of the manufacturing process it was possible to leak check the final two welds. Following the two w wicking material, consisting of several layers of bolting cloth of 70 was applied to the inner surface of the outer tube of the TES unit outer surface of the storage container, the flanges, and the hot cyli The distribution of the wick material is shown in Figure 57. Whereve wicking material was covering a heat transfer surface, the thickness c

AD-A040 895 XEROX CORP/ELECTRO-OPTICAL SYSTEMS PASADENA CALIF F/G 10/2
THERMAL ENERGY STORAGE DEMONSTRATION UNIT FOR VUILLEUMIER CRYOG--ETC(U)
FEB 77 R RICHTER F33615-75-C-2045
UNCLASSIFIED 2340-I-1 AFAPL-TR-76-110 NL

2 OF 2
AD A040895



END

DATE FILMED
7-77

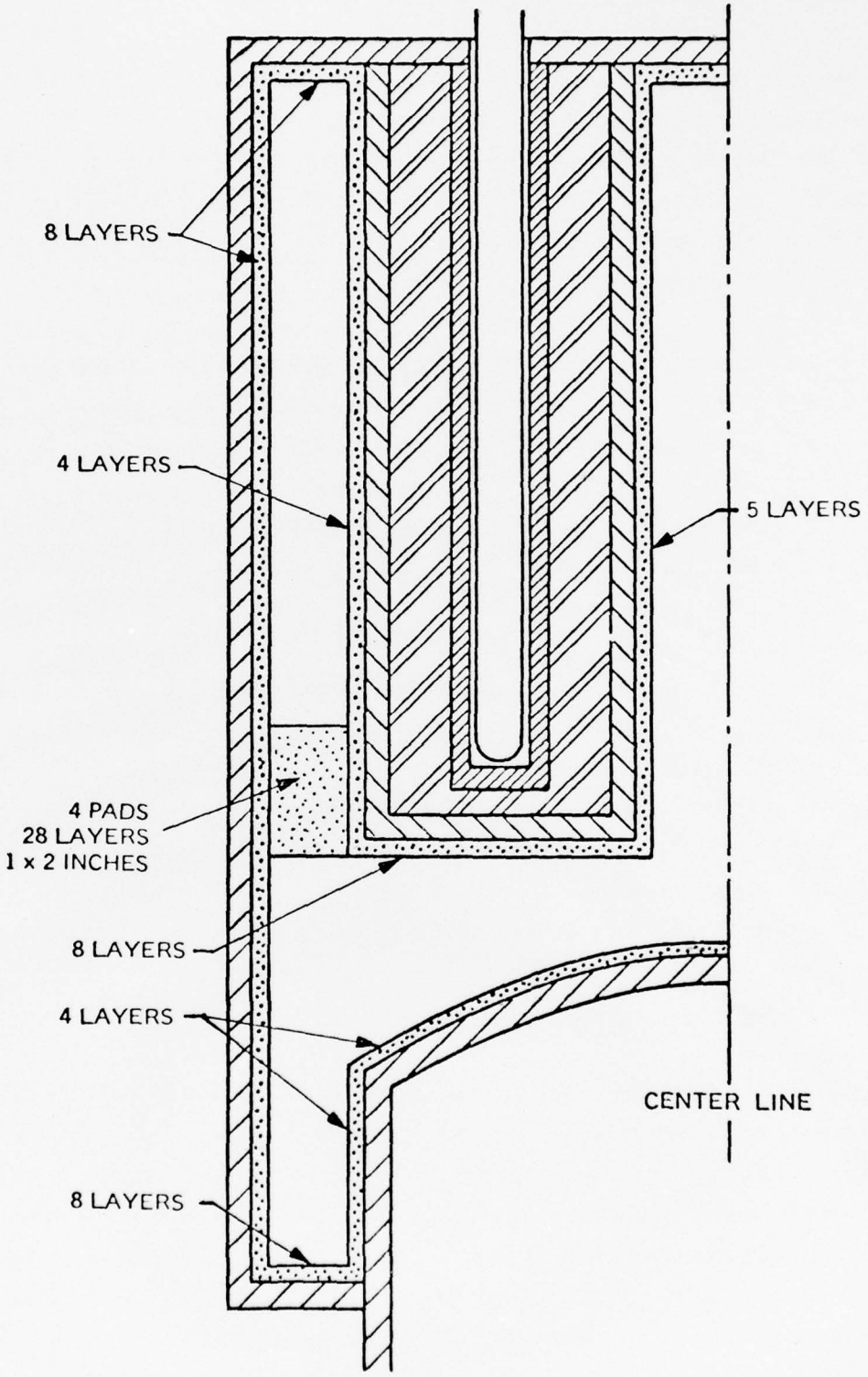



Figure 57. Distribution of Wick Material Consisting of Mesh 70 Bolting Cloth

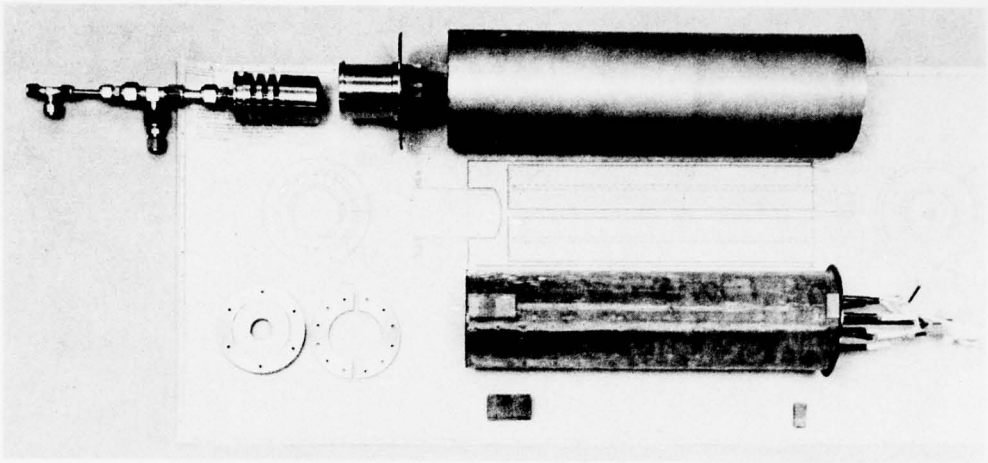
wick was made not larger than four layers of bolting cloth. All other surfaces were covered with eight layers of bolting cloth. The appearance of the thermal energy storage unit with all internal surfaces covered with the wicking material is shown in Figure 58. The locations of the eight pads which bridge the outside wick with the wick of the TES container are evident in this picture.

The assembly of the thermal energy storage unit was completed with the welding of the outer tube to the hot storage container. The completed thermal energy storage demonstrated unit is shown in Figure 59.

Sixteen nickel-chromium versus nickel-aluminum thermocouples were placed on the inside and the outside of the thermal energy storage unit. The locations of these thermocouples are shown in Figure 60. The outside thermocouples were attached to the surfaces by spot welding stainless steel ribbons to the Inconel over the thermocouple naked junctions. The thermal energy unit was then wrapped with five layers of 3/8-inch Flexible Min-K insulation and one layer of 1/2-inch 8 pound weight Cerafelt insulation. The insulation was completed with one wrap of aluminum foil. The predicted thermal losses for the thermal energy storage demonstration unit with this type of insulation are shown in Figure 61. The completely insulated TES unit ready for filling of its heat pipe with sodium is shown in Figure 62.

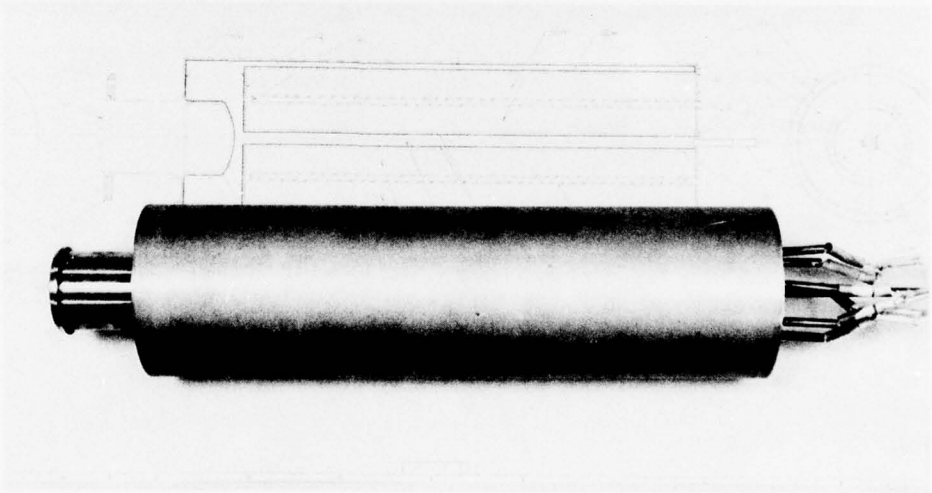
## 3.4 FILLING OF HEAT PIPE WITH WORKING FLUID

Based on the modified thermal energy storage demonstration unit design, the theoretical total wick volume was calculated to be 27.383 inches$^3$. For a wick constructed of a 70 Mesh wire screen, woven with a 0.00375 inch diameter wire, the void volume that is filled with sodium comprises 79.67 percent of the total wick volume. Thus, a sodium volume of 21.82 inches$^3$ was indicated for filling the heat pipe section of the thermal energy storage unit. At the operating temperature of 1250$^{\circ}$F, the specific weight of sodium is 0.7896 g/cm$^3$, which determined the total weight of the fill to



37626

Figure 58. TES Demonstration Unit after Application of Wicking Structure and Prior to Final Welding



4765

Figure 59. Completed Thermal Energy Storage Demonstration Unit

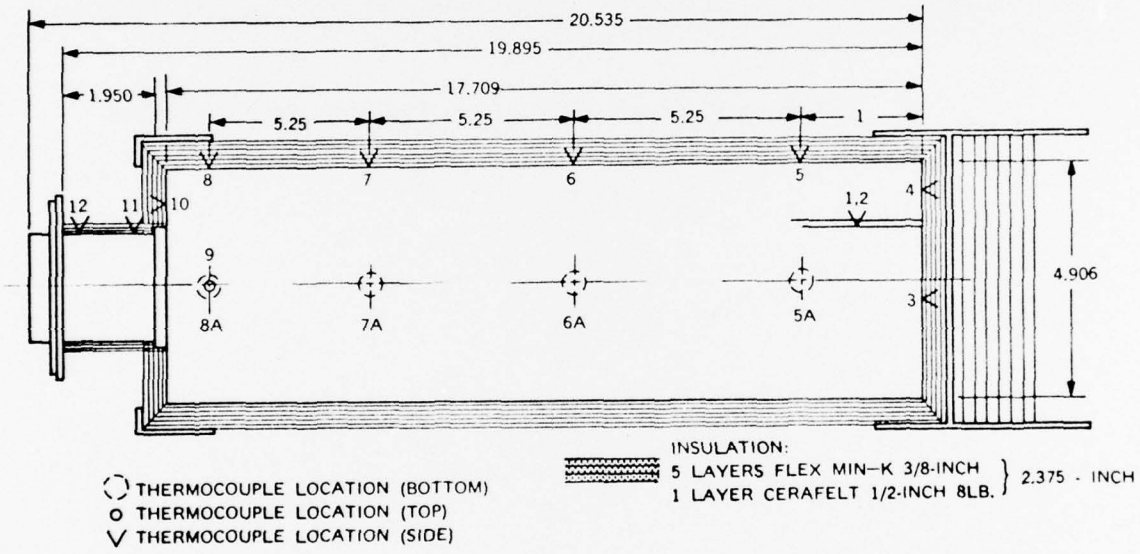
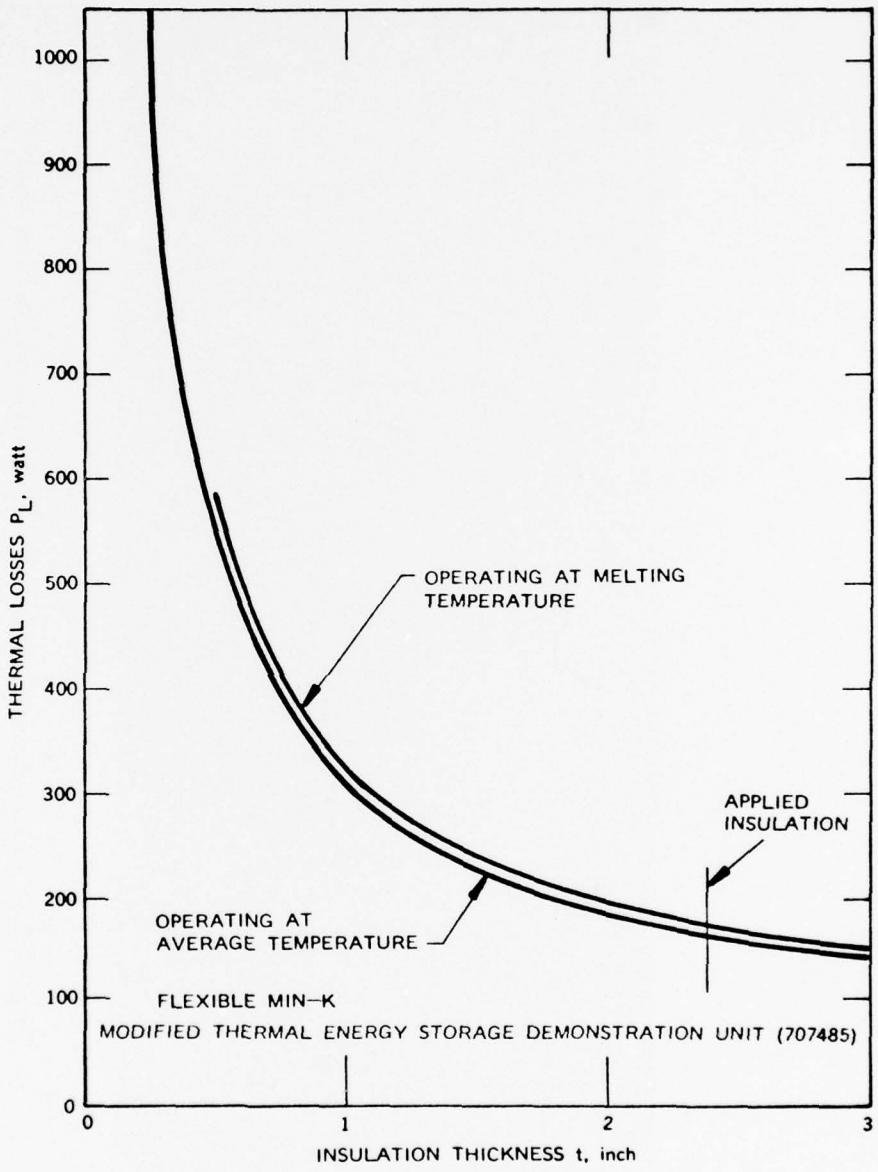



Figure 60. Insulation and Thermocouple Locations of Thermal Energy Storage Demonstration Unit for Vuilleumier Cooler Application

56754




56676

Figure 61. Predicted Thermal Losses from Thermal Energy Storage Demonstration Unt

5763

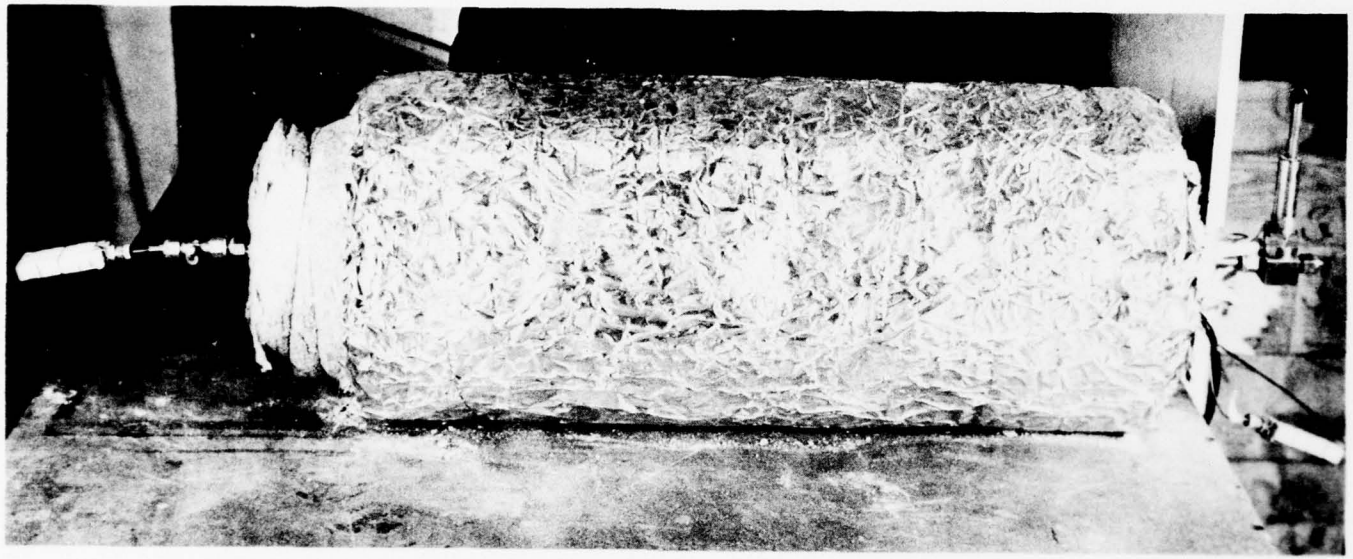


Figure 62. Fully Thermally Insulated TES Demonstration Unit

be 282.3 grams. Since the sodium was to be filled at a temperature of 320°F, at which the specific weight of the sodium is 0.913 gm/cm$^3$, a calibrated fill volume of 18.523 inches$^3$ was needed.

A fill volume was built from a stainless steel tube which had an O.D. of 1.250 inch, a wall thickness of 0.065 inch, and a length of 18.801 inch. The tube was weighed prior to and after filling it with sodium. The total amount of sodium in the tube was slightly more than 282.3 grams (i.e., 284.8 grams) because of the additional volume in the 1/4-inch tubes at the top and the bottom of the fill volume. After transferring the sodium into the thermal energy storage unit, the weight of the fill volume indicated that the heat pipe section had been filled with 281.1 grams of sodium.

It was attempted to fill the heat pipe section fairly accurately with the calculated required amount of sodium, although realistically the exact amount of sodium needed could not be verified until the thermal energy storage unit had been operated. Of all the individual wick volumes which comprise the total volume of the sodium, the eight layers of screen on the inner surface of the outer tube is the largest. Its calculated volume is 15.631 inches$^3$ comprising 57.1 percent of the total calculated wick volume alone. As it is difficult to achieve a perfect wick of consistent void volume with bolting cloth, the required amount of sodium for filling the the wick without surplus or dryness in certain areas has to be established by testing the heat pipe.

With the filling of the heat pipe with the working fluid the fabrication tasks were completed and the thermal energy storage unit was ready for testing.

SECTION IV

TESTING OF THERMAL ENERGY STORGE DEMONSTRATION UNIT

## 4.1 TEST SETUP

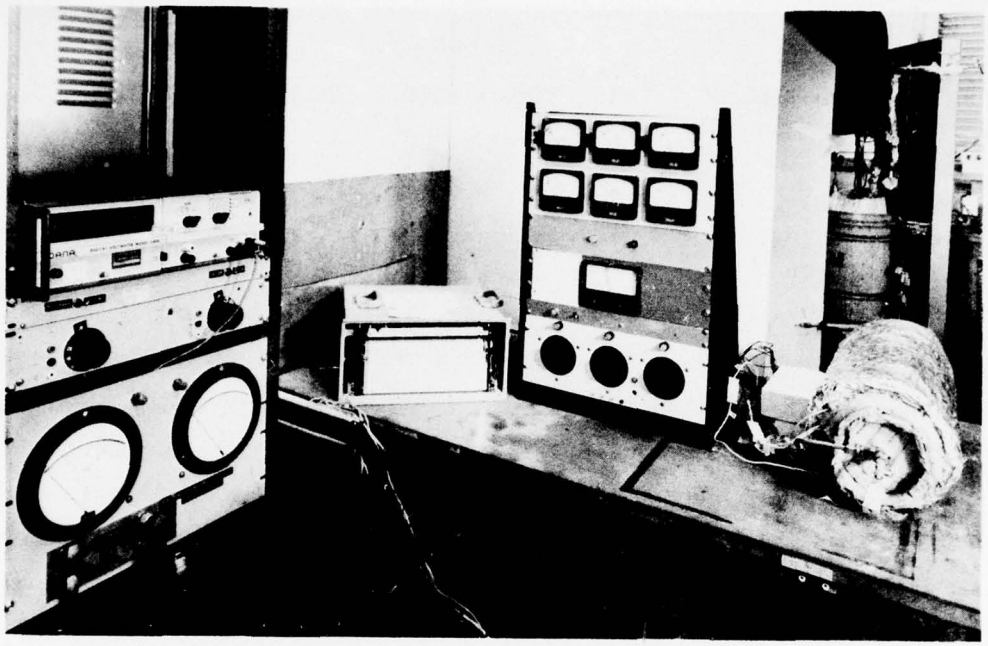
With completion of its fabrication the Thermal Energy Storage Demonstration Unit was integrated into the test setup which is shown in Figure 63. The thermal energy storage demonstration unit had been supplied with six individual heaters grouped in sets of two. The two heaters in each set were operated in parallel with each other, with their power being controlled by a variac. The average resistance of each heater was 18 ohms, so that at an applied voltage of 110 volts the power input was about 672 watts per heater for a possible total power input of about 4000 watts with all six heaters. Thus, even with only two heaters operating, it was possible to charge the thermal energy storage unit within one hour.

The three variacs could be adjusted and their power output determined by three sets of 1 percent full scale accurate ammeters and voltmeters. For controlling the temperature of the thermal energy storage unit, a temperature controller was used to turn off the power to the unit if the preset temperature was exceeded and to turn on the power when the temperature of the unit dropped below a preselected temperature.

While the temperature of all sixteen thermocouples could be determined from the output of a digital voltmeter, twelve of the temperatures were recorded continuously on a 24 point chart recorder. The gas flow for cooling the hot cylinder was controlled by the upstream pressure of a sonic orifice, and by observing the pressure downstream of the orifice to assure that, at all times during a test, sonic conditions at the orifice would exist. The pressures were measured with 1/2 percent accurate Bourdon pressure gages which can be seen in Figure 64.



PRECEDING PAGE BLANK-NOT FILMED



5762

Figure 63. Thermal Energy Storage Demonstration Unit Test Setup (View I)



5761

Figure 64. Thermal Energy Storage Demonstration Unit Test Setup (View II)

## 4.2 INITIAL TESTING

After completion of the test setup and the instrumentation of the thermal energy storage unit, testing of the unit was initiated. The first objective was to measure the steady state thermal losses from the unit as a function of the operating temperature, and to determine the effective thermal capacity of the unit, $(W\ c_p)_{eff}$.

### 4.2.1 STEADY STATE THERMAL LOSSES AND THERMAL CAPACITY

#### 4.2.1.1 Time Constant and Steady State Thermal Losses

The thermal energy storage unit comprises the main structure, the wick material, the heat pipe working fluid, sodium, and the thermal energy storage salt. The effective thermal capacities of the four components are:

| | | |
|---|---|---|
| Structural Material (Inconel) | 1.865 B/$^{o}$F | 27.80% |
| Thermal Energy Storage Salt | 4.459 B/$^{o}$F | 66.48% |
| Sodium | 0.190 B/$^{o}$F | 2.88% |
| Wick Material | 0.193 B/$^{o}$F | 2.83% |
| Total | 6.707 B/$^{o}$F | 100.00% |
| | $7.076 \times 10^{3}$ joules/$^{o}$F | |

During the solidification of the thermal energy storage salt, a total amount of thermal energy of $4.32 \times 10^{6}$ joules was expected to be released. It was predicted that the temperature of structural components of the thermal energy storage unit would decrease from 1275$^{o}$ to 1235$^{o}$F, while the average temperature of the thermal energy storage salt would decrease from 1310$^{o}$ to 1270$^{o}$F. The contribution of the sensible heat of the thermal energy storage unit would therefore be

$$E_{sensible} = 4.459 \times 40 + 2.248 \times 50 = 290.76B$$
$$= 0.307 \times 10^{6} \text{ joules}$$

This compares with the assumed total latent heat of the thermal energy storage salt of

$$E_{latent} = 4.32 \times 10^6 \text{ joules.}$$

The contribution of the sensible heat would thus be only 6.63 percent of the total thermal energy released.

The steady state heat losses from the thermal energy storage unit were to be obtained by correlating the power input with the steady state temperature of the unit. For predicting the time that would be required to bring the unit to steady state conditions, the time constant for the system had to be estimated.

The thermal losses at the average operating temperature of $1250^{o}F$ of the thermal energy storage unit were calculated to be about 180 watts. These losses are slightly higher than those shown in Figure 21. Thermal losses from the fill valve, which was to be left on the unit until the operation of the unit had been verified, and the heat losses at the hot cylinder end had to be added to the calculated losses. The effective time constant was estimated from the calculated thermal capacity of $7.076 \times 10^3$ $j/^{o}F$ and the predicted thermal losses at the operating temperature, i.e., 180 watt at $T = 1250^{o}F$, to be $t = 46.25 \times 10^3$ sec or 12.85 hours.

This indicated that the unit would require about two days to reach its steady state temperature at each test point. The test results are shown in Figure 65. Because of the long time constant, the plotted values are not absolutely accurate, as it would have required a considerably longer time than was available to obtain true steady state data. The process was speeded up by establishing the temperature loss correlation, estimating the losses at a given temperature, and adjusting the input power of the heaters to equal these losses when a given temperature was reached.

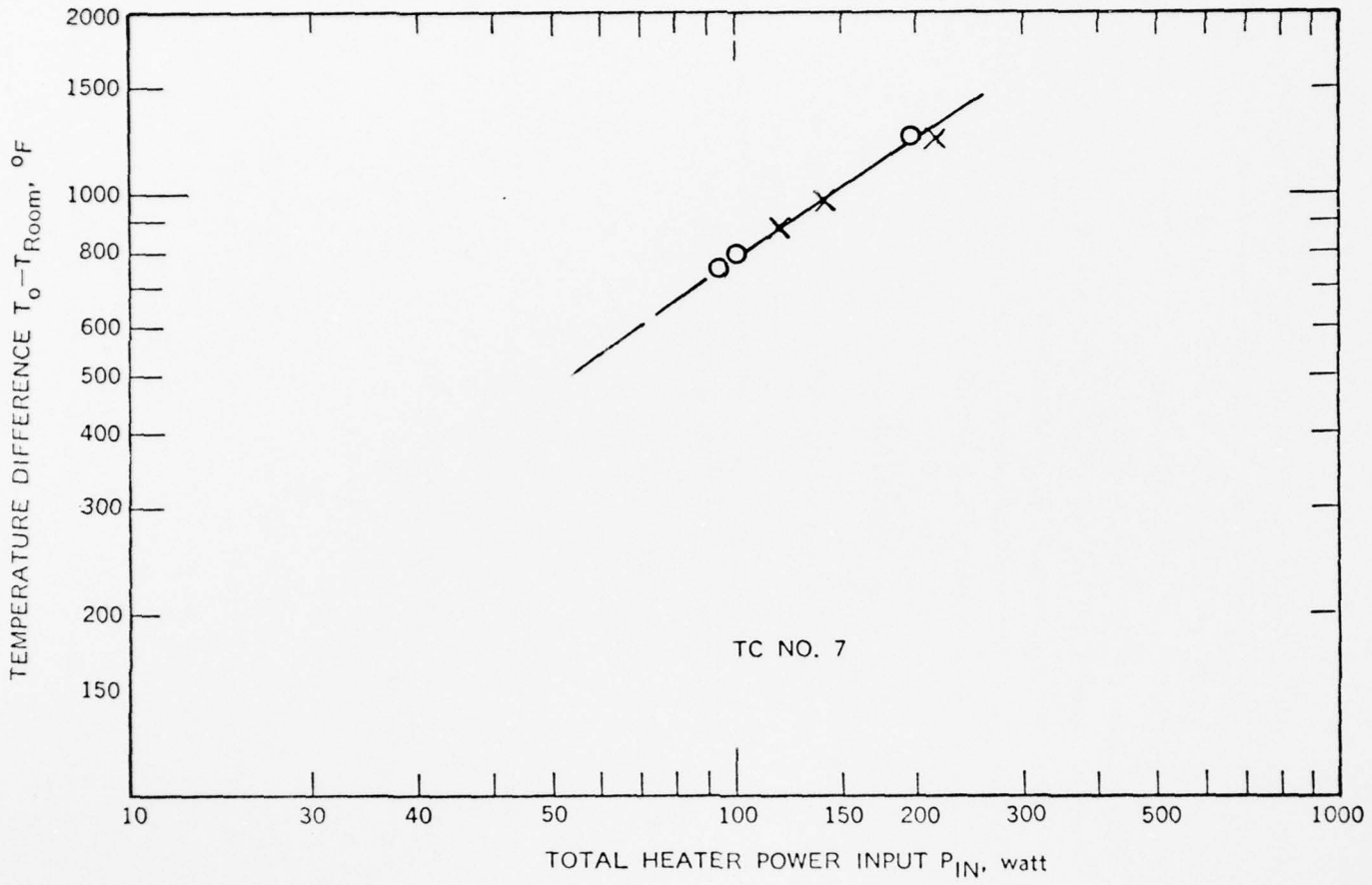
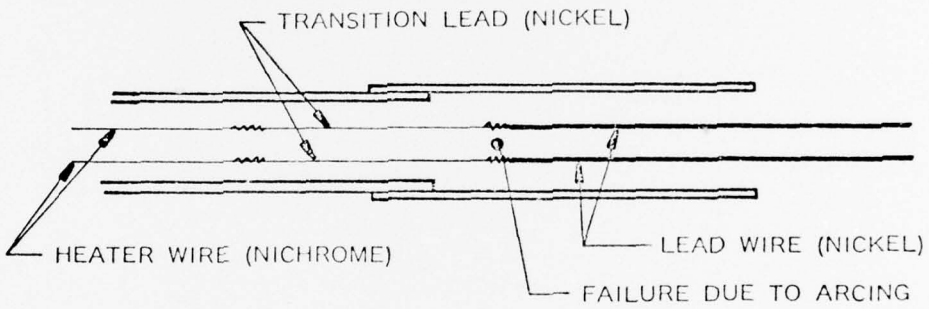



Figure 65. Energy Loss from Thermal Energy Storage Demonstration Unit (Insulation: 5 Layers 3/8-inch Flex Min-K, 1 Layer 1/2-inch 8 lb Cerafelt, 1 Sheet Aluminum)

During these initial tests, one of the three heater sets was used to supply the steady state power while the other two sets were employed to raise the temperature level. When the power of the two sets of heaters was raised for an average power output per heater of 162 watts (this compares with a design power output of 672 watts), three heaters failed almost simultaneously. Inspection of the heaters indicated that all three heaters had failed in the very same mode. Arcing between the two wires of each heater had occurred at the location where the transition wire had been welded to the lead wire, as shown in the sketch below.




56949

The heater vendor was contacted. Upon reviewing the heater design, the responsible manager conceded that a "human error" had occurred in the manfacturing process. It was felt that the remaining three heaters would not survive the planned testing, and that it would be appropriate to replace all heaters immediately with new heaters.

All six heaters were pulled out of the well after removing the insulation. New heaters from a different vendor were ordered and shipped from the east. Although the new heaters had the same power capacity as the original heaters, their power loading was considerably higher than that of the original heaters because each heater was only 29 inches long. This compared with the 70 inch length of the original heaters. Each heater was

bent into a hair pin and pushed into the heater well of the thermal storage unit. After replacing the insulation, testing of the thermal energy storage unit was continued.

During testing of the thermal energy storage unit, two of the six heaters of the second set of heaters failed by shorting internally to a dead short, although remaining isolated from the sheath. The vendor of the heaters was contacted who explained the failure by an accumulation of moisture at the cold end of the heater (i.e., the non-heated extension of the lead wires) where the short between the two lead wires occurred. He asked for the return of all six heaters for repair without charge. It was agreed that the heaters would be returned after completion of testing with the remaining four heaters. Since each heater had a capacity of over 1700 watts, ample capacity remained for continuing testing. The steady state heat loss data were found not to vary substantially from the original test data; indicating that the insulation was the same as before. The heat loss could be expressed as a function of temperature by

$$P_L = A(\Delta T)^n$$

where

$P_L$ = power loss, watt
$A$ = $3.318 \times 10^{-3}$
$n$ = 1.546
$\Delta T$ = temperature difference $T_o - T_{room}$, $^oF$

4.2.1.2 Thermal Capacity

With the correlation of the thermal losses against the operating temperature known, the effective thermal capacity of the thermal energy storage unit could be determined by the relation

$$(c_p W)_{eff} = \frac{\left(P_{in} - A \times (\Delta T)^n - P_{out}\right) dt}{dT}$$

where

$(c_p W)_{eff}$ = Effective sensible heat of the entire unit

$P_{in}$ = Power input supplied by the electric heaters

$P_{out}$ = Power extracted through the hot cylinder by cooling gas flow

A,n = Constants determined from steady state energy losses from the thermal energy storage unit

$\Delta T$ = Temperature difference between thermal energy storage unit temperature and ambient temperature

This relation was computerized to permit calculation of the effective thermal capacity, thermal losses, and power output. The required input data were the electrical power input and operating temperature of the unit at given time intervals.

Below and above the eutectic temperature of the thermal energy storage material the effective thermal capacity was expected to be relatively constant showing only a slight increase with increasing temperature. At the eutectic temperature, the effective heat capacity should, in the ideal case, approach infinity, as thermal energy is either stored or absorbed without increase in temperature. The computer program was expanded to also permit calculation of the energy extracted from or stored by the thermal energy storage material and the structural material of the thermal energy storage unit, and the total thermal energy extracted as a function of the temperature or the thermal energy storage unit.

### 4.2.2 TEST DATA EVALUATION

#### 4.2.2.1 Sensible Heat Capacity

After the initial tests, which provided the correlation between the temperature of the thermal energy storage unit and the thermal losses from

the unit, the unit was heated to a temperature that was assumed to be below the eutectic temperature of the thermal energy storage material. The maximum measured heater well temperature was 1303°F with a power input of 214 watts. Thus, no storage of thermal energy in form of latent heat of fusion should have occurred and all energy that would be released due to thermal losses from the unit through the insulation would be the total sensible heat of all materials of the unit. By determining the temperature of the unit as a function of time and applying the relation shown on page 42 it should be possible to verify the calculated thermal capacity of the unit, which must be known for evaluating the thermal capacity of the thermal energy storage material.

The measured correlations between thermal energy storage temperature and time are shown in Figures 66 and 67. The plotted test results immediately indicated that the temperatures do not correlate in the expected manner. Due to the higher thermal losses at the higher temperatures, a steeper drop in temperature at the beginning of the cooling cycle would have been predicted if the unit had a relatively constant thermal capacity. On the other hand the data indicated a much larger thermal capacity at the higher temperature. When the data were reduced, the thermal capacity was found to increase with temperature as shown in Figure 68.

In Figure 69, the temperatures of the thermal energy storage unit are shown as they were measured during the heating of the unit. The appearance of the heating curve is very similar to the appearance of the cooling curves, indicating that the effective thermal capacity of the unit is the same whether measured during cooling or during heating.

The test data made it appear that the effective thermal capacity of the thermal energy storage unit increased with increasing temperature. At the average operating temperature of T = 650°F, the effective thermal capacity of the unit appeared to be $7.22 \times 10^3$ joules/°F. This compared with the predicted effective thermal capacity of $7.1 \times 10^3$ joules/°F, a variation of 1.7 percent. The abnormal behavior was evident from the cooling curves as

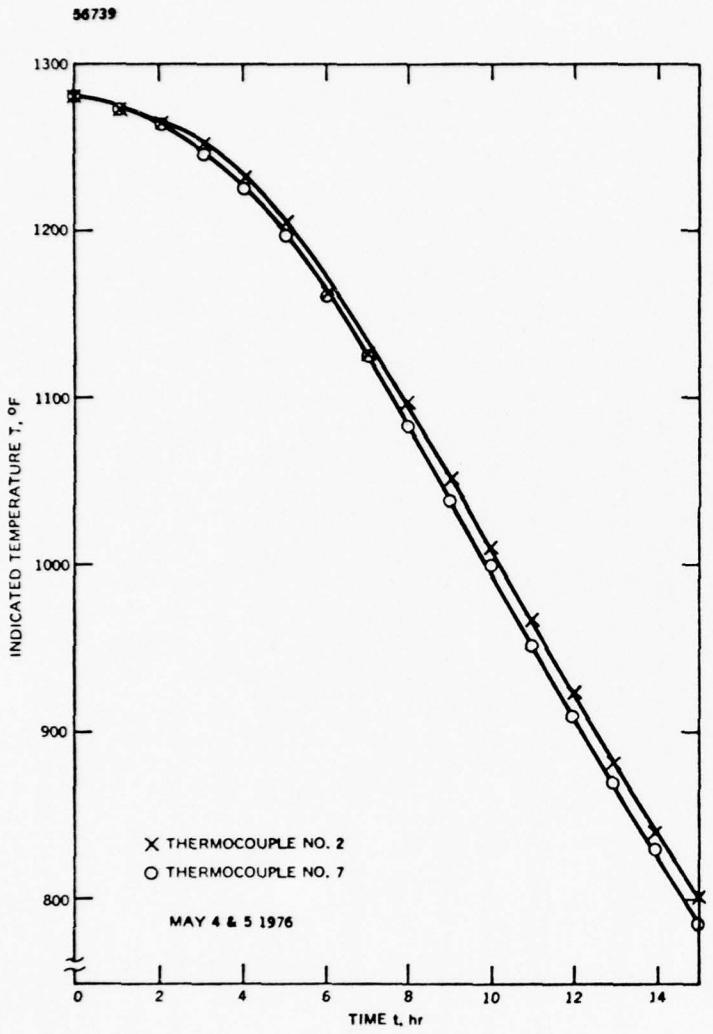



Figure 66. Temperature of Thermal Energy Storage Demonstration Unit During Cool-down

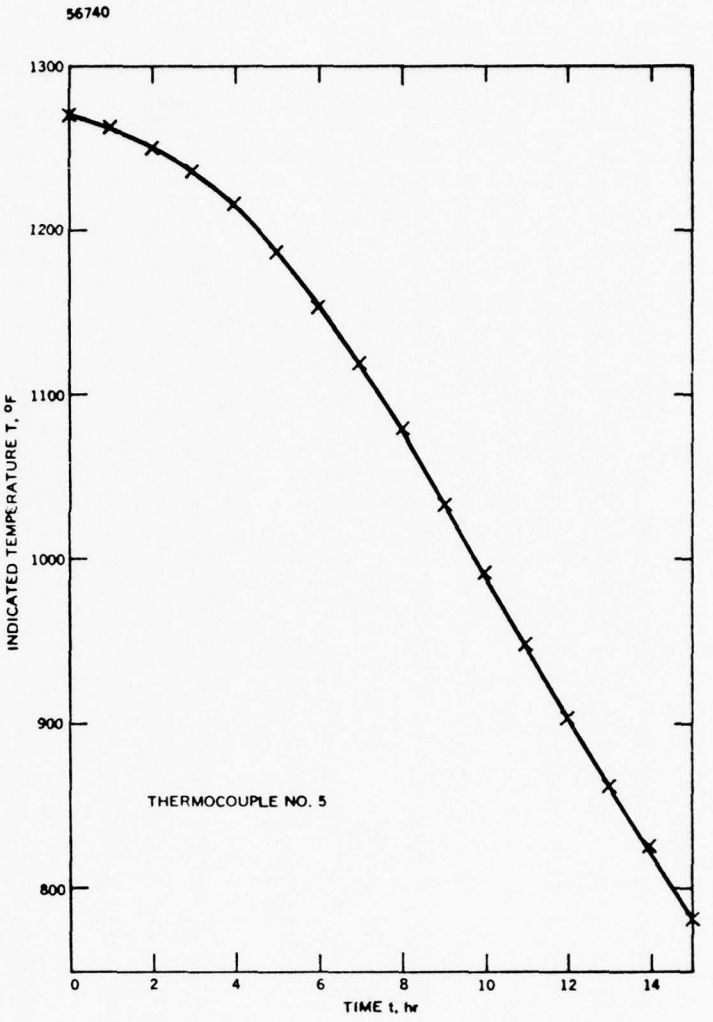
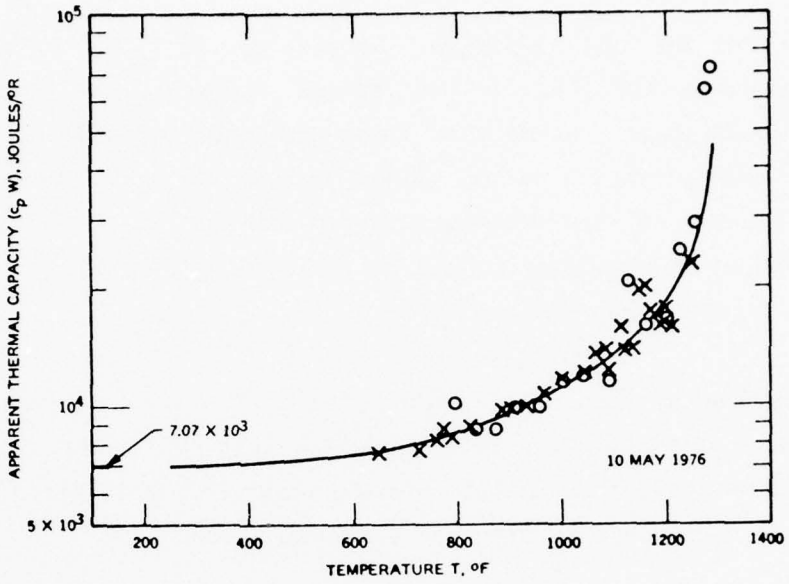
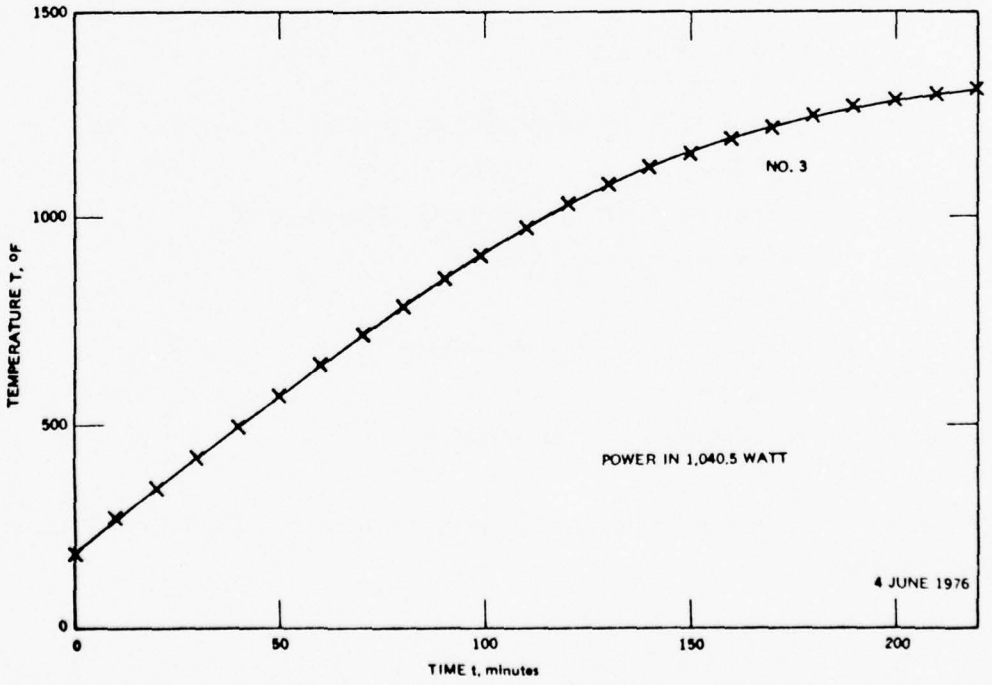



Figure 67. Temperature of Thermal Energy Storage Demonstration Unit During Cool-down




56724

Figure 68. Apparent Thermal Capacity of Thermal Energy Storage Unit




56737

Figure 69. Measured Temperature of Thermocouple No. 3 During Charging of TES Unit

well as from the heating curves. Despite the fact that no melting should have occurred, the slope of the curves changed their trend only below 950°F, which lies considerably below the reported melting point of the thermal energy storage salt. It was thought that the variable effective heat capacity of the thermal energy storage unit could possibly be explained by the varying amount of the working fluid of the heat pipe, sodium, in the vapor state.

With increasing temperature, the amount of sodium in the vapor state increases. The effective total specific heat of the sodium vapor due to evaporation and/or condensation in the vapor volume is given by the change of latent heat capacity with temperature, i.e.,

$$(W\, c_p)_{\text{eff Na}} = dC_{Na}/dT \text{ joules/}^{\circ}K \tag{1}$$

*where*

$$C_{Na} = \frac{\Delta H \times p_v \times V \times M}{RT} \tag{2}$$

$C_{Na}$ = latent heat of evaporation content of sodium vapor in the vapor volume, joules

$\Delta H$ = latent heat of evaporation, joules/gram

$p_v$ = vapor pressure, dynes/cm$^2$

$V$ = volume, cm$^3$

$M$ = molecular weight, grams/mole

$T$ = temperature, $^{\circ}K$

$R$ = gas constant, ergs/$^{\circ}K$-mole

The vapor pressure of sodium can be expressed as a function of temperature by the relation

$$p_v = A \exp(-E/T) \tag{3}$$

where

$$A = 3.363 \times 10^{10} \text{ dynes/cm}^2$$

$$E = 11973.4^{\circ}K$$

The latent heat of evaporization can be found by employing Clapeyron's relation

$$\Delta H = T(v_1 - v_2)\, dp_v/dT \tag{4}$$

where

$v_1$ = vapor volume

$v_2$ = fluid volume

Since

$$v_1 \gg v_2$$

the relation can be reduced to

$$\Delta H = T \times v_1 \times dp_v/dT \tag{5}$$

By differentiating relation 3 and employing the relation

$$p \times v = RT/M \tag{6}$$

the latent heat of evaporization can be found to be

$$\Delta H = RE/M \tag{7}$$

The effective thermal capacity of the sodium can then be expressed by

$$(c_p W)_{\text{eff Na}} = \frac{E \times (E/T - 1) \times V \times A \times \exp(-E/T)}{T^2} \text{ ergs/}^{\circ}K$$

The total volume V, of the vapor in the heat pipe of the unit was calculated to be 1243.9 $cm^3$.

When the above relation was evaluated, as shown in the following tabulation, the change of state of the sodium was found to have only a minor effect on the apparent thermal capacity of the entire system. It could not explain the observed change in thermal capacity of the system.

| T, $^oK$ | 300 | 500 | 750 | 1000 |
|---|---|---|---|---|
| $c_pW$, $j/^oK$ | $1 \times 10^{-10}$ | $1.8 \times 10^{-4}$ | 0.16 | 3.48 |

4.2.2.2 Latent Heat Capacity

After the completion of these initial tests, the temperature of the thermal energy storage unit was increased above the melting temperature of the thermal energy storage salt. The electric power to the heater was then turned off and the unit was permitted to cool solely by the losses through the insulation. The results of that test are shown in Figures 70 and 71. It can be seen that the solidification of the thermal energy storage salt started when the temperature of the thermocouple on the outside of the thermal energy storage unit reached 1280$^oF$.

When the data were reduced to determine the amount of thermal energy extracted from the unit as function of time and temperature, the distribution of the total energy between sensible heat and phase change energy as shown in Figures 72 and 73 were found. The results seemed to indicate that the total phase change energy, which had been expected to consist primarily of the fusion energy of the thermal energy storage material, was not released within a $\pm 25^oF$ temperature range.

The thermal energy storage unit design called for a thermal energy storage of $4.32 \times 10^6$ joules in the form of fusion energy. The amount of thermal energy storage material required was based on a fusion energy of

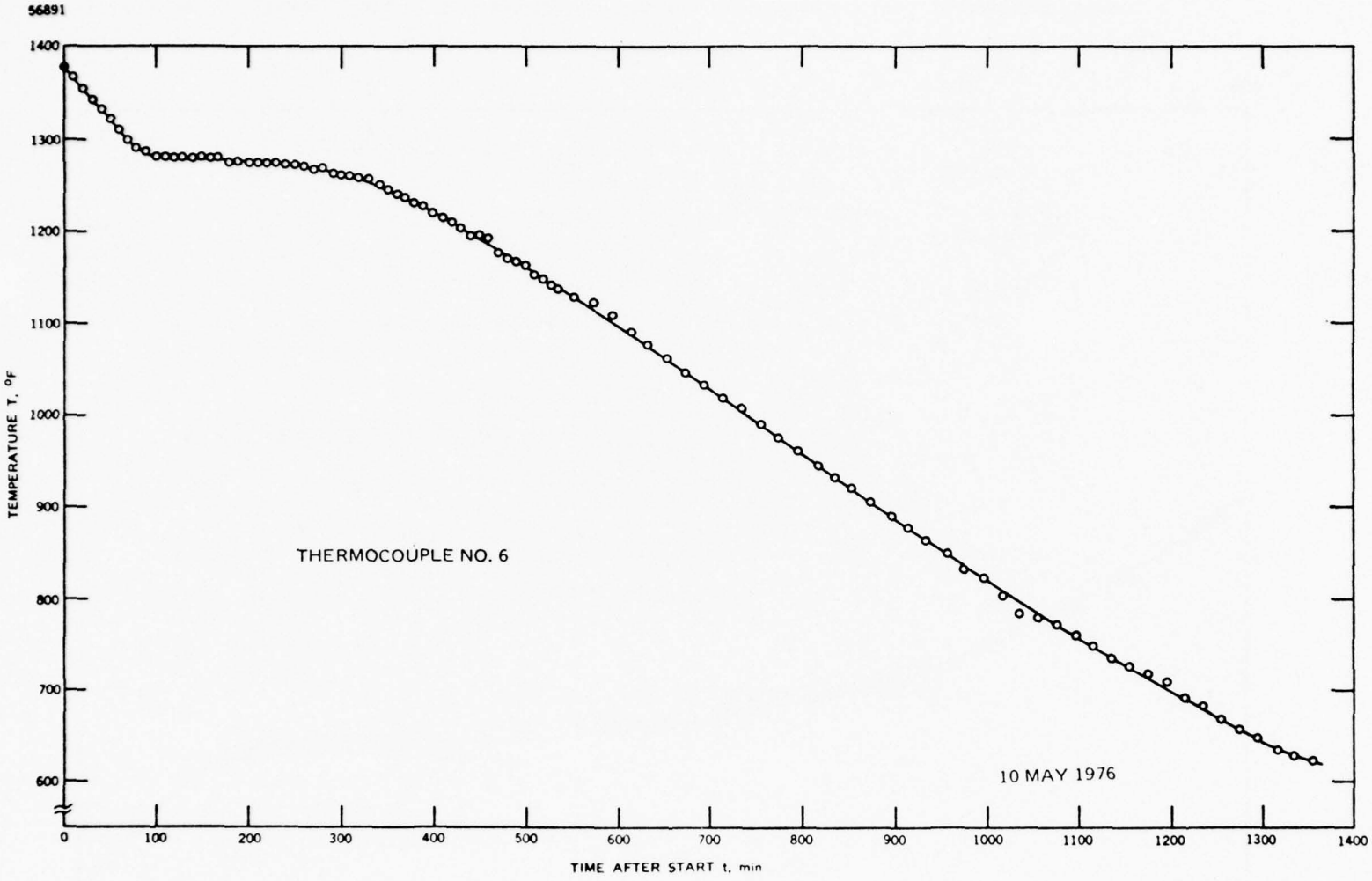



Figure 70. Cooling Data of Thermal Energy Storage Unit (Thermal Losses Only)

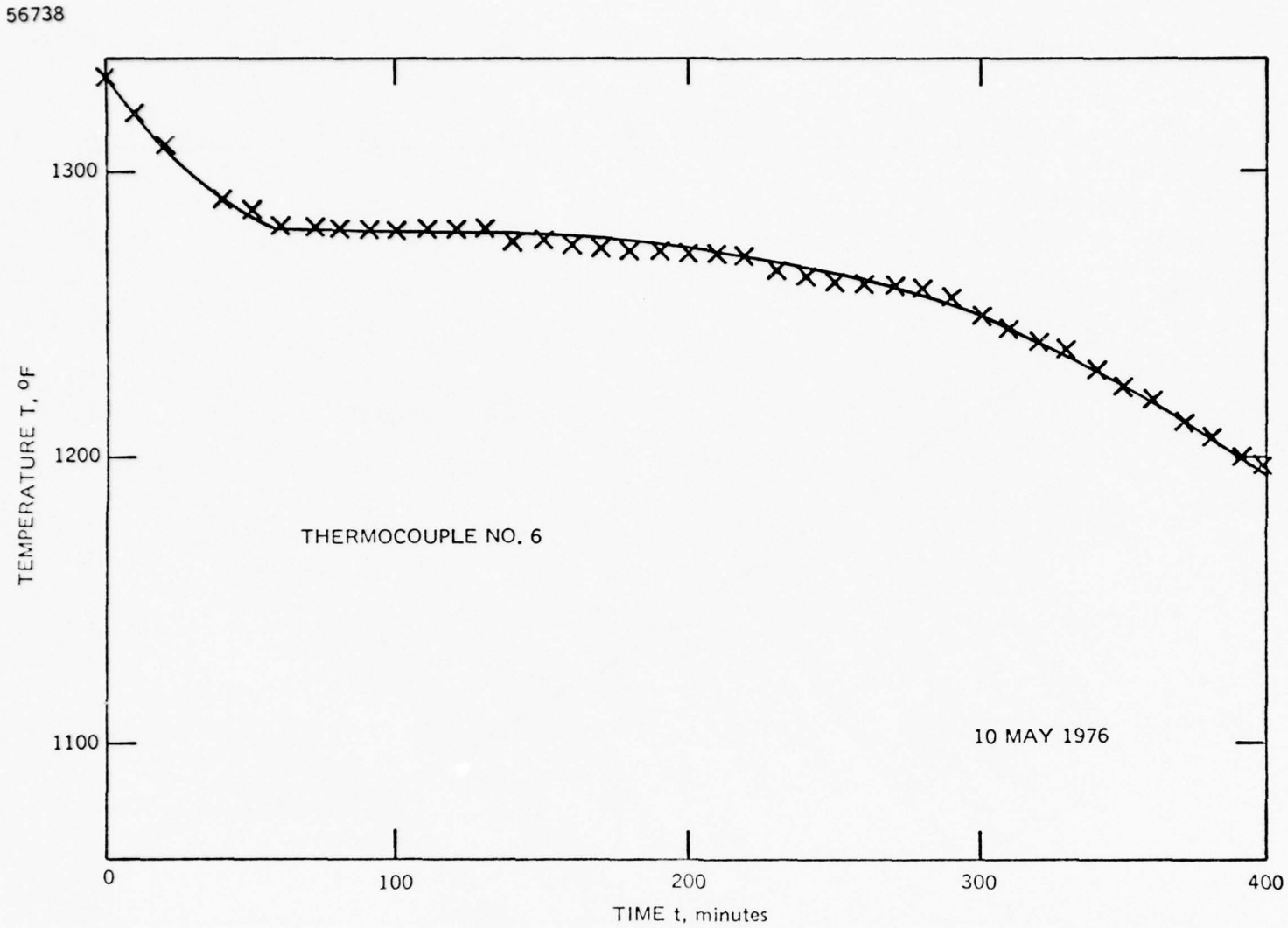



Figure 71. Temperature of Thermal Energy Storage Demonstration Unit During Cool-down

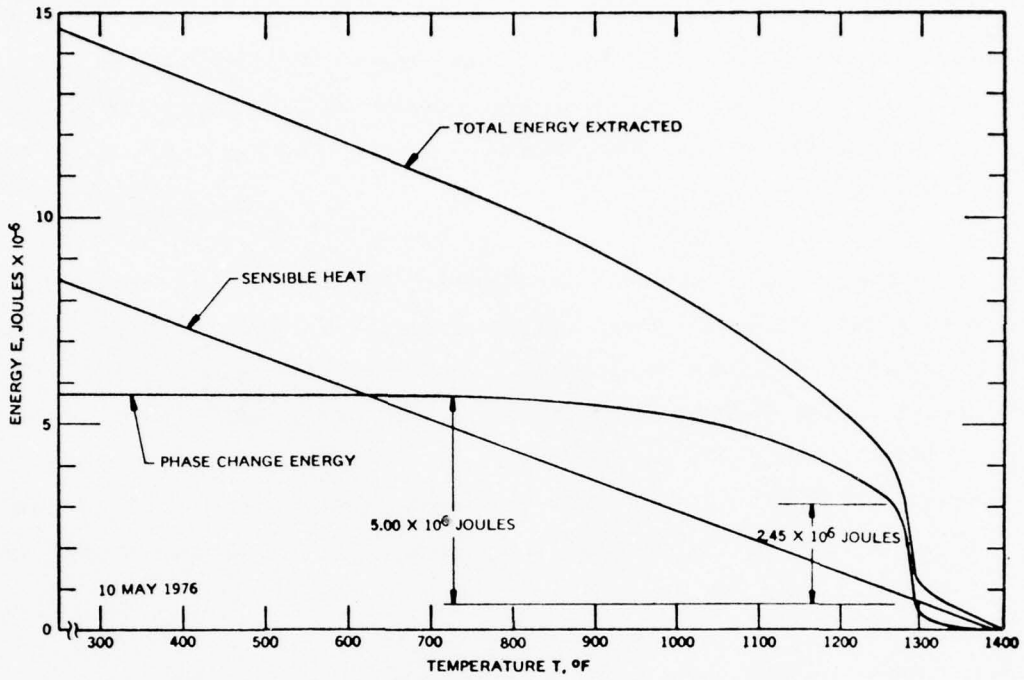



Figure 72. Extracted Energy (Cooling by Thermal Losses Only)

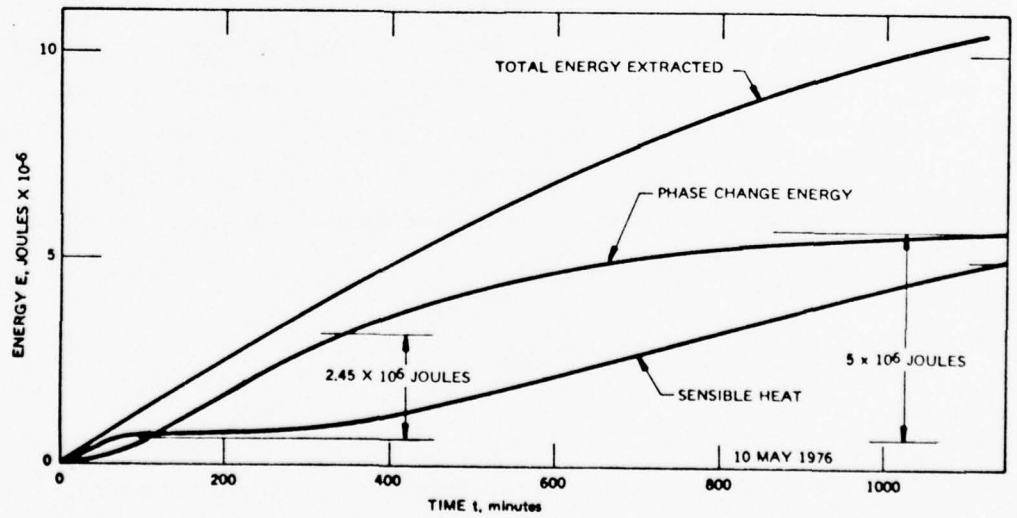



Figure 73. Extracted Energy (Cooling by Thermal Losses Only)

788.4 joules/gram (339.27 B/lb or 0.219 kW-hr/kg). This compares with the fusion energy of 944 joules/gram based on ideality of the ternary eutectic mixture of $MgF_2$-LiF-KF. Based on ideality, the total fusion energy available in the thermal energy storage unit would have been $5.17 \times 10^6$ joules.

From the results plotted in Figures 72 and 73 it appears that only $2.45 \times 10^6$ joules of phase change energy was released over a temperature range of $50^{\circ}F$. This is about 56.7 percent of the design energy. The total amount of the design energy was extracted over a temperature range of $1285^{\circ}$ to $1055^{\circ}F$, i.e., $230^{\circ}F$. The total amount of phase change energy appeared to be $5.07 \times 10^6$ joules. This is almost equal to the amount of energy that would have been calculated to be available as fusion energy based on ideality.

The same energy content in the TES salt as a function of temperature is exhibited in the heating curve as shown in Figure 74. This verifies that the energy content is independent of either the cooling or heating process of the salt.

The effective thermal capacity of the thermal energy storage unit as a function of time is shown in Figure 75. The curve shows two peaks in the effective thermal capacity of TES unit, one at about $1290^{\circ}F$ and the other at $1165^{\circ}F$. At these two temperatures thermal energy is released with the smallest drop in temperature. It is not known what phase change coincides with the second peak at $1165^{\circ}F$.

#### 4.2.2.3 Effect of Extraction Rate

The first evaluation of the thermal energy storage capacity was from test data obtained during a test in which the thermal energy storage unit was cooled only by its losses, which were a function of the temperature of the

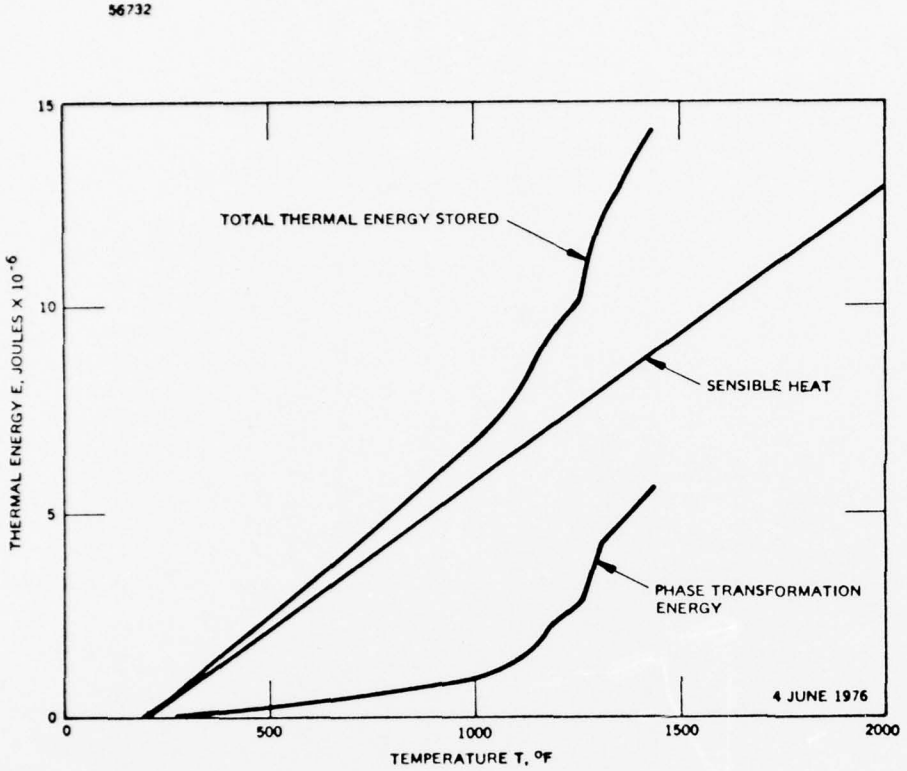



Figure 74. Amount of Stored Thermal Energy as Function of Temperature (Heating Curve)

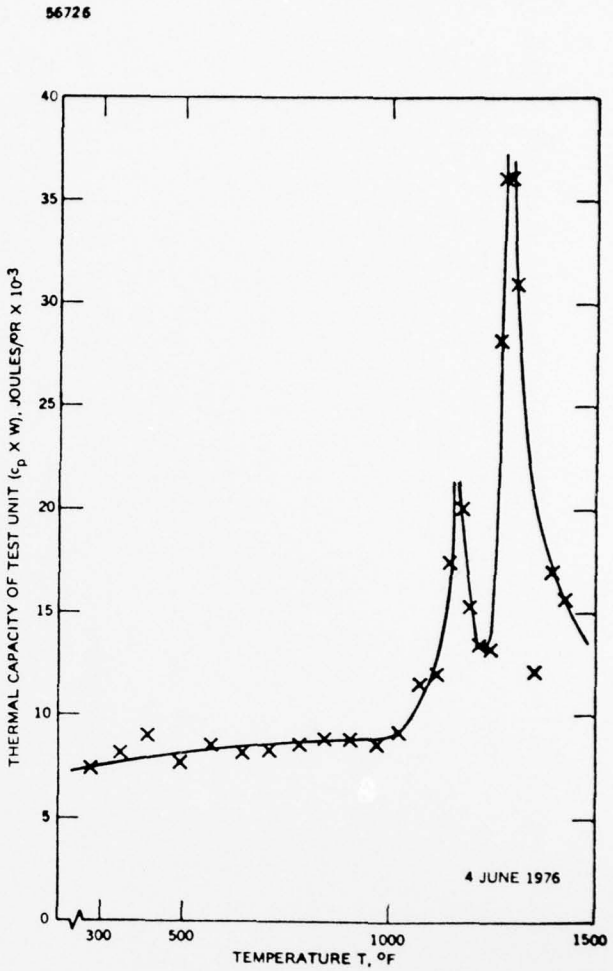


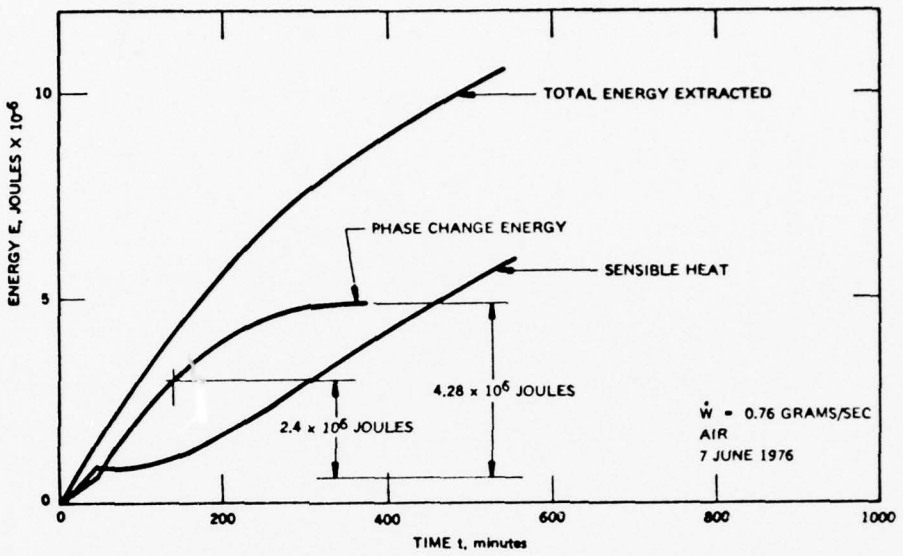

Figure 75. Apparent Thermal Capacity of Thermal Energy Storage Unit During Charging

unit. The initial loss was 213 watts decreasing with decreasing temperature, but remaining almost constant during the time at which the majority of the fusion energy was released.

Test results are shown in figures 76 and 77 of a test at which the initial total thermal power extraction from the unit was 555.6 watts. The power was extracted from the unit by losses through the insulation and by cooling the hot cylinder by an air flow of $\dot{W}$ = 0.76 gram/sec. At the eutectic point the power extraction rate was 475 watts. In a third test whose test data are presented in Figures 78 and 79, the gas flow rate was $\dot{W}$ = 3.7 gram/sec. At this flow rate the initial power extraction rate was 1799 watts, while at the eutectic temperature the extraction rate was 1067 watts, which was almost equal to the design extraction rate of 1200 watts, 200 watts of losses and 1000 watts of power carried away by the cooling gas in the hot cylinder.

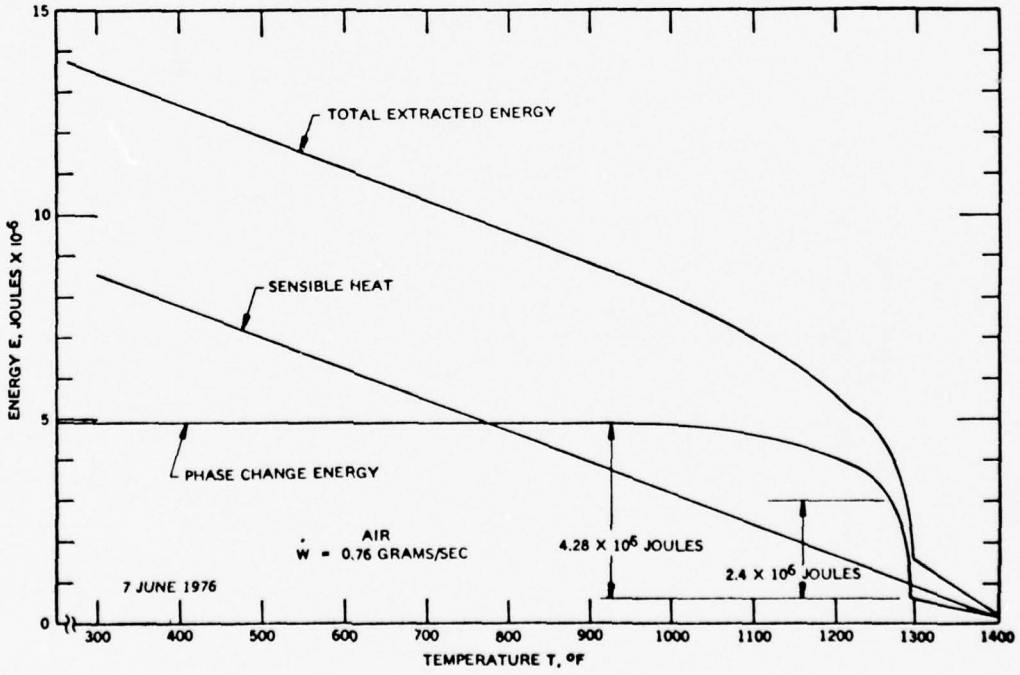
When the amount of energy extracted from the thermal energy storage material is correlated with the extraction rate, no effect of the extraction rate on the evaluated amount of available thermal energy can be found. The variations in the reduced data are within the accuracy with which the temperatures and the times could be measured.

Thus, the test data indicated that the behavior of the thermal energy storage material selected for this application was different from that anticipated. While lithium fluoride liberated the entire fusion energy at a specific melting point, the ternary eutectic salt made up of $MgF_2$, LiF, and KF, liberates phase change energy over a wide range of temperature. Since this temperature range was not known at the time of the design of the thermal energy storage unit, it was not included in the calculation of the temperature swing over which the hot cylinder would operate. Only the increasing temperature drop associated with the build-up of solidified thermal energy storage material had been considered. The overall effect of



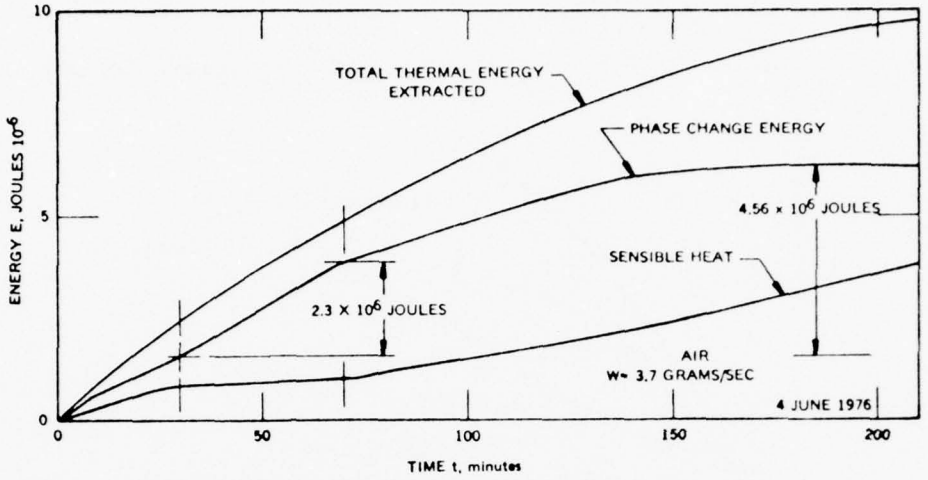

56736

Figure 76. Extracted Energy (Cooling by Thermal Losses and by Simulated V/M Cooler Operation with Flowing Air)



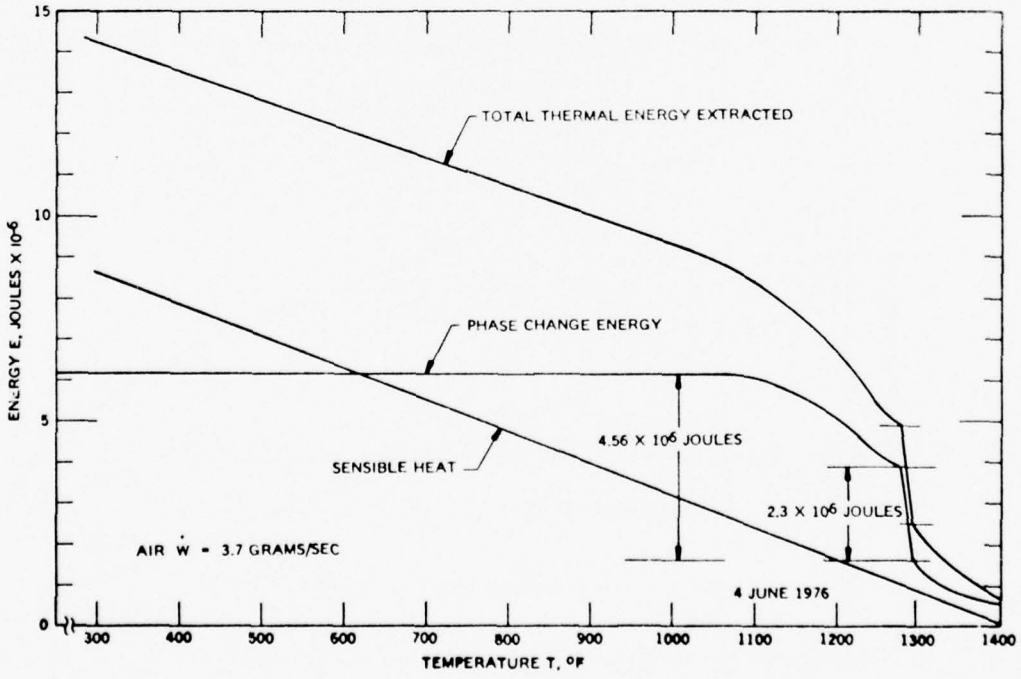

56733

Figure 77. Extracted Energy (Cooling by Thermal Losses and by Simulated V/M Cooler Operation with Flowing Gas)




56728

Figure 78. Extracted Energy (Cooling by Thermal Losses and by Simulated V/M Cooler Operation with Flowing Air)




56735

Figure 79. Extracted Energy (Cooling by Thermal Losses and by Simulated V/M Cooler Operation with Flowing Gas)

the unpredicted behavior of the chosen TES material is either the acceptance of a larger temperature swing over which the hot cylinder of the Vuilleumier cooler has to operate or a smaller energy storage density.

#### 4.2.2.4 Temperature Distribution

The design of the thermal energy storage unit was primarily aimed at extracting energy from the thermal energy storage material and transferring it to the hot cylinder with the smallest possible temperature drop. This would permit the use of a thermal energy storage material that had a melting temperature only slightly higher than the operating temperature of the hot cylinder of the Vuilleumier cooler. The best approach for achieving the desired operating characteristic of the thermal energy storage unit was the use of the heat pipe phenomenon by which energy could be transferred over a relatively large distance with a relatively small temperature drop.

When the thermal energy storage unit was tested with energy extraction at the hot cylinder, large temperature gradients were measured in the thermal energy storage unit. In Figures 80 and 81 the temperatures which were measured and recorded on a strip chart and whose locations are presented in Figure 60 are plotted against time. The gas flow rate through the hot cylinder was set to extract a total power of 1067 watts. Since the temperature differences did not exist during charging, as can be seen from Figure 82, the observed temperature gradients could not be attributed to faulty thermocouple readings.

All evidence indicated that the heat pipe functioned only partially. Some heat pipe effect was deducted from the fact, that the power transferred at the hot cylinder could not be conducted through the structural components of the the thermal energy storage unit with the indicated temperature gradients along the unit.

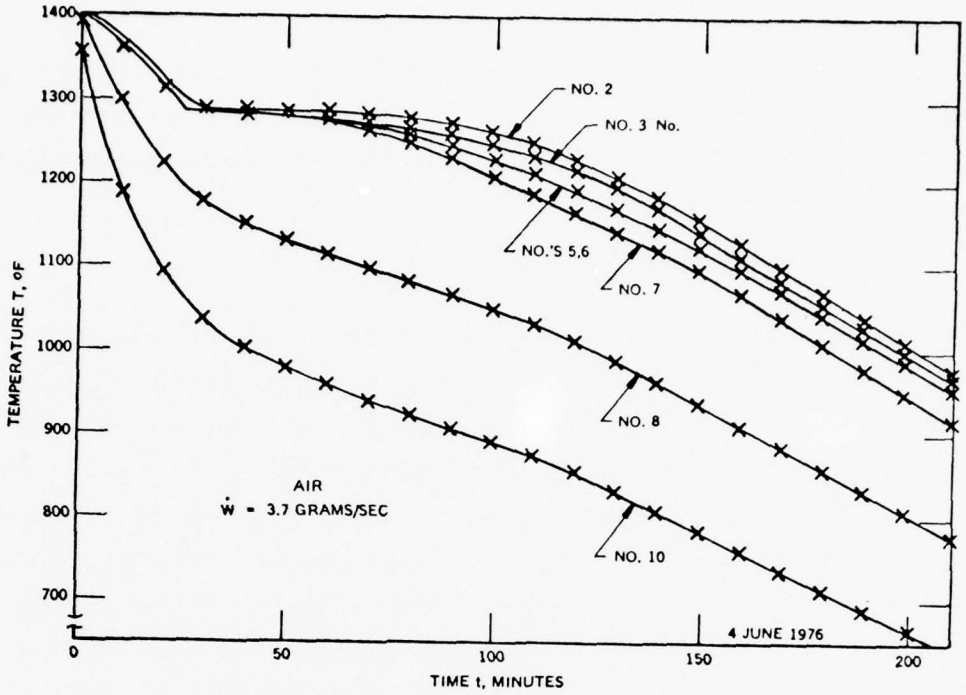



Figure 80. Measured Temperatures During Energy Extraction

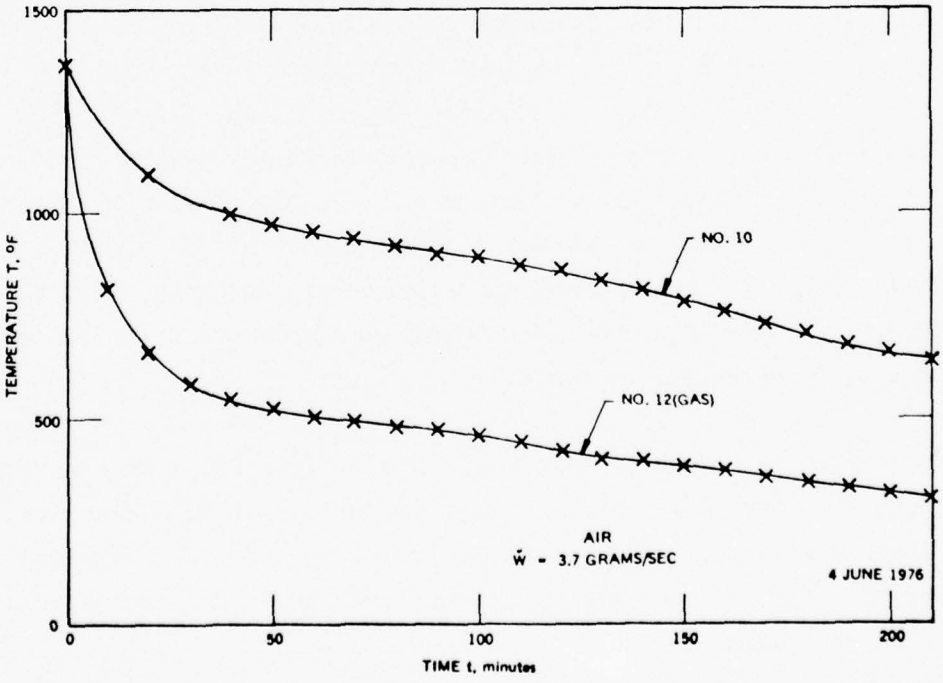



Figure 81. Measured Temperatures by Thermocuples Nos. 10 and 12

56727

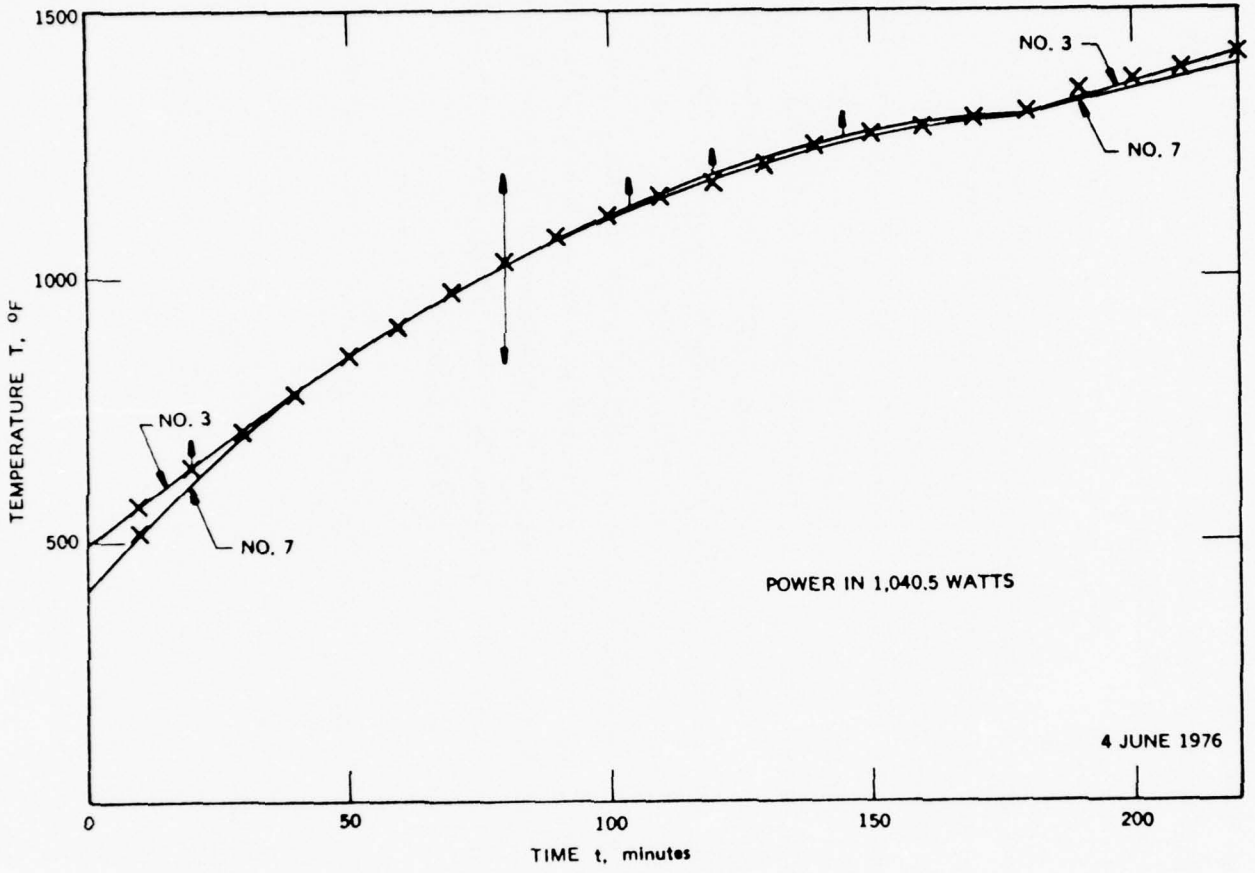



Figure 82. Temperatures During Charging of TES Unit

Three possible reasons for the malfunction of the heat pipe could be considered; (1) insufficient amount of working fluid (sodium), (2) failure of the wick, and (3) incondensable gas in the heat pipe. All three possible modes of heat pipe deficiency were investigated. (See Appendix B for wick study.) The failure was finally traced to a gas leak in the fill valve.

The heat pipe was reprocessed after the fill valve had been replaced by a new valve. When the stored energy was extracted from the unit by thermal losses and by cooling of the hot cylinder, the thermal energy storage unit exhibited the temperature distribution that had been predicted for the design (Figure 83). All temperatures along the outside of the unit remained equal, while the temperature measured inside the thermal energy storage unit (T.C. Nos. 1 and 2) was higher. The difference between the outside and inside temperatures was increasing with time as had been expected, when considering the heat transfer across the solidified TES material. The average power extraction rate was about 883 watts (figure 84) and the temperature differential between the outside temperatures and the inside temperature was $42^{o}F$. A temperature differential of $50^{o}F$ at an extraction rate of $1200^{o}$ watt had been predicted by the heat transfer analysis that was presented in Subsection 2.2.1.

The measured energy extracted as a function of temperature is shown in Figure 85.

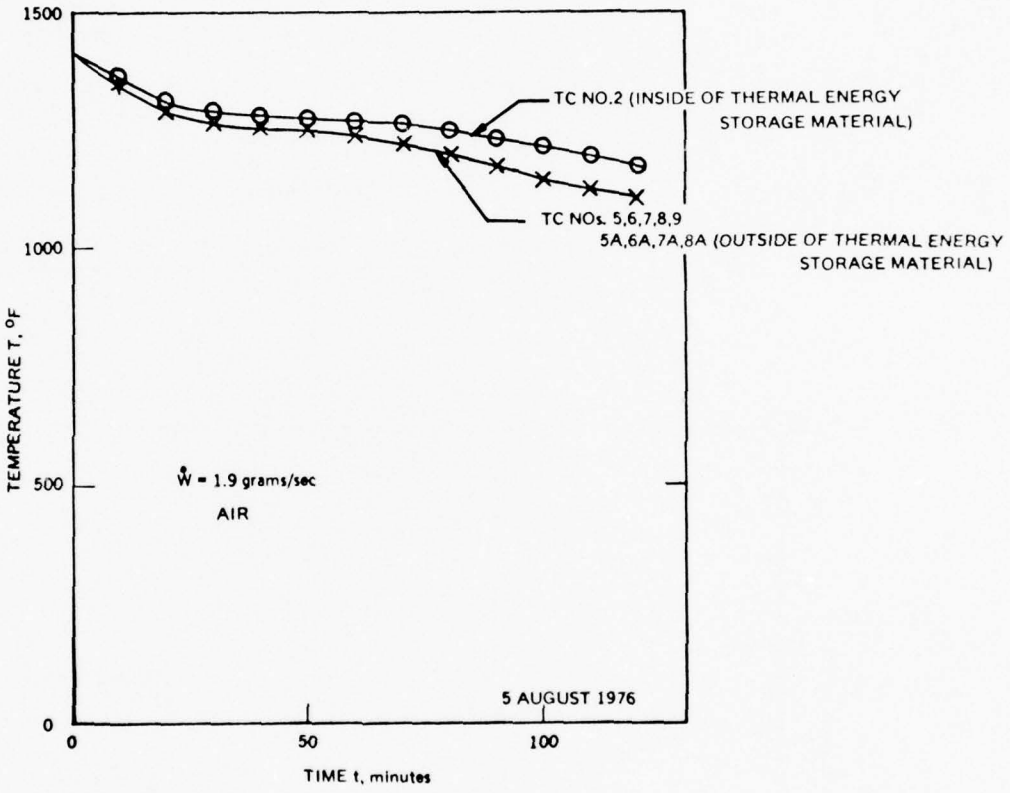
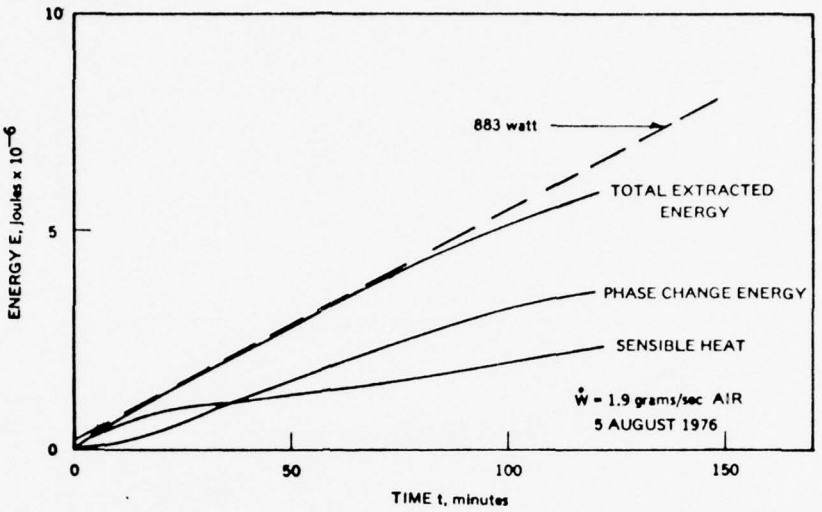


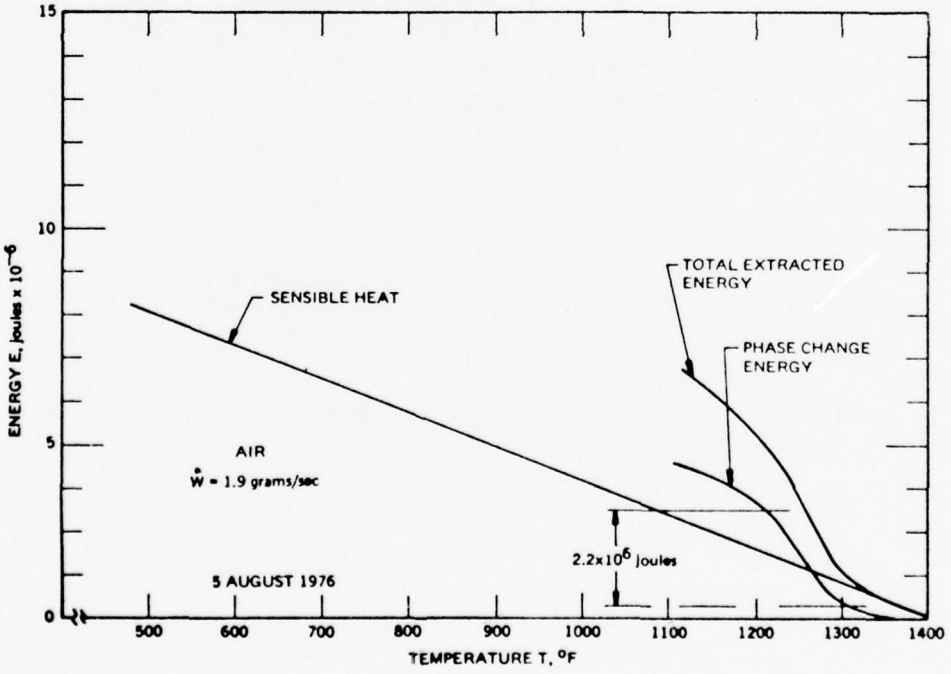

Figure 83. Measured Temperatures During Energy Extraction

56890




56689

Figure 84. Extracted Energy (Cooling by Thermal Losses and by Simulated V/M Cooler Operation with Flowing Air)




56688

Figure 85. Extracted Energy (Cooling by Thermal Losses and by Simulated V/M Cooler Operation with Flowing Gas)

## SECTION V

## CONCEPTUAL FLIGHT DEVICE PARAMETER DEVELOPMENT

### 5.1 BASIC REQUIRMENTS

For the evaluation of the thermal energy storage concept as applied to a high capacity Vuilleumier refrigerator, requirements for the refrigerator as shown in Table 6 were assumed.

TABLE 6. REFRIGERATOR REQUIREMENTS

| | |
|---|---|
| Orbit: | 12 hr |
| Eclipse Time: | 1 $\pm$0.1 hr |
| Operating Temperature: | 1250$^{o}$ $\pm$25$^{o}$F |
| Total Power Requirement: | 1000W |
| | 1500W |
| | 2000W |
| No. of Hot Cylinders: | 1 or 2 |

With the Vuilleumier cooler energy requirement given, it was further assumed that thermal losses would amount to about 10 percent of the cooler power, and that the thermal energy storage material is a ternary eutectic salt made up of 64 LiF - 30 $MgF_2$ - 6 KF, having an eutectic temperature of 1310$^{o}$F and a heat of fusion of 788.4 joules/gram (339.3 B/lb).

The main restrictions placed on the design of a thermal energy storage unit were:

a. The unit must be constructed from commercially available Inconel 600 pipes.

b. The unit must be tested in a 1-g environment.

c. The unit will be mated to the hot cylinder of the High Capacity refrigerator.

The stipulation that the design should incorporate commercially available Inconel 600 pipes was based on the experience gained in trying to procure specially made tubing from sheet metal stock. An intensive procurement inquiry produced only two vendors who were willing to undertake the fabrication of some but not all tubes to a given design. Despite quoting a price three times higher than that quoted by the first vendor, the second vendor was not even willing to guarantee the loosest tolerances required for final welding of the thermal energy storage unit. Thus, the available sources for tube fabrication from sheet metal stock proved to be too few and the fabrication cost appeared to be relatively high.

The nonfunctional requirement imposed on the design that the unit be able to operate in a 1-g environment, has to be accepted as long as the thermal energy storage unit has to be tested and its operation verified prior to launching and operation in space. This requirement imposes a dimensional constraint on the unit which is set by the height to which the working fluid of the heat pipe can be raised in a 1-g environment by the suction pressure due to capillary forces in the wick structure of the heat pipe.

## 5.2 CONCEPTUAL DESIGN PARAMETERS

### 5.2.1 BASIC DESIGN

The basic design that evolved from the above requirements and constraints is shown in Figure 86. The length, L, of the thermal energy storage unit is determined by the power requirement of the refrigerator which is shown in Figure 87.

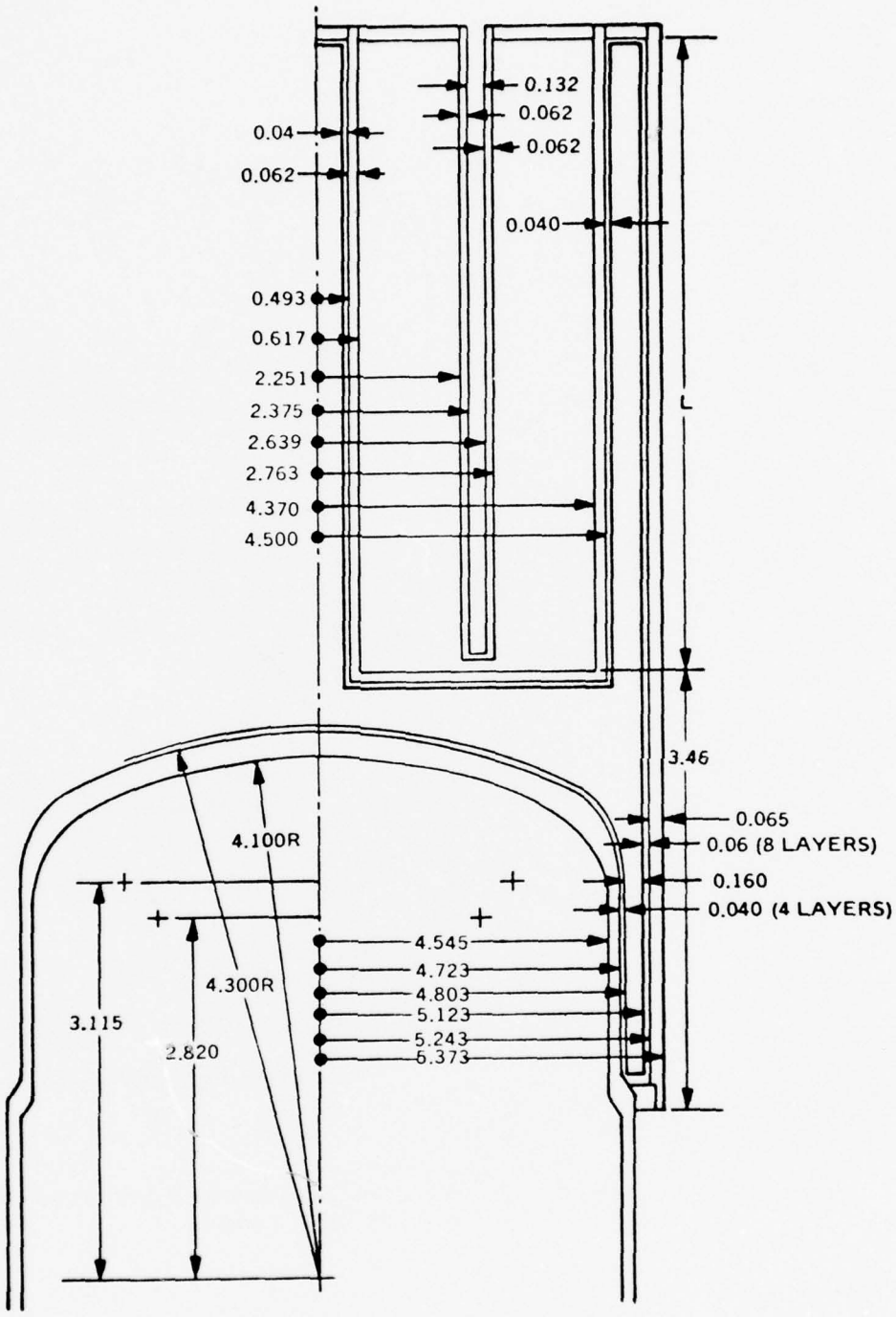



Figure 86. Thermal Energy Storage Unit Mounted on a Hi-Cap Hot Cylinder

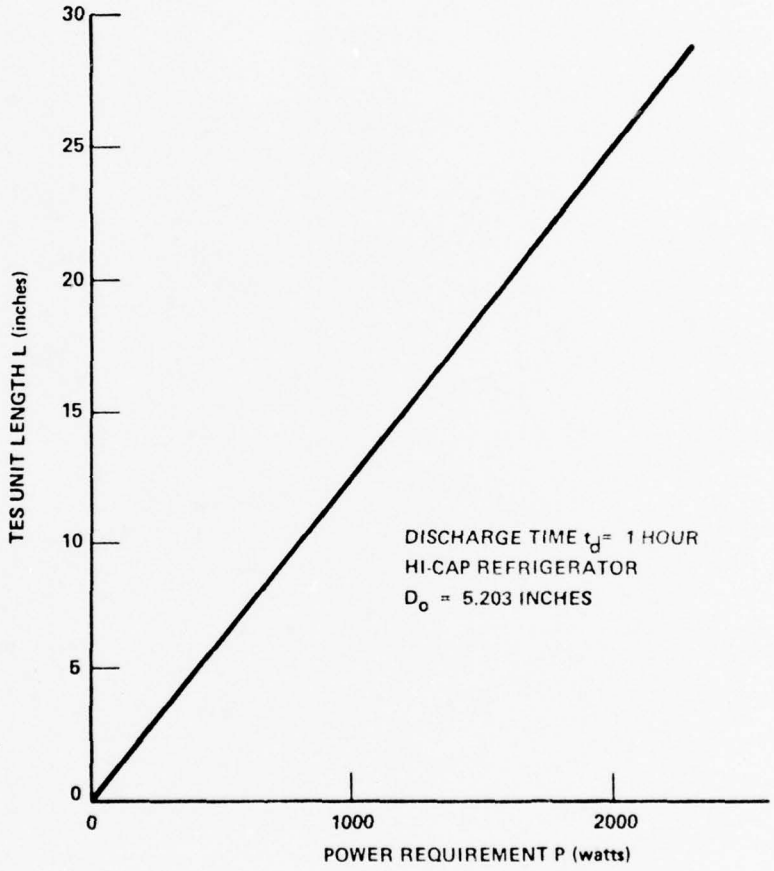



Figure 87. Correlation Between Power Requirement and TES Unit Length

54801

### 5.2.2 TEMPERATURE DISTRIBUTIONS

The temperature distribution in the thermal energy storage unit is shown in Figure 88. This temperature distribution is not affected by the length of the unit, because the temperature drop associated with the vapor flow pressure drop is very much less than $1^{\circ}F$. It remains negligible over the entire range of design lengths considered in this study.

The temperature drop across the thermal energy storage material as a function of the discharge time is shown in Figure 89. The effect of the temperature drop across the thermal energy storage material on the operating temperature of the Vuilleumier refrigerator is shown in Figure 90. At the beginning of the discharge cycle, the operating temperature is $1279^{\circ}F$, while at the end of the cycle the operating temperature will be either $1227^{\circ}F$ or $1219^{\circ}F$ for a 1-hour orbit, respectively. The operating temperature is therefore $29^{\circ}F$ above the design operating temperature of $1250^{\circ}F$ at the beginning of the eclipse and $23^{\circ}F$ below the design temperature.

The operating temperature of the Vuilleumier refrigerator over the entire 12-hour cycle, which includes the charging and discharging of the thermal energy storage unit, is shown in Figure 91. It would be interesting to compare this temperature variation and the cycle frequency of a hot cylinder operated with a thermal energy storage unit with the temperature history of a hot cylinder which is heated directly with a temperature controlled electrical heater.

### 5.2.3 WEIGHT

The total weight of the thermal energy storage unit including all necessary components of the unit, structural, wicking, working material, and insulation, is presented in Figure 92. For comparison, the probable weight of a nickel-hydrogen battery that can satisfy the same power requirements as the thermal energy storage unit are presented. The specific weight of the

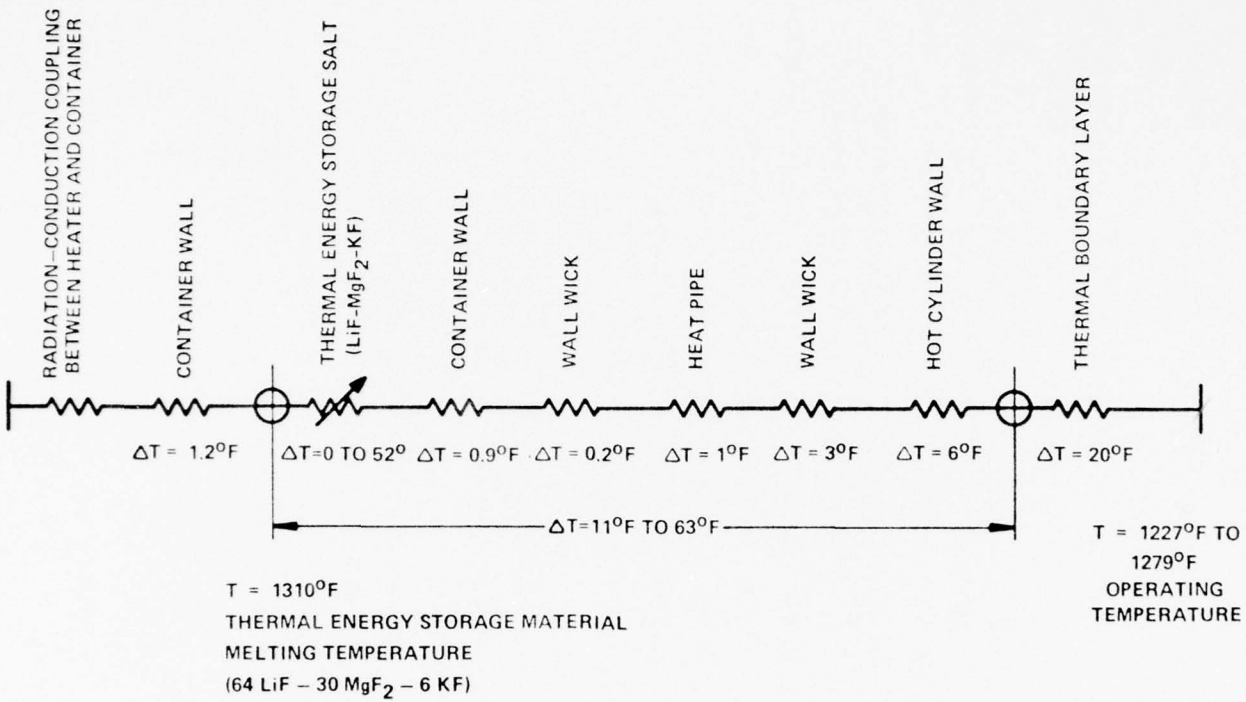
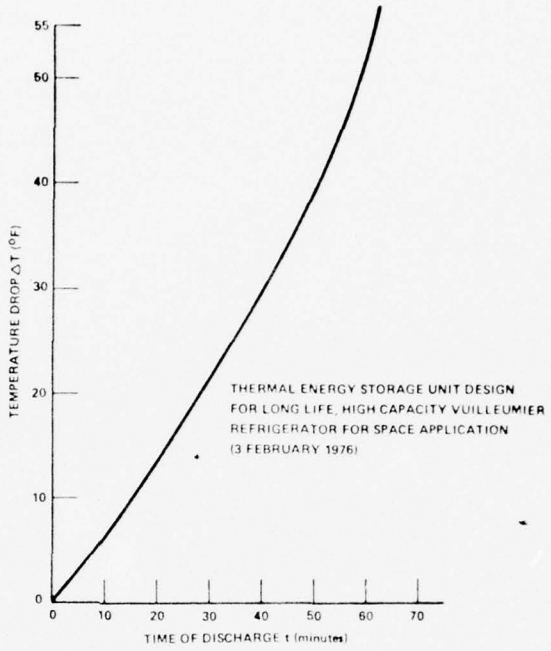
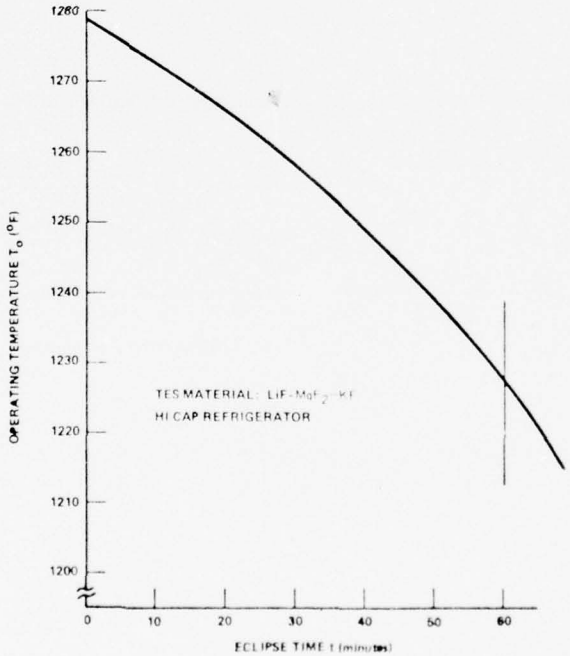



Figure 88. Temperature Distribution in the Thermal Energy Storage Unit and the Hot Cylinder of the Long Life, High Capacity Vuilleumier Refrigerator for Space Application




54796

Figure 89. Temperature Drop Across Thermal Energy Storage Material




54800

Figure 90. Vuilleumier Refrigerator Operating Temperature During Discharge of Thermal Energy Storage Unit

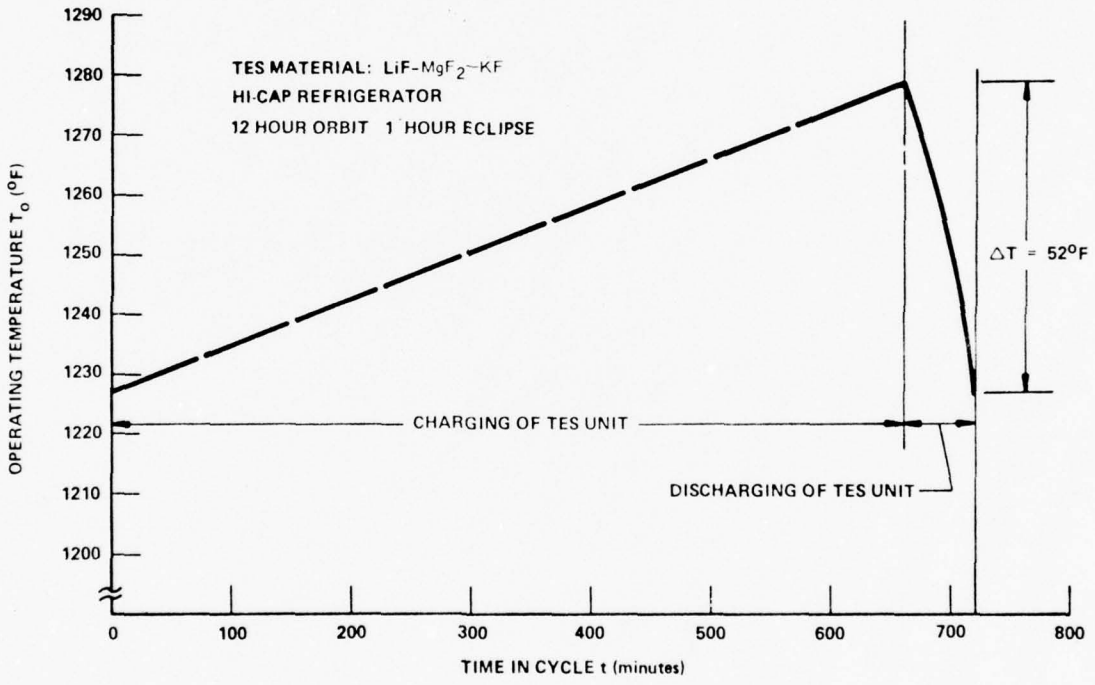
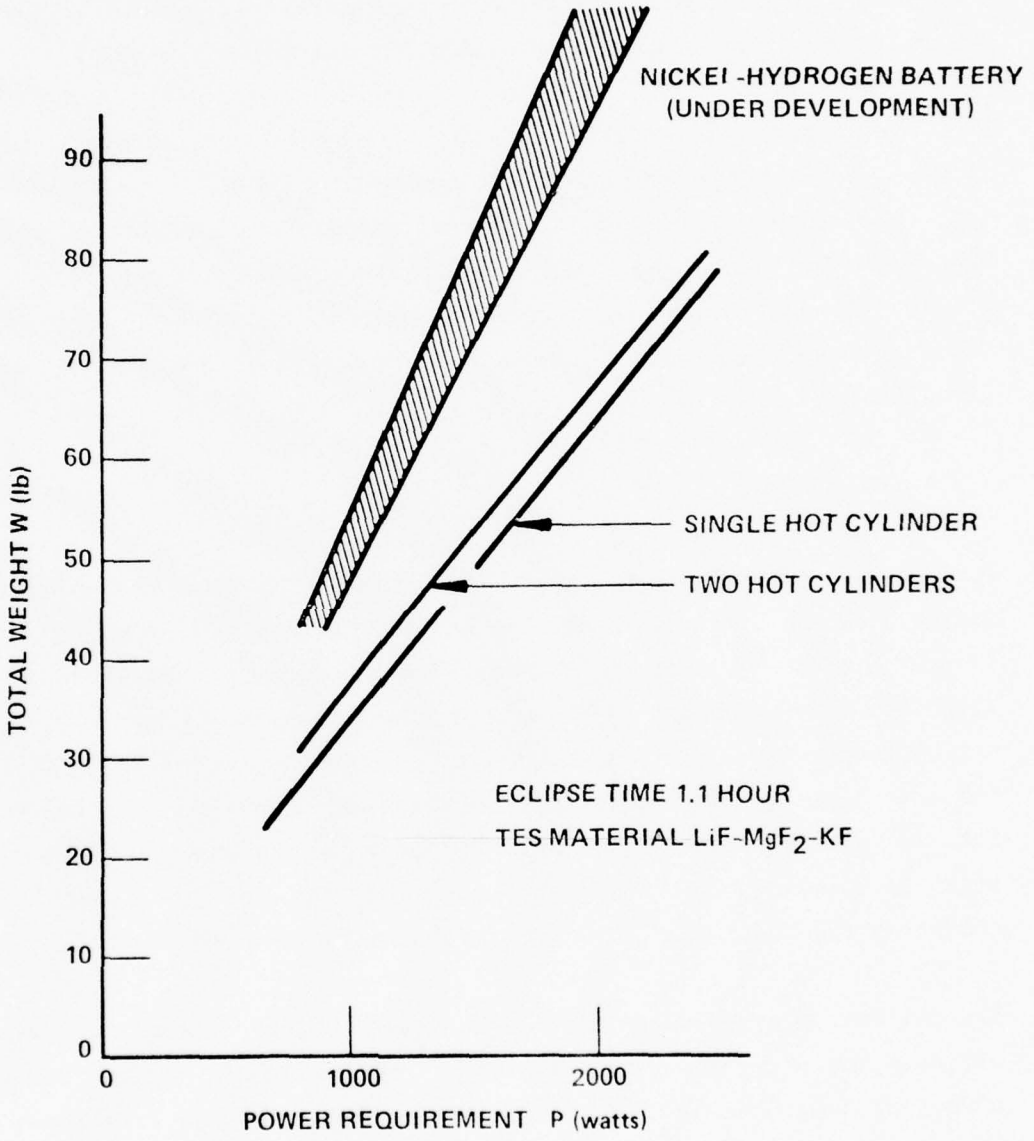



Figure 91. Operating Temperature of Vuilleumier Refrigerator During a Full Cycle of Charging and Discharging of the Thermal Energy Storage Unit

54799




54791

Figure 92. Total Weight of a Thermal Energy Storage Unit for a Vuilleumier Cooler

thermal energy storage unit is shown in Figure 93. With increasing power requirements, the specific weight approaches asymtotically 34 watt-hr/lb for a single hot cylinder Vuilleumier refrigerator, and slightly more than 32 watt-hr/lb for a dual hot cylinder refrigerator. The specific weights for batteries are being presented only for initial evaluation.

When comparing the weights of the thermal energy storage material (Figure 94) with the weights of the container (Figure 95), it can be seen that they are equal. While the thermal energy storage material weight is determined by the energy storage requirement, the container weight could conceivably be reduced if and when, by experience and long duration testing, the minimum material thickness for the container material has been established.

### 5.2.4 STRUCTURE

For the outer container, the wall thickness is determined by the collapsing criteria of the cylinder. The unit has to withstand a pressure difference of one atmosphere when the thermal energy storage unit is cold and a slightly lower pressure differential when the unit is operating at its design temperature. Correspondingly, the materials properties of Inconel 600 are changing with temperature as shown in Figure 96. The correlation between wall thickness of the outer cylinder and the collapsing pressure is shown in Figure 97. If a safety factor of 4 is employed, then the wall thickness for the design indicated in Figure 86 would be about 0.060 inch.

The collapsing pressure calculations assumed a long cylinder to cover the entire range of design. The calculations can be refined to incorporate the effect of length on the wall thickness requirements. A relatively short TES unit could be constructed with a slightly thinner wall than that indicated by Figure 97.

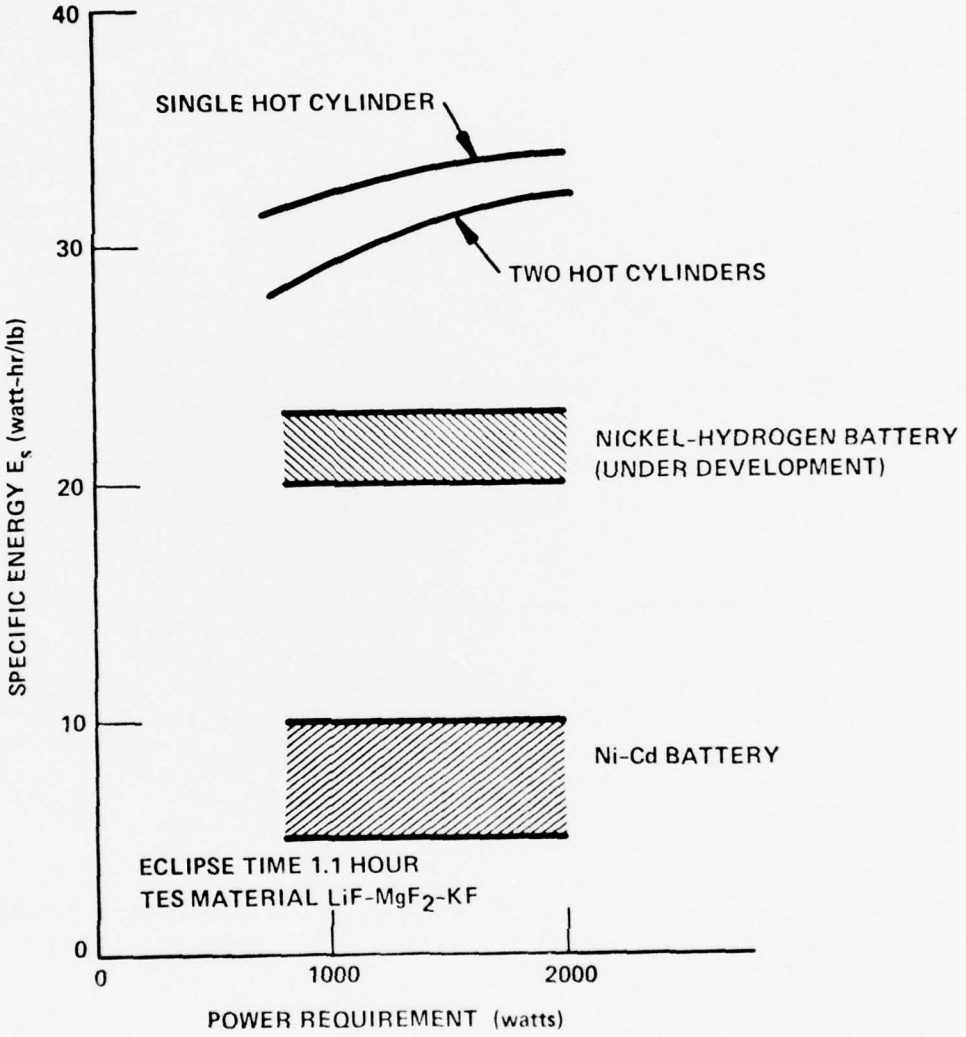



Figure 93. Specific Energy of a Thermal Energy Storage Unit for a Vuilleumier Cooler

54795

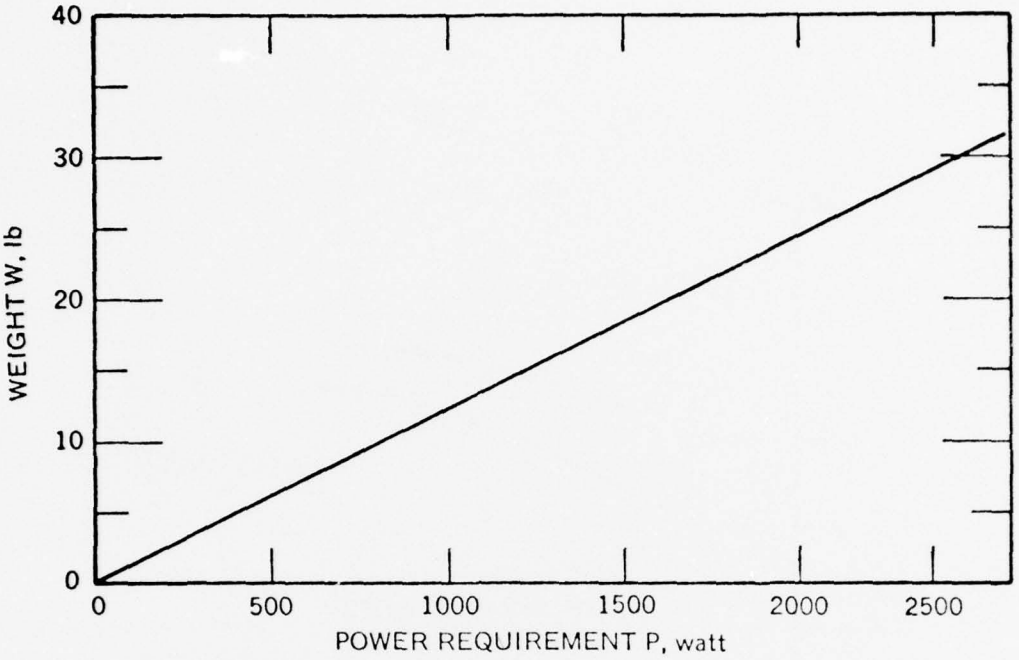



Figure 94. Thermal Energy Storage Material Weight

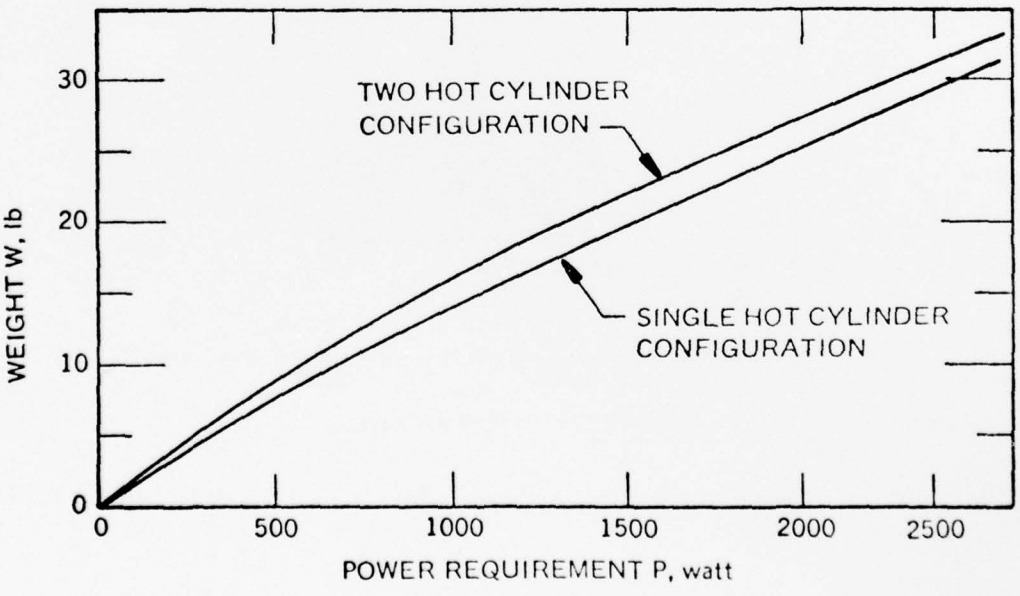
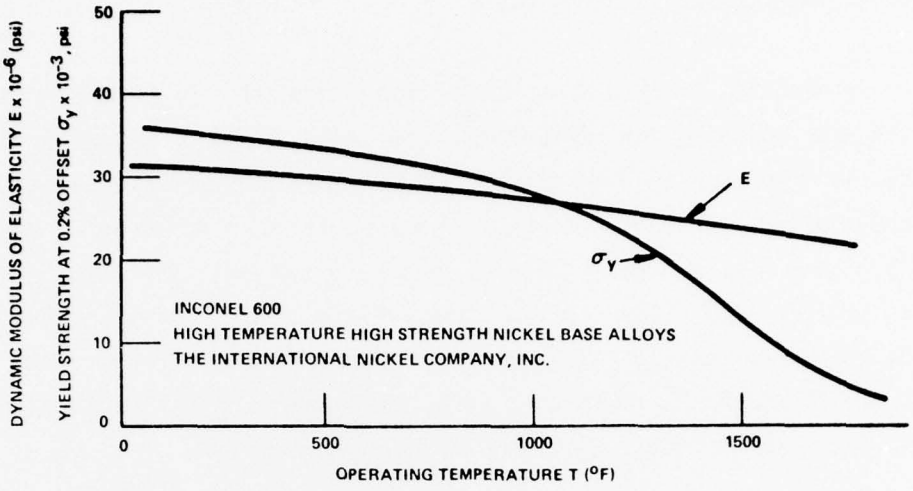


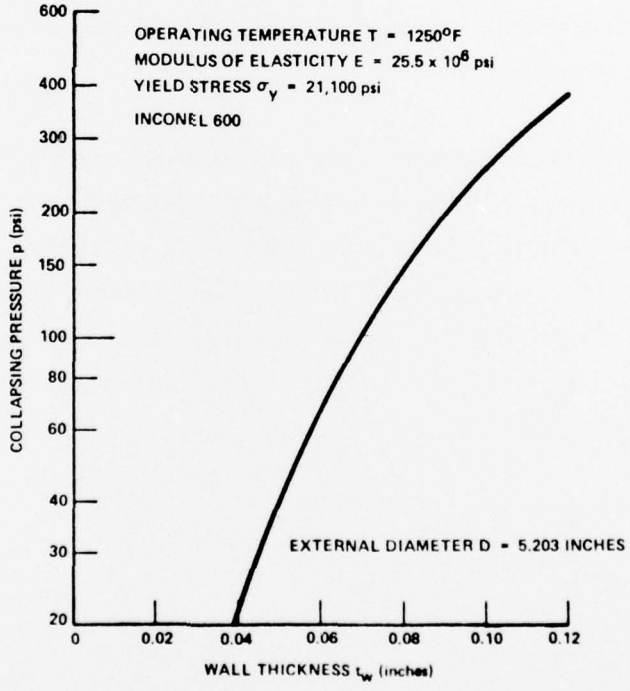

Figure 95. Total Container Weight Including Insulation and Heat Pipe Components

56883




54793

Figure 96. Dynamic Modulus of Elasticity E and Yield Strength of Inconel 600 Alloy




54794

Figure 97. Collapsing Pressure of Thin-Walled Vessel

### 5.2.5 CONCEPTUAL FLIGHT DEVICE

For a mission using a long life, high capacity Vuilleumier refrigerator with two opposing hot cylinders, the total thermal power requirement for the refrigerator is 1150 watts. This power has to be supplied to the two opposing hot cylinders, i.e., 575 watts to each cylinder. The low earth orbit would demand only 18 minutes of thermal energy to be supplied by the TES units. Using the design underlying the TES demonstration unit which called for an energy requirement of 1000 watts for 60 minutes, the length of the TES units for the long life, high capacity Vuilleumier refrigerator (Hi-Cap V/M) hot cylinders can be estimated to be

$$L = \frac{1150}{2 \times 1000} \times \frac{18}{60} L_{TESDU} = 0.1725 L_{TESDU}$$

The hot cylinder physical layout with the TES unit is shown in Figure 98 and Figure 99 shows the Hi-Cap V/M cooler with the TES units mounted on both hot cylinders. For comparison, Figure 100 shows the cooler without the TES units.

The available pipe sizes for the construction of the TES unit are boxed in black in Figure 32. Only Schedule 40 pipes are available for larger pipe sizes. The nominal 5-inch pipe has a wall thickness of 0.258 inch, which is about three times thicker than needed. Thus, an unmachined pipe would weigh about 10 pounds, but approximately two-thirds (6.5 pounds) would have to removed. The cost of the pipe is approximately $16/pound indicating a waste of about $100.

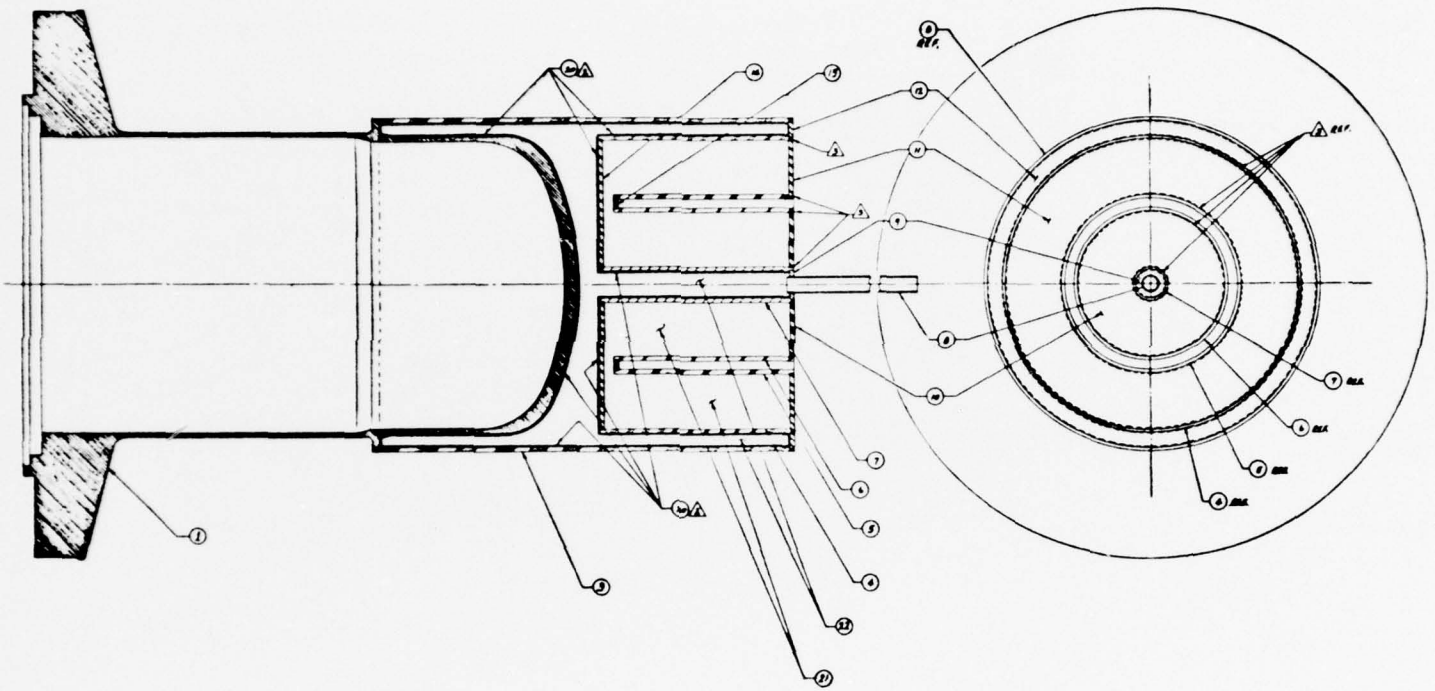


Figure 98. Conceptual Thermal Energy Storage Unit for Hi-Cap Vuilleumier Cooler

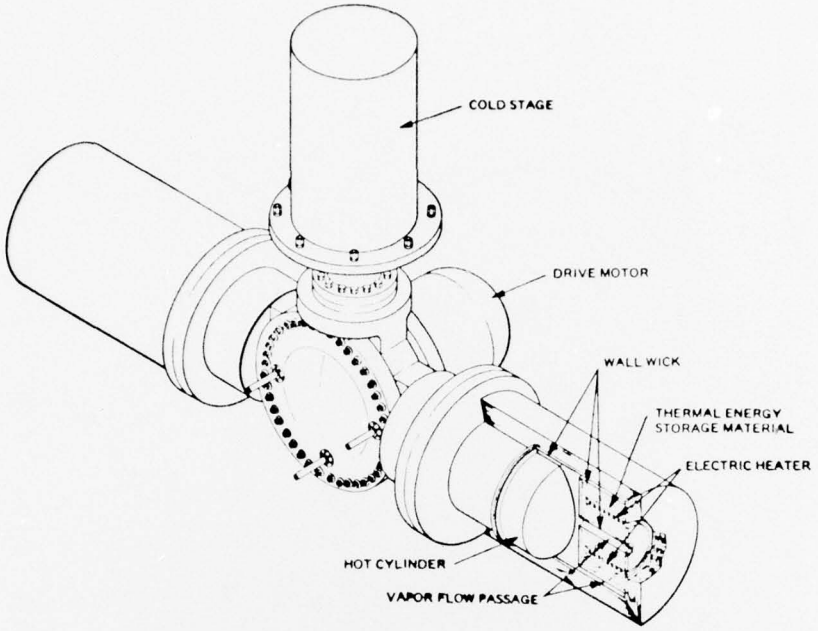



Figure 99. Long Life, High Capacity Vuilleumier Refrigerator with Thermal Energy Storage Units

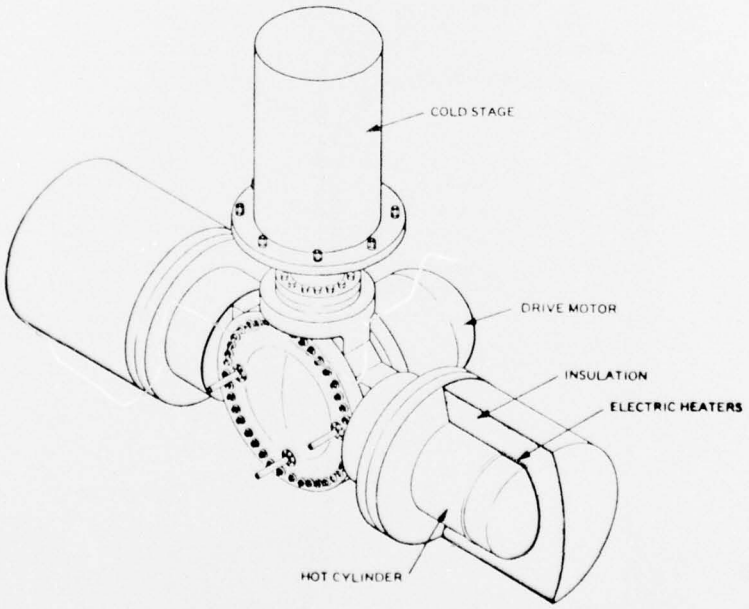



Figure 100. Long Life, High Capacity Vuilleumier Refrigerator with Battery Energized Electric Heaters (Present Hi-Cap Configuration)

# SECTION VI

# CONCLUSIONS

The Thermal Energy Storage Demonstration Unit program had as its objective proof of feasibility of storing energy in form of latent heat for powering a Vuilleumier cooler during the time a satellite is in the eclipse of the sun. The major technical areas that needed technical confirmation were the storing of thermal energy, the extraction of the energy over a limited temperature range, and the transfer of the thermal energy to the hot cylinder of the Vuilleumier cooler.

The design of the thermal energy storage unit confirmed the concept of storing energy from an electric heater in form of the latent heat of a thermal energy storage material. The stored thermal energy was extracted over a large area with a minimum of temperature drop and transferred to the hot cylinder by heat pipe action.

The testing of the thermal energy storage demonstration unit revealed rather unexpectedly that the phase change energy of the ternary eutectic salt, LiF-$MgF_2$-KF, was not released or absorbed entirely at the melting point of the salt, but over a relatively wide temperature range. It appeared that only about 50 percent of the "ideal" fusion energy is absorbed during heating or released during cooling at the eutectic temperature of about 1310$^{o}$F. Phase transformation with energy absorption upon heating apparently takes place at temperatures below the eutectic temperature. This produces the appearance of a specific heat which is much more temperature dependent than kinetic theory would predict.

The thermal energy storage demonstration unit program demonstrated a TES unit that stored energy in the form of fusion energy, released the stored

energy at the eutectic temperature and below, and could transfer the energy by heat pipe action to the hot cylinder of a Vuilleumier cooler. The large amount of thermal energy released at the eutectic temperature and during the solidification of the thermal energy storage salt was transferred over a temperature range of about $42^{\circ}F$. This agreed well with the design prediction, confirming the capability of designing TES units to specific requirements when the thermodynamic properties of the TES material are known.

The evaluation of weight contributions of the various TES unit components pointed to the most fruitful areas of further investigation of all aspects of thermal energy storage, if this concept should prove to be a valid alternative to storing energy in an electrical battery. A considerable reduction of the wall thicknesses of the container could be possible, if material compatibility for long duration operation could be proven to exist between the storage salt, the heat pipe working fluid, and the container material.

# APPENDIX A

## EFFECT OF NONCONDENSABLE GAS ON HEAT PIPE OPERATION

When large temperature differences along the heat pipe section of the thermal energy storage unit were observed, an attempt was made to explain this apparent malfunction of the heat pipe by assuming the possibility of noncondensable gas in the heat pipe section of the thermal energy storage unit. In Figure A-1, the temperature difference between thermocouple No. 6 and thermocouple No. 10 were plotted. The temperature difference could be explained by a vapor pressure difference of the working fluid which has been calculated for the operating temperature and which has also been plotted in Figure A-1. The calculated pressure differentials which are based on the observed temperature differentials, are considerably higher than those which were calculated for the vapor flow, as can be seen from the pressure differentials shown in Figures 16, 17 and 18 of Subsection 2.2.2.3. Only the presence of noncondensable gas in the heat pipe could explain such large vapor pressure differentials. If the presence of noncondensable gas at a pressure of 1.67 mm Hg at room temperature is assumed, then temperature differentials as shown in Figure A-1 could be expected. The calculated temperature differential curve has apparently a different trend than the curve which was constructed from the measured temperature differentials. Nevertheless, some similarity in behavior seems to exist.

It was interesting to show that, if noncondensable gas should have an effect on the heat pipe operation, a heat pipe operating with potassium as the working fluid would be less affected than a heat pipe operating with sodium at the same operating temperature. This can be seen in Figure A-2. The reason for this diffeence between the two working fluids can be found

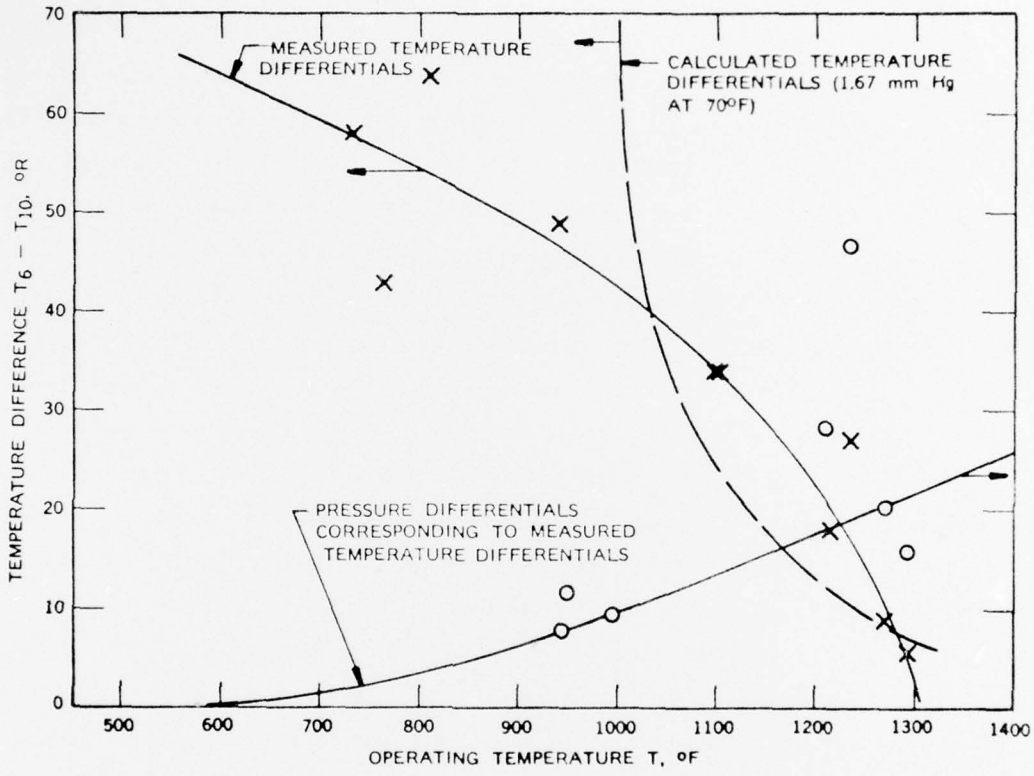



Figure A-1. Temperature Differentials and Pressure Differentials

56744

56742

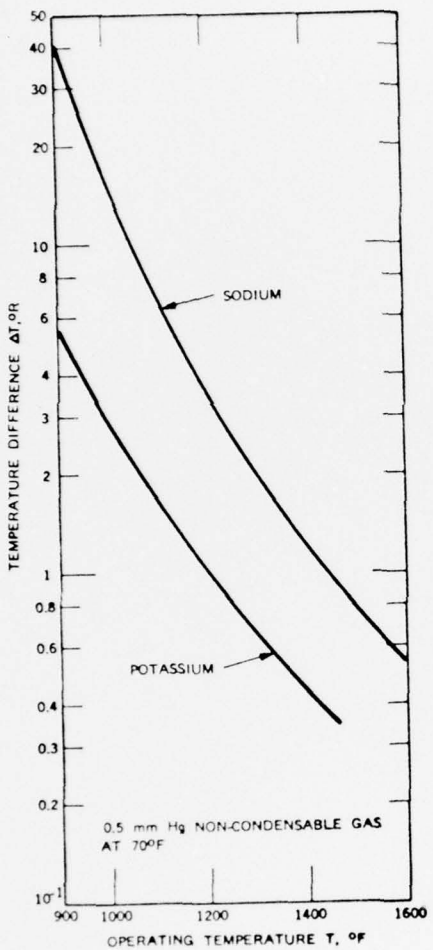



Figure A-2. Temperature Differential Due to Noncondensable Gas

56882

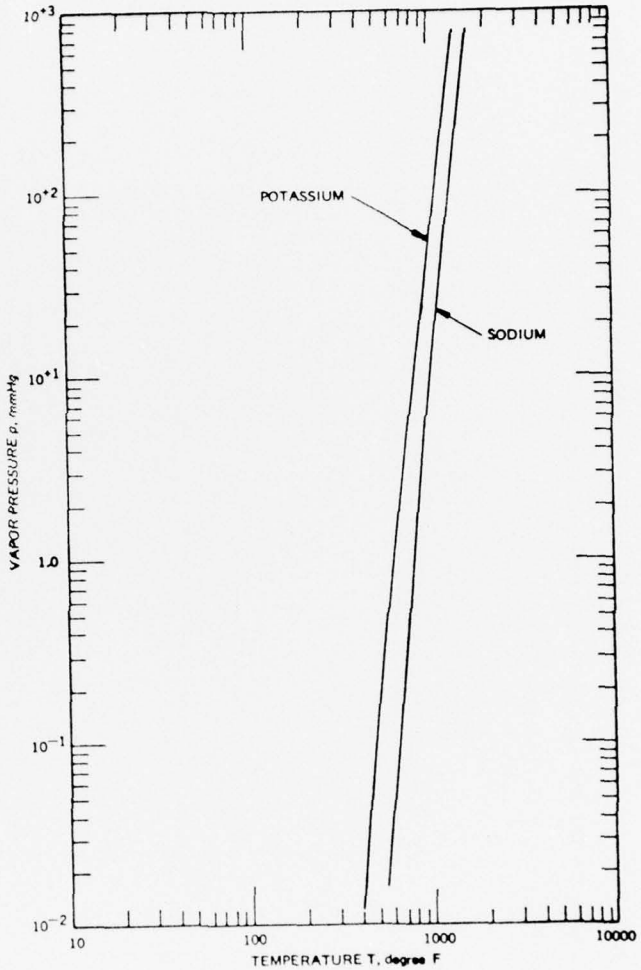



Figure A-3. Vapor Pressure of Sodium and Potassium

from the graph showing the vapor pressure of sodium and potassium (Figure A-3). For the thermal energy storage unit operating at around $1300^{o}F$, potassium would be quite acceptable as heat pipe working fluid, as the vapor pressure at that temperature is only slightly above 1/2 atm. The unit has to be designed for a pressure differential of 1 atm to satisfy the condition in the laboratory.

## APPENDIX B

## TRANSIENT WICK EFFECTS

When initially it was not possible to verify the presense of noncondensable gas in the heat pipe section of the thermal energy storage unit, and it appeared that the heat pipe section had been fully evacuated, the capacity and performance of the wick structure was investigated in an informative experiment to verify the wick design.

The wick of the heat pipe was constructed with a 70 Mesh bolting cloth which has a wire diameter of 0.00375 inch. For a fluid the wicking height is

$$h = \Delta p_c / \rho g$$

where:

$h$ = height, cm
$\rho$ = specific gravity of water, $g/cm^2$
$g$ = gravitational constant, 981 $cm/sec^2$
$\Delta p_c$ = capillary pressure, dynes/cm

$$\Delta p_c = 2\sigma \cos\phi / r_c$$

where:

$\sigma$ = surface tension of water against air, dynes/cm
$\phi$ = contact angle, degrees
$r_c$ = effective pore radius, cm

$$r_c = 0.707\ (1/M - d)$$

where:

$M$ = Mesh, $cm^{-1}$

$d$ = wire diameter, cm

For distilled water at room temperature, the surface tension is

$\sigma$ = 72.75 dynes/cm,

and the wicking height is found to be:

$h$ = 3.086 inch.

Figure B-1 shows a fixture that was built to simulate the wick structure in the heat pipe section of the thermal energy storage unit. In step one, the dry structure was weighted. In step two, the wick structure was soaked with water and the structure was weighted again. In step three, the structure was held horizontally in water, after which it was weighted again. In the fourth step, the wick was permitted to soak up water after most of the water had been shaken out of the wick. The structure was weighted again. The fully filled 4.9 inch high screen appeared to hold 7.0 grams of water. When standing vertically, it retained 4.5 grams of water. This indicated that the height of the water in the wick was

$$h = h_o \times W/W_o$$

$h$ = 3.15 inch

This compared with the predicted value of $h$ = 3.086 inch. After the fourth step, the water weight was $W$ = 3.6 grams, which corresponded to a wicking height of $h$ = 2.52 inch, or about 80 percent of the maximum wicking

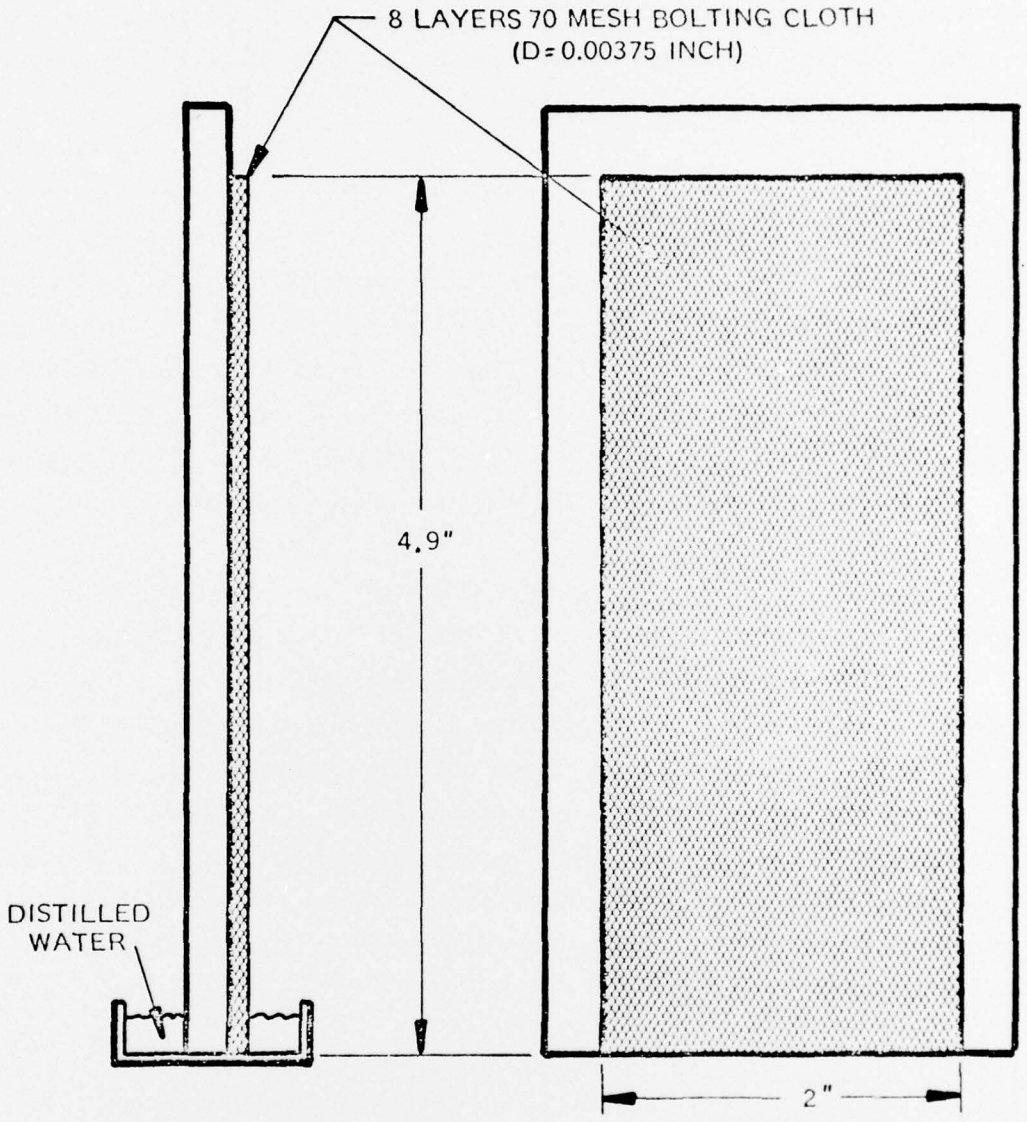



Figure B-1. Test Fixture for Wick Investigation

56741

height. The data of Ref. 3 are difficult to correlate and do not pertain to sodium. Nevertheless it is indicated that time is a strong parameter which determines the height during continuous operation to which the wick will remain wet in a heat pipe whose diameter is close to the calculated maximum wicking height.

The small informative test indicated that some basic data should be generated in support of the design of full scale thermal energy storage units. Wick data in the literature and of other investigators are very speculative and sketchy and can therefore not be used for designs in which the limit of the capability of wick structures is being approached. The permeability investigation of wicking structures, which was performed under the previous program, proved the need for such basic studies in connection with the design of a major hardware component.

Tests might be needed to ascertain whether the heat pipe section of the thermal energy storage unit is not subject to the fast start-up phenomenon which was observed with the 15-ft long heat pipe. At an extraction rate of 1200 watts, 0.2772 g/sec of sodium has to circulate. This is equivalent to 997.92 g/hr of sodium. The entire heat pipe section contains 329 grams of sodium, indicating that the sodium has to be wicked back three times an hour during operation. This rate might make the heat pipe operation marginal for a wick height which is more than 75 percent of the maximum wicking height. Some basic investigations with water should be able to answer these questions.

---

3. H. R. Knuz, L. S. Langston, B. H. Hilton, S. S. Wyde, and G. H. Nashick, "Vapor-Chamber Fin Studies - Transport Properties and Boiling Characteristics of Wicks," NASA Contractor Report No. NASA CR-812, June 1967.



☆ U. S. GOVERNMENT PRINTING OFFICE: 1977 — 757-001/317